

UNCLASSIFIED

AD NUMBER

AD478353

LIMITATION CHANGES

TO:

Approved for public release; distribution is unlimited.

FROM:

Distribution authorized to U.S. Gov't. agencies and their contractors;
Administrative/Operational Use; FEB 1966. Other requests shall be referred to Arnold Engineering Development Center, Arnold AFB, TN.

AUTHORITY

AEDC ltr 31 May 1991

THIS PAGE IS UNCLASSIFIED

AEDC-TR-65-255

AD-478 353

1967
OCT 19 1967

OCT 15 1970

MAR 12 1991

MAY 30 1991



DIFFUSER AUXILIARY EJECTOR DEVELOPMENT FOR THE DESIGN OF THE J-3 LEM DESCENT EXHAUST SYSTEM

J. W. Hale and W. C. Gobbell

ARO, Inc.

**TECHNICAL REPORTS
FILE COPY**

**PROPERTY OF U. S. AIR FORCE
AEDC LIBRARY
AF 40(600)1200**

**PROPERTY OF U.S. AIR FORCE
AEDC TECHNICAL LIBRARY**

February 1966

Approved for public release; distribution unlimited.

~~This document is subject to special export controls
and each transmittal to foreign governments or foreign
nationals may be made only with prior approval of
Arnold Engineering Development Center.~~

**ROCKET TEST FACILITY
ARNOLD ENGINEERING DEVELOPMENT CENTER
AIR FORCE SYSTEMS COMMAND
ARNOLD AIR FORCE STATION, TENNESSEE**

NOTICES

When U. S. Government drawings specifications, or other data are used for any purpose other than a definitely related Government procurement operation, the Government thereby incurs no responsibility nor any obligation whatsoever, and the fact that the Government may have formulated, furnished, or in any way supplied the said drawings, specifications, or other data, is not to be regarded by implication or otherwise, or in any manner licensing the holder or any other person or corporation, or conveying any rights or permission to manufacture, use, or sell any patented invention that may in any way be related thereto.

Qualified users may obtain copies of this report from the Defense Documentation Center.

References to named commercial products in this report are not to be considered in any sense as an endorsement of the product by the United States Air Force or the Government.

DIFFUSER AUXILIARY EJECTOR DEVELOPMENT
FOR THE DESIGN OF THE
J-3 LEM DESCENT EXHAUST SYSTEM

J. W. Hale and W. C. Gobbell
ARO, Inc.

This document is subject to special export controls
and each transmittal to foreign governments or foreign
nationals may be made only with prior approval of
Arnold Engineering Development Center.

FOREWORD

The work reported herein was sponsored by the Arnold Engineering Development Center (AEDC), Air Force Systems Command (AFSC), under Program Element 65402234.

The results of research presented were obtained by ARO, Inc. (a subsidiary of Sverdrup and Parcel, Inc.), contract operator of the AEDC, AFSC, Arnold Air Force Station, Tennessee, under Contract AF 40(600)-1200. The research was conducted in Propulsion Research Areas (R-2C-2 and R-2D-1) of the Rocket Test Facility (RTF) from September 1964 to April 1965 under ARO Project No. RW3543, and the manuscript was submitted for publication on November 9, 1965.

This technical report has been reviewed and is approved.

Forrest B. Smith, Jr.
Propulsion Division
DCS/Research

Donald R. Eastman, Jr.
DCS/Research

ABSTRACT

A four-phase investigation was conducted to select a rocket engine diffuser auxiliary ejector configuration. The configuration was required to maintain test cell pressure sufficiently low to keep the rocket engine nozzle flowing full at 10 percent of full power while operating against an exit pressure of approximately 1.50 psia. The investigation was in support of the LEM Descent test program scheduled for the J-3 test cell. The annular-type auxiliary ejector was selected because of its superior performance over the centerbody-type ejector. A successful model rocket engine throttling demonstration to 10 percent of full power was made with the annular-type auxiliary ejector. An ejector second throat (having a contraction area ratio of 0.62) was used to increase the limiting diffuser exit pressure. Pressure distribution through the J-3 model ducting was obtained at various exhaust header pressures.

CONTENTS

	<u>Page</u>
ABSTRACT.	iii
NOMENCLATURE.	viii
I. INTRODUCTION	1
II. APPARATUS	
2.1 Simulated Rocket Engines	2
2.2 Model Liquid-Propellant Rocket Engine	2
2.3 Diffuser and Auxiliary Ejector Test Configurations	2
2.4 Simulated Rocket Engine and Ejector Driving Fluid. .	4
2.5 Instrumentation.	4
III. TEST PROCEDURE	
3.1 Phase I	5
3.2 Phase II	5
3.3 Phase III.	6
3.4 Phase IV.	6
IV. RESULTS AND DISCUSSION	
4.1 Phase I	7
4.2 Phase II	9
4.3 Phase III.	11
4.4 Phase IV.	17
V. SUMMARY OF RESULTS	21
APPENDIX I: Force Balance Analysis for Test Configurations 3a, b, and c	25
REFERENCES	33

ILLUSTRATIONS

Figure

1.	Details of Simulated Rocket Engine Nozzles and Model Rocket Engine	
a.	Configuration A.	35
b.	Configuration B.	35
c.	Configuration C.	36
d.	Configuration D.	36
2.	Model Rocket Engine Propellant System for Configuration D Engine Throttling.	37
3.	Details for Centerbody-Type Ejector Configura- tions 1 through 9	38

<u>Figure</u>		<u>Page</u>
4.	Details of Centerbody-Type Auxiliary Ejector Configuration 10.	40
5.	Test Configurations 2a and b for Centerbody-Type Ejector Configuration 10	41
6.	Test Configurations 2c, d, and e for Centerbody-Type Ejector Configurations 10, 10a, and 10b	42
7.	Details of Annular-Type Auxiliary Ejector Configurations 11 and 11a	43
8.	J-3 Model Installation in Propulsion Research Area (R-2C-2) for Test Configurations 3a, b, and c. .	44
9.	Details of Centerbody-Type Ejector Configuration 12	45
10.	J-3 Model Installation in Propulsion Research Area (R-2C-2) for Test Configuration 4	46
11.	Performance Evaluation of Phase I, Test Configurations with Diffusers having Normal Shock Contraction	
	a. Centerbody-Type Ejector Position Limitation for Various Nose Cone Angles . . .	47
	b. Centerbody-Type Ejector Position Effect on Driving Pressure Ratio for Various Centerbody Nose Cone Angles.	47
12.	Diffuser Contraction Area Ratio Effect on Driving Pressure Ratio for Various Centerbody Nose Cone Angles	48
13.	Centerbody-Type Ejector Performance for Test Configurations 2a and b having $(L/D)_c = 2.6$ and 8.0	
	a. Secondary-to-Primary Mass Ratio Influence on the Limiting Driving Pressure Ratio	48
	b. Secondary-to-Primary Mass Ratio Influence on Cell-to-Driving Pressure Ratio	49
	c. Secondary-to-Primary Mass Ratio Influence on Rise Ratio	49
14.	Centerbody-Type Ejector Performance for Test Configurations 2c, d, and e	50

<u>Figure</u>		<u>Page</u>
15.	Air-Driven Rocket Engine and Steam-Driven Centerbody-Type Ejector Performance for Test Configurations 2c through e	
	a. Diffuser Limiting Second-Throat Exit Static Pressure Performance.	51
	b. Ejector Limiting Exit Static Pressure Performance	52
	c. Minimum Cell Pressure and Rocket Engine Nozzle Lip Static Pressure Performance . . .	53
16.	Steam-Driven Rocket Engine and Steam-Driven Centerbody-Type Ejector Performance for Test Configuration 2e	
	a. Diffuser Limiting Second-Throat Exit Static Pressure Performance	54
	b. Ejector Limiting Exit Static Pressure Performance	55
17.	Nomogram of Rocket Engine Chamber Pressure Throttling Limitations for Test Configurations 2c and e	56
18.	Annular-Type and Centerbody-Type Ejector Performance for Test Configurations 3a, 3b, and 4. .	57
19.	Steam-Driven Rocket Engine and Steam-Driven Annular-Type Ejector Performance for Test Configurations 3a and b	
	a. Diffuser Limiting Second-Throat Exit Static Pressure Performance	58
	b. Ejector Limiting Exit Static Pressure Performance	59
	c. Minimum Cell Pressure and Rocket Engine Nozzle Lip Static Pressure Performance . . .	60
	d. Rocket Engine Jet Boundary Impingement Variation with Change in Chamber Pressure . .	61
20.	Throttling Performance of N ₂ O ₄ and AZ-50 Liquid- Propellant Rocket Engine for Test Configurations 3c and 4	
	a. Annular-Type Ejector Test Configuration 3c . .	62
	b. Centerbody-Type Ejector Test Configuration 4 .	63
	c. Rocket Engine Jet Boundary Change with Position for Test Configuration 3c	64

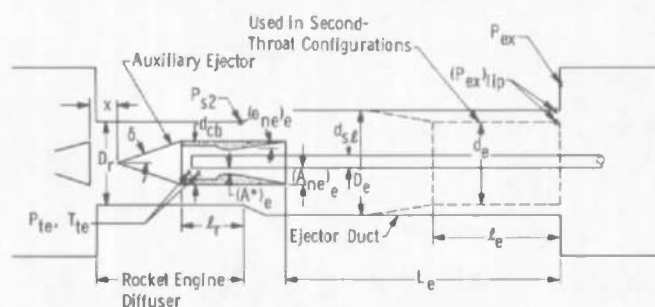
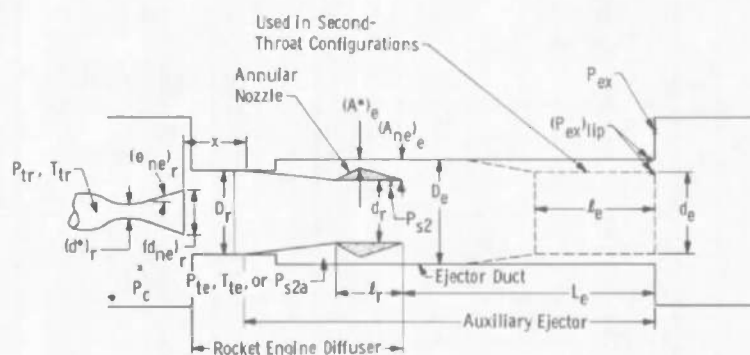
<u>Figure</u>		<u>Page</u>
21.	J-3 Model Duct Pressure Distribution for Test Configuration 3c with $P_{te} = 43$ psia and Throttling from $P_{tr} = 50$ to 10 psia	
	a. $(P_t)_{ex} = 0.55$ psia.	65
	b. $(P_t)_{ex} = 1.5$ psia	65
	c. $(P_t)_{ex} = 2.0$ psia	65
22.	J-3 Model Duct Pressure Distribution for Test Configuration 3c with $P_{te} = 40$ psia and Throttling from $P_{tr} = 100$ to 20 psia	
	a. $(P_t)_{ex} = 0.64$ psia.	66
	b. $(P_t)_{ex} = 0.85$ psia.	66
	c. $(P_t)_{ex} = 1.25$ psia.	66
23.	J-3 Model Duct Pressure Distribution for Test Configuration 3c with $P_{te} = 56$ psia and Throttling from $P_{tr} = 100$ to 10 psia	
	a. $(P_t)_{ex} = 1.7$ psia	67
	b. $(P_t)_{ex} = 2.0$ psia	67
24.	Typical Transient of Rocket Engine Chamber Pressure.	68
25.	Nomogram of Rocket Engine Chamber Pressure Throttling Limitations for Test Configurations 3a, b, and c	69

TABLES

I.	Description of Rocket Engine Nozzle Configurations	71
II.	Description of Test Configurations	72
III.	Summary of Cold-Flow Centerbody-Type Ejector Blockage Study (Phase I)	73

NOMENCLATURE

A	Cross-sectional area, in. ²
D	Diameter of diffuser duct, in.
d	Diameter, in.
F	Total stream thrust or impulse, lbf



g_c	Dimensional constant, $32.174 \text{ ft-lb}_m/\text{lb}_f\text{-sec}^2$
L	Length of constant-area diffuser duct, in.
ℓ	Length of second-throat duct, in.
M	Mach number
\dot{m}	Mass flow rate, lb_m/sec
O/F	Oxidizer-fuel mass ratio
P	Pressure, psia
R	Specific gas constant, $\text{ft-lb}_f/\text{lb}_m\text{-}^\circ\text{R}$
T	Temperature, $^\circ\text{R}$
x	Distance from rocket engine nozzle exit to the beginning of second throat or to the tip of the centerbody-type ejector nose cone, in.
γ	Ratio of specific heats
δ	Centerbody-type ejector nose cone half-angle, deg
θ	Nozzle divergent half-angle, deg
$\mu(M)$	Function of Mach number

SUBSCRIPTS

31 , 32 , and 33	J-3 model duct stations
act	Actual
c	Test cell
cb	Centerbody
d	Diffuser
e	Ejector
ex	Exit
i	Inbleed
isen	Isentropic
lip	Lip
ne	Nozzle exit
ns	Normal shock
p	Primary
pred	Predicted
r	Rocket engine
ramp	Ejector second-throat ramp
s	Secondary
sl	Supply Line
st	Second throat
s ₂	Rocket engine diffuser second-throat exit lip
s _{2a}	Rocket engine diffuser second-throat external exit
t	Total or stagnation
w	Wall
x	Upstream of normal shock
y	Downstream of normal shock

SUPERSCRIPTS

*	Nozzle throat
'	Primary
''	Secondary

SECTION I INTRODUCTION

A variable thrust capability to provide more versatility for space rendezvous has recently become a rocket engine requirement. Some proposed test programs at AEDC involve rocket engines which have operational thrust ranges from maximum power down to 10 percent of maximum. The experimental determination of throttleable rocket engine performance requires an installation in which a relatively constant test cell pressure is maintained during throttling.

The objective of the program reported herein was to develop a rocket engine diffuser auxiliary ejector configuration for Propulsion Engine Test Cell (J-3) in support of the Lunar Excursion Module (LEM) Descent program. This configuration must maintain a test cell pressure sufficiently low to keep the rocket engine nozzle flowing full during transient thrust variation from full power to 10-percent power when operating against an exhaust pressure of approximately 1.50 psia. During operation, the auxiliary ejector driving fluid mass flow was to be kept at a minimum for the available diffuser exit pressure.

The investigation was conducted to select the type of auxiliary ejector (annular-type or centerbody-type) which would satisfy the objective and requirements. To evaluate the types of auxiliary ejectors, the program was divided into four phases:

- I. Cold-flow centerbody-type ejector blockage study
- II. Centerbody-type ejector performance study
- III. Diffuser-ejector performance evaluation of the centerbody- and annular-type ejectors with a simulated rocket engine.
- IV. Diffuser-ejector performance evaluation of the centerbody- and annular-type ejectors with a model liquid-propellant rocket engine.

SECTION II APPARATUS

The basic test hardware used in the four phases of the investigation included a dummy centerbody-type ejector to simulate blockage, a small nozzle area ratio centerbody-type ejector, a large nozzle area ratio centerbody-type ejector, and an annular-type ejector. The centerbody-type or annular-type ejector configurations were used in tandem with a simulated rocket engine nozzle or a model liquid-propellant rocket engine.

2.1 SIMULATED ROCKET ENGINES

Three axisymmetric conical nozzles used to simulate rocket engines are shown in detail in Figs. 1a through c as configurations A, B, and C. A description of the nozzle configurations is given in Table I.

2.2 MODEL LIQUID-PROPELLANT ROCKET ENGINE

The liquid-propellant rocket engine configuration D (Fig. 1d) is a pressure-fed unit utilizing nitrogen tetroxide (N_2O_4) and Aerozene-50 as the propellant. The nozzle was contoured and had an area ratio of 40. A description of the engine nozzle configuration is given in Table I.

The propellant lines to the engine were provided with valves and orifices to accommodate thrust variation by changing propellant flow rate at constant tank pressure. The details of this arrangement are shown in Fig. 2.

2.3 DIFFUSER AND AUXILIARY EJECTOR TEST CONFIGURATIONS

2.3.1 Phase I

A schematic of the test configuration is shown in Fig. 3, and a description is given in Table II. The dummy centerbody-type ejector (configurations 1 through 9) used to produce blockage in the diffuser was changed in diameter and nose cone shape and used with two diffuser sizes. Details of the nine configurations tested are shown in Fig. 3. The dummy centerbody-type ejector position with respect to the simulated rocket engine was made variable by a screw mechanism attached to the simulated ejector driving fluid supply line.

2.3.2 Phase II

Details of the centerbody-type ejector (configuration 10) with a 15-deg half-angle nose cone and nozzle area ratio of 7.54 are shown in Fig. 4. Test configuration 2 (Table II) consisted of a test cell 12 in. in diameter and 21 in. long, into which atmospheric air was bled in through a control valve to the nozzle plenum shown in Fig. 5. Two lengths of the 3.48-in. -diam duct were used, giving an $(L/D)_e = 2.6$ or 8.

2.3.3 Phase III

The test configurations used in Phase III are described as 2c, d, and e and 3a and b in Table II. Test configuration 2c was the same as that used in Phase II (test configuration 2a) except that a simulated rocket engine (nozzle configuration B, Fig. 1b) was used in place of the atmospheric inbleed system shown in Fig. 5. Modifications were made by adding two sizes of second throats to the ejector, giving test configurations 2d and e. Figure 6 gives the details of these test configurations (2c, d, and e).

The annular-type ejector configurations 11 and 11a used in test configurations 3a and b were the annular type. This rocket engine diffuser-ejector configuration consisted of a 7.68-in. -diam duct contracted through a 12-deg half-angle to a 5.87-in. -diam duct forming the diffuser second throat. Connected to the second throat was a symmetrical expanding annular nozzle having an area ratio of 16.62 and a throat area of 1.86 in.². The annular nozzle discharged into a 9.93-in. -diam constant area duct, forming ejector configuration 11. A 7.82-in. -diam ejector second throat was added to give configuration 11a. Details of the annular-type ejector are shown in Fig. 7. The test configuration shown in Fig. 8 is an approximate 1/10-scale (based on diameters) model of the J-3 test cell ducting. The simulated rocket engine (nozzle configuration C, Fig. 1c) was used in test configurations 3a and b.

2.3.4 Phase IV

The test configurations (Table II) were used with rocket engine configuration D (Table I). One test configuration (3c) used the same annular-type ejector as in Phase III but used the model rocket engine configuration D rather than the simulated rocket engine configuration C. This test configuration is also shown in Fig. 8.

The second test configuration had a centerbody- instead of the annular-type ejector. The centerbody-type ejector configuration 12 was built with the same basic geometrical parameters as the annular-type ejector, as shown in Table II. Dimensional details of the centerbody-type ejector nozzle configuration 12 are presented in Fig. 9. The rocket engine and centerbody-type diffuser-ejector installation and diffuser details are presented in Fig. 10.

Test configuration 4 (Fig. 10) is the same as 3e except that the annular-type ejector was replaced by the centerbody-type ejector.

2.4 SIMULATED ROCKET ENGINE AND EJECTOR DRIVING FLUID

Air from the VKF 4000-psi storage tank or 200-psig saturated steam from the AEDC central plant provided the driving medium for the simulated rocket engine and auxiliary ejector. A plenum total pressure range from 0 to 100 psia for air or steam was supplied to the simulated rocket engine and/or the auxiliary ejector. The diffuser exhaust pressure was varied from 0 to approximately 10 psia by means of a valve or held constant at a predetermined value by the exhaust machines.

2.5 INSTRUMENTATION

The parameters of primary interest were cell pressure, rocket engine and ejector driving fluid total pressure and temperature, and rocket engine diffuser and auxiliary ejector exit pressure. The investigation included both steady-state and transient instrumentation.

The steady-state pressure sensing instrumentation consisted of diaphragm-activated dial gages which were periodically calibrated to ensure that the readings were within the calibration range. The temperatures were measured with copper-constantan thermocouples and were read on compensating millivoltmeters.

The transient instrumentation consisted of pressures sensed by transducers and recorded on oscillographs and strip charts by null-balance, potentiometer-type recorders. The transient pressures were obtained by a galvanometer having a frequency response of 60 cps.

All pressure transducers were laboratory calibrated against a secondary standard before installation. Prior to and after each test, all pressure transducers were resistance-calibrated in place to verify the electrical portion of the transducer and data acquisition system.

Only a 0 to 100 psia transducer was used to measure the rocket engine chamber pressure, P_{cr} , for both 100 and 10-percent power. The accuracy of measuring the chamber pressure in the 10-psia range on the 0 to 100 psia transducer is not good; therefore, the chamber pressure to which throttling was accomplished (10 to 20 psia) may be in error.

The rocket engine oxidizer and fuel flows were sensed by turbine-type flowmeters, indicated visually on frequency-to-dc converters, and recorded on an oscillograph in cycles per second.

SECTION III TEST PROCEDURE

This investigation consisted of four phases: (I) cold-flow centerbody-type ejector blockage study with air as the simulated rocket engine driving fluid, (II) centerbody-type ejector performance study with air, (III) diffuser-ejector performance evaluation of the steam-driven centerbody- and annular-type auxiliary ejectors with a simulated air-driven and steam-driven rocket engine, and (IV) diffuser-ejector performance evaluation of the steam-driven centerbody- and annular-type auxiliary ejectors with a model liquid-propellant rocket engine.

3.1 PHASE I

The procedure for the cold-flow centerbody-type ejector blockage study for all test configurations was the same. Rocket engine diffuser starting characteristics were checked at a low steady-state value of diffuser exit pressure $[(P_{ex})_{ltp} = 0.50 \text{ psia}]$ by increasing the rocket engine driving pressure from 0 to 100 psia for various positions of the centerbody nose cone with respect to the rocket engine nozzle exit plane. The range of centerbody positions covered was from 0 to 6 in. downstream of the rocket engine nozzle exit plane in increments of 1 in. or greater. At each centerbody position tested where the diffuser was started, the diffuser exit pressure was increased at a constant (100 psia) rocket engine driving pressure until breakdown. The limiting centerbody positions at which the diffuser would remain started were checked by varying the centerbody position with the rocket engine chamber pressure held at 100 psia and a low (0.50 psia) diffuser exit pressure maintained.

3.2 PHASE II

The ejector performance on test configurations 2a and b (Table II) was obtained at various values of secondary atmospheric inbleed airflow in the following manner: A set value of secondary inbleed flow was made by adjusting the inbleed valve (Fig. 5) while the ejector was operating. The ejector was operated at a constant driving pressure and the diffuser exit pressure, $(P_{ex})_{ltp}$, was varied to determine optimum performance for each value of secondary inbleed flow. The ejector was driven at pressures between 45 and 75 psia.

3.3 PHASE III

The procedure was the same for obtaining the diffuser performance during operation of the ejector, the simulated rocket engine, and with both the ejector and simulated rocket engine. The diffuser-ejector exit pressure was varied for diffuser breakdown and start at various ejector and simulated rocket engine driving pressures. When both ejector and simulated rocket engine were operating together (test configurations 2c through e and 3a and b) diffuser breakdown and start pressure ratios were obtained by varying exit pressure. In most cases the ejector driving pressure was maintained constant while the simulated rocket engine driving pressure was varied.

3.4 PHASE IV

For the model rocket engine phase (test configurations 3c and 4), the ejector driving pressure was set at a predetermined level (optimum), and then firings were made at various diffuser exit pressures with the rocket engine chamber pressure throttled to various values. The chamber pressure level was varied by the propellant tank pressures and the orifice sizes used, as shown in Fig. 2. The predetermined or optimum ejector driving pressure was selected such that the rocket engine diffuser exit pressure, P_{s2} , would be sufficiently low for the diffuser to be started at the throttled chamber pressure. The optimum diffuser-ejector exit static pressure, $(P_{ex})_{lip}$, was set at the maximum level which would permit the ejector to be started (minimum cell pressure obtained). The rocket engine firings were made after sufficient time had elapsed for conditions in the test cell to stabilize.

The conditions set during the rocket engine tests included an average O/F ratio of 1.90 and flows necessary to give a combustion chamber pressure of 100 or 50 psia. The average oxidizer flows for 100- and 50-psia chamber pressures were 0.210 and 0.115 lb_m/sec, respectively. The average specific heat ratio of the exhaust gas was assumed to be approximately 1.28.

Throttling was initiated after the rocket engine chamber pressure had stabilized (approximately 5 sec after ignition).

SECTION IV RESULTS AND DISCUSSION

This investigation was a four-phase program consisting of (I) cold-flow centerbody-type ejector blockage study with air as the simulated

rocket engine driving fluid, (II) centerbody-type ejector performance study with air, (III) diffuser-ejector performance evaluation of the steam-driven centerbody-type and annular-type auxiliary ejectors with a simulated air-driven and steam-driven rocket engine, and (IV) diffuser-ejector performance evaluation of the steam-driven centerbody-type and annular-type auxiliary ejectors with a model liquid-propellant rocket engine. The results are shown in Figs. 11 through 25 and Table III.

4.1 PHASE I

Since a centerbody-type ejector was under consideration, three questions had to be answered concerning its use as an auxiliary ejector in tandem with a throttlable rocket engine. The diffuser required had to be designed such that it (1) would start and operate at the highest exit pressure possible and (2) would require the least work for the ejector. This requirement demands the use of a second-throat-type diffuser as presented in Ref. 1. To keep the overall length of the diffuser-ejector system as short as possible, the second-throat contraction should be provided by the centerbody-type ejector. A contraction area ratio equal to normal shock contraction, $A_{st}/A_d = 1/(A_d/A^*)_r (P_{ty}/P_{tx})$, was selected. The normal shock contraction area ratio is a conservative value, and it will allow the driving pressure ratio to be equal to the pressure ratio across a normal shock as shown in Refs. 1 and 2. A centerbody-type ejector producing a reduction of this magnitude in area had not been used at RTF. This raised three questions concerning the use of the centerbody-type ejector: (1) Will it work? (2) Is the nose cone angle of the centerbody critical? (3) Does the spacing of the centerbody-type ejector in relation to the rocket engine nozzle exit affect the performance of the diffuser?

Phase I of the test program was conducted in an attempt to answer the three questions. The test configurations described in Table II and shown in Fig. 3 were used. The centerbody nose cone angle and shape as well as position were varied for the various contraction area ratios. Contraction area ratios as low as 0.510 and as high as 0.648 were investigated with two diffuser sizes.

The sizing of the hardware was initially based on the following equations:

$$\left(\frac{\gamma M_{ne}^2}{\sqrt{M_{ne}^2 - 1}} \right)_{\text{model}} = \left(\frac{\gamma M_{ne}^2}{\sqrt{M_{ne}^2 - 1}} \right)_{\text{full scale}}$$

$$(M_d)_{\text{model}} = (M_d)_{\text{full scale}}$$

$$(A_{st}/A_d)_{\text{normal shock}} = (A_{st}/A_d)_r$$

$$= \frac{1}{(A_d/A^*)_r (P_{ty}/P_{tx})}$$

The full-scale rocket engine and diffuser parameters, and the model parameters, calculated from the full-scale values by these three equations, are:

	γ_r	θ_{ne}, deg	$(A_{ne}/A^*)_r$	$(M_{ne})_r$	$(A_d/A^*)_r$	$(M_d)_r$	$(A_{st}/A_d)_r$
Full Scale	1.28	10.14	49	4.92	75.93	5.33	0.583
Model (Required)	1.40	10.14	16.28	4.92	32.39	5.33	0.643

An existing conical nozzle to simulate the rocket engine and an existing diffuser were used; only the dummy centerbody-type ejector had to be fabricated. The existing hardware did not exactly meet the required model parameters. The following table is a comparison of the actual and required model parameters:

	θ_{ne}, deg	$(A_{ne}/A^*)_r$	$(M_{ne})_r$	$(A_d/A^*)_r$	$(M_d)_r$	γ_r
Required	10.14	16.28	4.48	32.39	5.33	1.40
Actual	9.00	10.51	3.98	29.05	5.19	1.40

Results of testing the nine test configurations (Table II and Fig. 3) are summarized in Table III and Figs. 11 and 12. Figure 11a presents the relation of $(P_c/P_t)_r / (P/P_t)_{\text{is.en}}$ with centerbody-type ejector position for normal shock contraction. The ratio is a constant for the centerbody positions at which the diffuser is started even for the smaller contraction area ratios as shown in Table III. Presented in Fig. 11b for normal shock contraction is the variation of the ratio of the driving pressure ratio to normal shock total pressure ratio $(P_{ex}/P_{tr} / P_{ty}/P_{tx})$ with centerbody-type ejector position for different centerbody nose cone angles and shapes. This ratio is highest when the centerbody-type ejector is at the zero position except for test configuration 1g. No nonstart positions between 0 and 6 in. existed for test configuration 1a, which had a centerbody nose cone angle of 15 deg. For the same nose cone angle, the position at which the diffuser would start became more limited as the contraction area ratio decreased. This is shown in Table III. Figure 12 gives the variation of $P_{ex}/P_{tr} / P_{ty}/P_{tx}$ with contraction ratio. The smallest effective nose cone angle had the highest value of the ratio $(P_{ex}/P_{tr} / P_{ty}/P_{tx})$. This ratio increased as contraction ratio decreased, as expected from Ref. 1.

Test configuration 1a had only one nose cone reflected shock off the duct wall which missed the exit of the centerbody. All other test configurations had more than one nose cone reflected shock in the minimum area section.

Test configuration 1b was the same as 1a except that the diffuser size was smaller (3.47-in. -diam), resulting in a smaller contraction area ratio (0.527). Test configuration 1c was the same as 1a except that the centerbody diameter was increased from 2.39 to 2.82 in. to give approximately the same contraction area ratio (0.510) that existed for test configuration 1b. The performance of test configurations 1b and c was essentially the same, as shown in Table III.

The position of the centerbody-type contracted diffuser is limited especially with near-critical contraction area ratio. This limiting positioning is a characteristic phenomenon observed with second-throat-type diffusers and is reported in Refs. 3 and 4. Test configurations 1d, e, and f were the same except that the contraction area ratio was changed by changing the centerbody diameter from 2.82 to 2.61 to 2.40 in., respectively. As shown in Table III for these three configurations, the smaller the contraction area ratio, the more limited was the centerbody position for diffuser starting. Test configurations 1a, g, h, and i had essentially the same contraction area ratio (0.643) but were different only in centerbody nose cone angle. The greater the centerbody nose cone angle became, the more limited was the centerbody position for diffuser starting.

4.2 PHASE II

A $\gamma = 1.40$ normal shock contraction area ratio diffuser produced by a centerbody-type ejector (test configuration 1a) proved to perform satisfactorily in Phase I for a 15-deg centerbody-type ejector nose cone. An existing 15-deg nose cone centerbody-type ejector as shown in Fig. 4 was used to build up test configurations 2a and b (Fig. 5). The inlet duct was sized from the centerbody diameter to give near-normal shock contraction area ratio (0.643 for $\gamma = 1.40$). The actual contraction area ratio obtained was 0.633. The centerbody-type ejector diffuser duct was sized from an area ratio $(A_d/A^*)_e = 40.95$ for $A^*_e = 0.1963$ in.² based on the equation

$$(A_d/A^*)_{e, \text{ model}} = (A_d/A^*)_{e, \text{ full scale}} = 40.95$$

The actual $(A_d/A^*)_e$ obtained was 44.43. Two diffuser-ejector lengths were used to make test configurations 2a $[(L/D)_e = 2.6]$ and 2b $[(L/D)_e = 8.0]$ (see Fig. 5 and Table II).

This phase of the investigation was to determine the performance for the steam-driven centerbody-type ejector with two diffuser lengths with various amounts of air as secondary mass flow. Presented in Fig. 13a is the effect of diffuser $(L/D)_e$ on the limiting driving pressure ratios, $(P_{ex})_{lip}/P_{te}$, for various secondary-to-primary mass flow ratios, m_s/m_p . For an $(L/D)_e = 8$, the limiting $(P_{ex})_{lip}/P_{te}$ is practically a constant for the various values of m_s/m_p . The limiting $(P_{ex})_{lip}/P_{te}$ decreases directly proportional with an increase in m_s/m_p for the $(L/D)_e = 2.6$ configuration.

The variations of P_c/P_{te} and $(P_{ex})_{lip}/P_c$ with m_s/m_p for test configurations 2a and b are shown in Figs. 13b and c. The $(L/D)_e$ change from 2.6 to 8 had no effect on the ratio of test cell-to-ejector driving pressure, but did affect the rise ratio, $(P_{ex})_{lip}/P_c$. The increase in P_c/P_{te} with m_s/m_p is linear above an m_s/m_p of 0.07.

The equivalent mass ratio of $m_s/m_p = 0.0982$ which was required by the model (test configuration 2a) to simulate the mass ratio ($m_s/m_p = 0.028$) for full scale was obtained from the equation

$$(m_s/m_p)_{model} = \frac{K_{model}}{K_{full\ scale}} (m_s/m_p)_{full\ scale}$$

where

$$K = \left[(R'/R'') (\gamma''/\gamma') (T_1'/T_1'') \right]^{1/2}$$

The difference in static conditions of the secondary fluid (air for model and exhaust products for full scale) required a difference in mass ratio for similarity in performance to exist between the model and full-scale centerbody ejector.

The P_c/P_{te} versus $(P_{ex})_{lip}/P_{te}$ performance for the $(L/D)_e = 2.6$ and 8.0 test configurations 2a and b with no secondary mass flow is shown in Fig. 14 along with the isentropic pressure ratio and the normal shock downstream static-to-upstream total pressure ratio. The actual P_c/P_{te} obtained divided by the isentropic ratio was

$$\left[(P_c/P_{te})_{act} \right] / \left[(P/P_t)_{isen} \right] = 1.52$$

The limiting driving pressure ratio, $(P_{ex})_{lip}/P_{te}$, divided by the static-to-total normal shock pressure ratio was $\left[(P_{ex})_{lip}/P_{te} \right] / (P_y/P_{tx}) = 0.887$. There was no difference in P_c/P_{te} or $(P_{ex})_{lip}/P_{te}$ performance at start or breakdown for $(L/D)_e = 2.6$ and 8.0 when the ejector was pumping no secondary flow. This is also shown in Figs. 13a and b. A difference in $(P_{ex})_{lip}/P_{te}$ at start and breakdown for the $(L/D)_e = 2.6$ was expected.

4.3 PHASE III

The diffuser-ejector performance evaluation of the steam-driven ejector for an air-driven and steam-driven simulated rocket engine was obtained for centerbody- and annular-type auxiliary ejector configurations. Both types were investigated with and without an ejector second throat.

4.3.1 Centerbody-Type Ejector Test Configurations 2c through e

A simulated rocket engine nozzle without the atmospheric inbleed system was used in test configuration 2a to give test configuration 2c. Two second-throat inserts were added to configuration 2c to make configurations 2d and e (Fig. 6). The resulting test configurations 2d and e had ejector contraction area ratios of 0.535 and 0.637, respectively, and $(A_{st})_e / (A_{st})_r$ ratios of 1.12 and 1.34, respectively.

The simulated rocket engine nozzle (an existing nozzle) was selected based on the equations:

$$\left(\frac{\gamma (M_{ne})_r^2}{\sqrt{(M_{ne})_r^2 - 1}} \right)_{\text{model}} = \left(\frac{\gamma (M_{ne})_r^2}{\sqrt{(M_{ne})_r^2 - 1}} \right)_{\text{full scale}}$$

$$(\theta_{ne})_{r, \text{model}} = (\theta_{ne})_{r, \text{full scale}}$$

and

$$(M_{dr})_{\text{model}} = (M_{dr})_{\text{full scale}}$$

The existing nozzle (Fig. 1b) did not exactly meet the required model parameters as calculated from the above equations. The following table is a comparison of the actual and required model rocket engine parameters.

	$(\theta_{ne})_{r, \text{deg}}$	$(A_{ne}/A^*)_r$	$(M_{ne})_r$	$(A_d/A^*)_r$	$(M_d)_r$	γ_r
Required	10.14	16.28	4.92	32.39	5.33	1.40
Actual	13.25	11.77	4.11	32.11	5.32	1.40

The individual performance of the centerbody-type ejector is presented in Fig. 14 for test configurations 2c, d, and e for no secondary mass flow with the isentropic pressure ratio and the downstream static-to-upstream total normal shock pressure ratio. The second throats in the ejector extended the limiting driving pressure ratio from 0.887 to 1.03 times the normal shock ratio (P_y/P_{tx}). The difference shown in Fig. 14 for P_c/P_{te} with and without the ejector second throat occurred because the transition section of the second-throat insert was too close to the ejector nozzle exit.

The simulated rocket engine diffuser for test configuration 2d would not start with the ejector operating above approximately 10 psia. This configuration had a contraction area ratio of $(A_{st}/A_d)_e = 0.535$ and a ratio of $(A_{st})_e / (A_{st})_r = 1.12$. Results similar to this were experienced in the test reported in Ref. 2. When the contraction area ratio was increased from 0.535 to 0.637 (test configuration 2e), giving the ratio of $(A_{st})_e / (A_{st})_r = 1.34$, the simulated rocket engine diffuser would start and operate with an ejector driving pressure of 50 psia as long as the simulated rocket engine chamber pressure was above 20 psia. The rocket engine diffuser would remain started with a chamber pressure of approximately 10 psia when the ejector driving pressure was reduced to approximately 22 psia. This result indicates that the ejector second-throat area cannot be as small as the rocket engine diffuser second-throat area while the rocket engine second-throat contraction area ratio is no larger than the normal shock contraction area ratio.

The limiting simulated rocket engine diffuser exit pressure, P_{s2} , was determined for various values of air-driven rocket engine chamber pressure, P_{tr} , and different steam-driven ejector driving pressures, P_{te} . This relationship is presented in Fig. 15a. The data are shown in relation to the normal shock static pressure, $(P_y)_r$. The limiting P_{s2} data are approximately equal to the normal shock value, $(P_y)_r$, for simulated rocket engine chamber pressures up to 40 psia. For chamber pressure above 40 psia, the limiting P_{s2} was approximately 0.90 times the normal shock value. The data shown in Fig. 15a are for test configurations 2c (no ejector-second throat) and 2e, $(A_{st}/A_d)_e = 0.637$. At $P_{te} = 50$ psia, P_{s2} was unstable below a chamber pressure of 20 psia because the ejector nozzle lip static pressure was higher than the required P_{s2} to keep the diffuser started. The auxiliary ejector requires a condition of static pressure equilibrium in the secondary and primary streams according to Ref. 5. To obtain static pressure equilibrium requires the limiting P_{s2} to equal the ejector nozzle lip static pressure. This explains why the unstable condition shown in Fig. 15a is eliminated when the ejector driving pressure is reduced from 50 psia. The reduction in ejector driving pressure reduces the ejector nozzle lip static pressure proportionally. The limiting P_{s2} (P_{s2} at breakdown) was determined with only the simulated rocket engine operating and with both the ejector and simulated rocket engine operating as shown in Fig. 15a.

Presented in Fig. 15b is the limiting diffuser-ejector exit static pressure variation with air-driven simulated rocket engine chamber pressure and various values of ejector driving pressure. When only the simulated rocket engine was operating with test configuration 2c, the limiting diffuser-ejector exit static pressure was approximately 9 percent higher than the corresponding normal shock value as shown in Fig. 15b. The performance of test configuration 2c, which was tested with both simulated rocket engine and ejector operating, is also shown in Fig. 15b. An improvement in limiting diffuser-ejector exit static pressure over that obtained by not

having the ejector operating was experienced with the ejector operating. References 2 and 6 show similar results. The higher ejector driving pressure gives the higher limiting $(P_{ex})_{lip}$ but also limits the minimum simulated rocket engine chamber pressure to a higher value. From Fig. 13a, the limiting $(P_{ex})_{lip}/P_{te}$ decreased as the secondary-to-primary mass ratio increased for m_s/m_p up to approximately 0.15. At a P_{tr} of 5 psia in Fig. 15b, m_s/m_p is equal to 0.162, which would correspond to limiting $(P_{ex})_{lip} = 0.93$ psia from Fig. 13a for $P_{te} = 50$ psia. This limiting $(P_{ex})_{lip} = 0.93$ psia is in good agreement with that shown in Fig. 15b for $P_{tr} = 5$ psia.

Test configuration 2e, which consisted of an ejector second-throat insert having $(A_{st}/A_d)_e = 0.637$ or $(A_{st})_e/(A_{st})_r = 1.34$, was tested at almost the same conditions as test configuration 2c. The performance is shown in Fig. 15b to be no different from that obtained for test configuration 2c. The limiting $(P_{ex})_{lip}$ was expected to be higher for the second-throat configuration 2e than it was for the no-second-throat configuration 2c; however, this did not occur. It is believed that the cooling of the two-phase steam (ejector driving fluid) by the cold secondary air (simulated rocket engine driving fluid) caused a large decrease in specific volume of the mixture. No appreciable difference was noted in diffuser-ejector start and breakdown especially at low P_{tr} values (less than 30 psia).

Presented in Fig. 15c is the relationship of simulated rocket engine nozzle lip static pressure, $(P_{ne})_r$, and test cell pressure, $(P_c)_r$, with simulated rocket engine chamber pressure. The ejector was driven at 50 psia, and the diffuser-ejector exit static pressure was held equal to or below its limiting value as shown in Fig. 15b. Also shown in Fig. 15c is the corresponding isentropic relationship. The actual simulated rocket engine nozzle lip static pressure is approximately 1.19 times the isentropic value. The cell pressure curve crosses the corresponding isentropic line because of a Reynolds number influence as presented in Refs. 7 and 8. The limiting minimum simulated rocket engine chamber pressure for a $P_{te} = 50$ psia was approximately 20 psia.

A check was made on test configuration 2e by substituting steam in place of air for the simulated rocket engine driving fluid to eliminate the temperature difference. This performance is shown in Fig. 16. Presented in Fig. 16a is the variation of the limiting diffuser exit static pressure, P_{s2} , with various values of simulated rocket engine chamber pressure for two ejector driving pressures. The data are higher than the normal shock value as shown in Fig. 16a because of a possible error in the data. It was very difficult to obtain these data because the P_{s2} pressure line continually filled with water, giving a higher than actual pressure.

An increase of approximately 1 psia in the limiting diffuser-ejector exit static pressure was obtained for the steam-driven rocket engine over

that obtained for the air-driven rocket engine with $P_{te} = 50$ psia (Fig. 16b). The performance was obtained on only the second-throat test configuration 2e with a steam-driven rocket engine.

This phase of the investigation indicates that static pressure equilibrium in the secondary and primary stream must exist for stable operation. The limiting minimum rocket engine chamber pressure depends on the ejector nozzle area ratio and driving pressure as well as the rocket engine diffuser area ratio and contraction ratio.

By knowing the relationship of the diffuser exit pressure, P_{s2} , to the normal shock static pressure and the relationship of the ejector nozzle lip exit static pressure to its isentropic value, the minimum rocket engine chamber pressure for a given ejector driving pressure can be determined from the static pressure equilibrium principle

$$[(P_{ne})_e = P_{s2}]$$

Figure 17 presents these relationships for test configurations 2c and e. The lip exit static pressure for the 13-deg half-angle simulated rocket engine (nozzle configuration B) was 1.19 times the isentropic value (shown in Fig. 15c); therefore, it is reasonable to assume that the centerbody-type ejector, which has a nozzle half-angle of 10 deg, would have a lip exit static pressure of approximately 1.15 times the isentropic value as indicated in Fig. 17 for $\gamma = 1.30$. The P_{s2} value was almost equal to the normal shock static pressure in the range of $P_{tr} = 0$ to 40 psia as shown in Fig. 15a for $\gamma_r = 1.40$; therefore, the normal shock static pressure is shown equal to P_{s2} in Fig. 17. For an ejector driving pressure of 50 psia, the minimum simulated rocket engine chamber pressure is shown in Fig. 17 to be 19 psia to satisfy the static pressure equilibrium principle. This is in agreement with the data shown in Fig. 15a where the rocket engine diffuser exit pressure becomes unstable. This is true even if the diffuser-ejector exit static pressure, $(P_{ex})_{lip}$, is below the limiting value shown in Fig. 15b for the air-driven rocket engine and Fig. 16b for the steam-driven rocket engine.

4.3.2 Annular-Type Ejector J-3 Model Test Configurations 3a through c

The diffuser and auxiliary annular-type ejector were designed for the existing model rocket engine, shown in Fig. 1d, to simulate the J-3 test engine. The test requirements included throttling to 10 percent of full power without losing altitude simulation with a diffuser-ejector exit pressure from 1.5 to 2.0 psia at full engine power. Since the model engine used the same propellant as the full-scale engine, the scaling was direct.

The ejector nozzle was designed for static pressure equilibrium according to Ref. 5. A steam-driven simulated rocket engine nozzle was selected based on the equations

$$\left(\frac{\gamma M_{ne}^2}{\sqrt{M_{ne}^2 - 1}} \right)_{\text{steam rocket}} = \left(\frac{\gamma M_{ne}^2}{\sqrt{M_{ne}^2 - 1}} \right)_{\text{live rocket}}$$

$$(\theta_{ne})_{\text{steam rocket}} = (\theta_{ne})_{\text{live rocket}}$$

and

$$(M_d)_{\text{steam rocket}} = (M_d)_{\text{live rocket}}$$

The existing nozzle selected (configuration C, Fig. 1c) did not fully satisfy the equations. A comparison of the required with the actual is:

	$(\theta_{ne})_r, \text{deg}$	$(A_{ne}/A^*)_r$	$(M_{ne})_r$	$(A_d/A^*)_r$	$(M_d)_r$	γ_r
Required	9.75	32.54	4.65	63.80	5.33	1.30
Actual	18	18.57	4.14	61.89	5.30	1.30

The test configurations 3a and b are shown in Fig. 8. The individual ejector performance is shown in Fig. 18. The actual P_c/P_{te} and $(P_{ex})_{lip}/P_{te}$ divided by isentropic and normal shock values from Ref. 9 are

Ejector Configuration	$P_c/P_{te} / (P/P_t)_{isen}$	$\frac{(P_{ex})_{lip}/P_{te}}{P_y/P_{tx}}$
11	1.74	0.62
11 a	1.74	0.94

The $P_c/P_{te} / (P/P_t)_{isen}$ for the centerbody-type ejector configuration was 1.52 as given in Phase II. Steam-driven axisymmetrical 18-deg nozzles (Ref. 10) pumped the following values:

A_{ne}/A^*	A_d/A^*	$\frac{P_c/P_{te}}{(P/P_t)_{isen}}$
18	38.60	1.35
10.8	39.82	1.76

The annular-type ejector performance is in good agreement with this performance. The breakdown performance is in good agreement with that reported in Ref. 3.

The diffuser second-throat limiting exit static pressure, P_{s1} , and the limiting pressure to which the flow from the rocket engine diffuser

discharged, P_{s2a} , are presented in Fig. 19a for test configurations 3a and b. With only the rocket engine operating, the limiting P_{s2} and P_{s2a} with and without the ejector second throat (test configurations 3a and b) are approximately equal to the downstream normal shock static pressure. The limiting value of P_{s2} when the ejector was driven at $P_{te} = 50$ psia for test configuration 3a was lower than the normal shock value. For test configuration 3b, the limiting value of P_{s2} was still lower and unstable above $P_{tr} = 30$ psia. It is believed that the P_{s2} pressure tap was located in a separated flow region when the ejector was operating, thus giving a lower value. The separated flow region is influenced by the addition of the ejector second-throat insert for test configuration 3b, further lowering P_{s2} as shown in Fig. 19a. The minimum value of the limiting P_{s2} obtained with the ejector driven at $P_{te} = 50$ psia was 0.14 psia and was constant for rocket chamber pressures below $P_{tr} = 10$ psia. This value of P_{s2} was lower than the ejector nozzle lip static pressure, which indicates that the ejector flow was expanding beyond the nozzle exit and reaching static pressure equilibrium at an area smaller than the rocket engine diffuser second-throat area. The smaller area could cause a separated region near the end of the second throat. The unstable conditions experienced with the centerbody-type ejector test configurations 2c and e (Fig. 15a) were not evident with test configurations 3a and b when the rocket engine chamber pressure was reduced to zero.

A comparison of the diffuser-ejector limiting exit static pressure, $(P_{ex})_{lip}$, for test configurations 3a and b is presented in Fig. 19b. The limiting $(P_{ex})_{lip}$ when only the rocket engine was operating is approximately 1.26 times the normal shock value. The limiting $(P_{ex})_{lip}$ was approximately doubled when the ejector was operating at $P_{te} = 50$ psia for test configuration 3a. An additional increase of approximately 50 percent in the limiting $(P_{ex})_{lip}$ was obtained by adding the ejector second-throat insert for test configuration 3b. The insert gave the ratio of $(A_{st})_e / (A_{st})_r = 1.77$. The limiting $(P_{ex})_{lip}$ is practically a constant for rocket chamber pressures from 0 to 15 psia. For test configuration 3b, this constant value is the same as that obtained when only the ejector is operating. This characteristic was not the case with the centerbody-type configuration as shown in Figs. 15b and 16b.

The relationship of the test cell pressure and rocket engine nozzle lip static pressure for stepwise steady-state chamber pressure decrease to zero is presented in Fig. 19c. The relationship is typical for an ejector driving pressure of $P_{te} = 50$ psia and $(P_{ex})_{lip}$ equal to or less than the limiting value shown in Fig. 19b. Similar relation is shown in Ref. 2. Note in Fig. 19c that, when P_c becomes equal to $(P_{ne})_r$, a further decrease in chamber pressure causes nozzle flow separation to occur and then cell pressure starts to increase. The $(P_{ne})_r$ data are 1.125 times the isentropic value.

The Reynolds number effect discussed in Refs. 7 and 8 influences the test cell pressure for the low chamber pressures. The effect is increased by the jet boundary impingement region on the diffuser if the second throat is not properly located as discussed in Ref. 3. At a chamber pressure of 26.04 psia, the jet boundary calculated by the method given in Ref. 11 impinges on the second-throat transition near the intersection with the diffuser as shown in Fig. 19d. The jet boundary for a chamber pressure of $P_{1r} = 79.68$ psia impinges on the diffuser upstream of the beginning of the second-throat transition.

The equivalent mass ratio of $m_s/m_p = 0.059$ for test configurations 3a and b was required to simulate the full-scale value of 0.028 for a full-scale rocket engine chamber pressure of 11 psia and ejector mass flow rate of 125 lb_m/sec. This mass flow ratio of $m_s/m_p = 0.059$ was obtained when the annular ejector was driven at 50 psia and the simulated rocket engine chamber pressure was 7.45 psia.

The results of this phase of the investigation indicate that the model rocket engine (Fig. 1d) can be throttled to 10-percent power with the auxiliary annular-type ejector (Fig. 7) in the J-3 model test configuration 3b (Fig. 8). From Figs. 19b and c, the diffuser-ejector exit static pressure can be as high as 1.64 psia for an ejector driving pressure of 50 psia.

The diffuser-ejector exit static pressure was checked by a force balance calculation for test configurations 3a and b (see Appendix I). The predicted limiting $(P_{ex})_{ltp}$ pressure from the force balance analysis was in good agreement with the measured value for test configuration 3a, but the predicted value was low for test configuration 3b.

4.4 PHASE IV

This phase concluded the investigation with the model rocket engine used both with the auxiliary annular-type ejector from Phase III and an auxiliary centerbody-type ejector having equal geometric parameters to the annular-type ejector. The performance evaluation included pressure distribution in the J-3 model ducting from the diffuser-ejector exit to the simulated J-1 exhaust header into which the J-3 model discharged.

4.4.1 Annular-Type Ejector Test Configuration 3c

The test configuration (3c, Fig. 8) was the same as 3b except for the rocket engine. The rocket engine configuration D (Table I and Fig. 1d) was used.

Engine throttling simulation was accomplished by an orificed bypass line and valving arrangement as shown in Fig. 2. The orifices were sized for the propellant flow rates from a constant pressure supply to give the desired chamber pressure when the main flow was cut off. The performance was obtained with two sets of orifices, which allowed throttling from 95 to 20 psia and from 48 to 12 psia.

The end points of the transient throttling demonstration for test configuration 3c are presented in Fig. 20a. The isentropic values of test cell and rocket engine nozzle lip static pressures are shown for comparison with the actual data. The rocket engine had a contoured nozzle with an area ratio of 40 as shown in Fig. 1d. The engine nozzle lip static pressure was 2.07 times the isentropic value corresponding to the area ratio of 40 as shown in Fig. 20a. The cell pressure was 0.52 times the corresponding isentropic value when the nozzle was properly located with respect to the beginning of the diffuser second throat. For the case shown in Fig. 20a with the nozzle 1.194 in. farther downstream, the cell pressure was approximately two times the isentropic value. The jet boundary impingement on the diffuser for the two positions is shown in Fig. 20c.

Shown in Fig. 20a are the data that represent the maximum ejector driving pressure for the cell pressure to be a minimum and the diffuser-ejector exit static pressure to be at or near the limiting value. The limits were established by maintaining low $(P_{ex})_{lip}$ for different throttling runs at various ejector driving pressures. The maximum P_{ie} was defined as the value above which the minimum possible cell pressure corresponding to the throttled chamber pressure could not be maintained. For this maximum P_{ie} , various throttling runs were made at different diffuser-ejector exit static pressures. The limiting $(P_{ex})_{lip}$ was determined when a higher value would cause test cell pressure to increase at the throttled chamber pressure. These performance data are in good agreement with the cold-flow data for test configuration 3b in Phase III (Figs. 19a and b) except that the ejector driving pressure had to be approximately 15 percent lower.

Presented in Figs. 21, 22, and 23 are the J-3 model duct pressure distributed from the diffuser-ejector exit static pressure to the exhaust header. The magnitude of the pressures is shown in Fig. 21 for pre-fire (ejector operating alone), firing at $P_{tr} \approx 48$ psia, and at throttled $P_{tr} \approx 12$ psia. The ejector driving pressure was approximately 45 psia. The survey was made for three exhaust header pressures from $(P_t)_{ex} = 0.55$ to 2.0 psia as shown in Figs. 21a through c. At the low exhaust pressure level, there is a rather large difference between pre-fire and $P_{tr} = 48$ psia. The difference decreases as the exhaust pressure increases. Figure 21e shows the condition for maximum P_{ie} and $(P_{ex})_{lip}$ for minimum P_c when $P_{tr} = 13.04$ psia after throttling from $P_{tr} = 48.93$ psia.

Figure 22 is a similar set of curves but for a rocket driving pressure of $P_{tr} \approx 93$ psia and throttling to $P_{tr} \approx 20$ psia. The ejector driving pressure was maintained at approximately 42 psia. Note that a greater difference exists between pre-fire and maximum P_{tr} for these conditions than for those presented in Fig. 21. The duct appears to be choked for the conditions shown in Figs. 22a and b for maximum P_{tr} since the increase in $(P_t)_{ex}$ did not alter the pressures upstream.

Presented in Fig. 23 is a set of curves for the same throttling conditions as those in Fig. 22 except the ejector driving pressure was increased to $P_{te} = 58.44$ psia. Figure 23b is for the condition shown in Fig. 20a.

A typical rocket engine chamber pressure transient for the two throttling conditions is shown in Fig. 24.

4.4.2 Centerbody-Type Ejector Test Configuration 4

Test configuration 4 was the same as 3c except that the annular-type ejector was replaced by the centerbody-type configuration. Test configuration 4 is shown in Fig. 10. All geometric parameters for the centerbody-type ejector associated with performance were equal to the corresponding parameters for the annular-type ejector.

The performance investigation was similar to that for the annular-type ejector test configuration. Throttling was attempted for $P_{tr} = 95$ to 10 psia, 95 to 20 psia, and 48 to 12 psia (Fig. 20b). The diffuser would start and pump the minimum cell pressure at the $P_{tr} = 95$ -psia condition for an ejector driving pressure as high as 50.25 psia. When throttling was accomplished, the test cell pressure increased even when the diffuser-ejector exit static pressure was as low as 0.91 psia. The ejector driving pressure was as low as 40.23 psia, which is lower than the values for test configuration 4. The diffuser would not start at $P_{tr} = 48.11$ psia, $P_{te} = 44.27$ psia, and $(P_{ex})_{lip} = 0.78$ psia for the centerbody-type configuration, but it would start at $P_{tr} = 48.93$ psia, $P_{te} = 46.58$ psia, and $(P_{ex})_{lip} = 1.46$ psia for the annular-type configuration. When the rocket engine nozzle exit plane was moved 1.194 in. farther upstream, no improvement in performance was experienced.

The individual centerbody-type ejector performance is presented in Fig. 18. The P_c/P_{te} was 0.97 times the isentropic value. This is much better than the no-secondary-flow performance obtained with the annular-type ejector configuration. The $(P_{ex})_{lip}/P_{te}$ was 1.07 times the normal shock value, P_y/P_{tx} . This is also an improvement over the value obtained for the annular-type ejector.

The main difference between this centerbody-type ejector (Fig. 9) and the one used in Phase III with test configuration 2e (Fig. 4) was that the nozzle area ratio and the nose cone half-angle (20 deg instead of 15 deg) was larger. The larger nozzle area ratio was used to give a lower nozzle exit static pressure for the same driving pressure. From the static pressure equilibrium principle, the lower $(P_{ne})_e$ would allow the diffuser exit static pressure, P_{s2} , to be lower, therefore allowing chamber pressure after throttling to be lower. A 20-deg instead of a 15-deg nose cone was used to conserve the length of the centerbody since the full-scale diffuser-ejector length was limited. The location of the ejector 20-deg half-angle nose cone with respect to the rocket engine nozzle exit plane was such that $(L/D)_e = 0.41$. According to the results of Phase I (Fig. 11a), no diffuser starting problem should exist for a spacing such that $(L/D)_e = 0.56$ for a 22-deg half-angle nose cone.

A comparison of the performance with test configurations 3c and 4 indicates that the annular-type ejector in test configuration 3c was best. Rocket engine throttling to 10 percent of full power capability was demonstrated with the annular-type ejector.

For the annular-type ejector with a second throat, the performance can be predicted using both a steam-driven rocket engine and the model rocket engine by a nomograph, as shown in Fig. 25. The diffuser second-throat exit static pressure is equal to from 0.90 to 1.0 times the downstream normal shock static pressure for a second-throat contraction area ratio equal to normal shock contraction based on $(A_d/A^*)_e$. This is shown in Figs. 15a, 16a, and 19a. To have optimum ejector performance, satisfying primary and secondary flow static pressure equilibrium requires the ejector nozzle lip exit static pressure to equal the diffuser second-throat exit static pressure $[(P_{ne})_e = P_{s2}]$. This can be determined by knowing the geometry of the ejector nozzle, especially the area ratio $(A_{ne}/A^*)_e$, and the relationship of the actual to the isentropic value of the lip static pressure. The actual P_{ne} for a conical nozzle will be approximately 10 to 15 percent higher than the isentropic value based on nozzle area ratio (Figs. 15c and 19c). The performance for test configurations 3a, b, and c indicates that, for a range of rocket engine chamber pressure from 0 to 15 psia, the diffuser-ejector limiting exit static pressure is a constant and approximately equal to the limiting value when only the ejector is operating as shown in Fig. 19b. The value of the diffuser-ejector limiting exit static pressure is determined by the ejector area ratio, length-to-diameter ratio, and the contraction area ratio. The effect of contraction ratio is shown in Figs. 14 and 18, and the $(L/D)_e$ effect is shown in Fig. 13a. This limiting exit static pressure for test configurations 3a and b is found by:

Test Configuration	$(A_{gt}/A_d)_e$	$\frac{(P_{ex})_{lip} / P_{te}}{(P_y/P_{tx})_e}$
3 a	1.00	0.62
3 b	0.62	0.94

This information, properly arranged, gives the nomograph shown in Fig. 25. Enter the nomograph at the desired throttled rocket engine chamber pressure and proceed to the proper diffuser second-throat exit pressure; thence vertically along the constant pressure line to the line representing the proper ejector nozzle lip exit static pressure; thence, move along a horizontal line crossing the $P_{te} = P_{tr}$ scale to $(P_y)_e$ scale and intersecting the diffuser-ejector exit static pressure line which determines $(P_{ex})_{lip}$. The data from test configurations 3a, b, and c presented in Figs. 19b and 20a are in good agreement with this nomograph.

A force balance analysis was made for test configuration 3c to determine the diffuser-ejector exit static pressure. The method is presented in Appendix I. The predicted value was higher than the measured value. This difference could be caused by data inaccuracies, the method of calculation of the ejector ramp pressure, the correction factor applied to the theoretical exit static pressure to get the predicted value, and the omission of wall friction forces.

SECTION V SUMMARY OF RESULTS

The investigation consisted of four phases: (I) cold-flow centerbody-type ejector blockage study, (II) centerbody-type ejector performance study, (III) diffuser-ejector performance evaluation of the centerbody- and annular-type ejectors with a simulated rocket engine, and (IV) diffuser-ejector performance evaluation of the centerbody- and annular-type ejectors with a model liquid-propellant rocket engine. The results of the investigation are summarized as follows:

1. A centerbody-type ejector sufficiently large to give a normal shock contraction area ratio diffuser configuration based on the ratio of rocket engine diffuser-to-nozzle throat areas can be used without affecting cell pressure with certain limitations. The nose cone half-angle must be sufficiently small and the spacing of the centerbody-type ejector must be as near as possible to the rocket engine nozzle exit plane. The small nose cone angle allows

- the spacing of the centerbody-type ejector with respect to the rocket engine nozzle exit plane to be less critical. A smaller diffuser contraction area ratio allows an increase in limiting driving pressure ratio but makes the spacing of the ejector nose cone more critical.
2. A short diffuser $[(L/D)_e = 2.6]$ for a centerbody-type ejector allows the limiting driving pressure ratio to decrease for an increase up to 0.15 in secondary-to-primary mass flow ratio. The limiting driving pressure ratio increases only slightly (practically a constant) for a long diffuser $[(L/D)_e = 8.00]$ for an increase of 0.15 in secondary-to-primary mass flow ratio. The rise ratio is lower for the short $(L/D)_e$ mixing duct at the same secondary-to-primary mass flow ratio than for the long $(L/D)_e$ one.
3. A second-throat having a normal shock contraction area based on $(A_d/A^*)_e$ inserted in the diffuser-ejector permits the limiting driving pressure ratio to be increased to approximately the normal shock value, P_y/P_{tx} . No effect was noted on the cell-to-driving pressure ratio during operation without secondary mass flow.
4. The rocket engine second-throat limiting diffuser exit static pressure is approximately equal to the downstream normal shock static pressure based on the $(A_d/A^*)_e$ at start and breakdown for either a centerbody-type or an annular-type diffuser-ejector.
5. During rocket engine operation, the limiting annular- or centerbody-type ejector exit static pressure was increased proportionally to driving pressure when the ejector was operating. The ejector second throat $[(A_{st})_e / (A_{st})_r = 1.34]$ for a rocket engine diffuser having a normal shock contraction will allow an additional increase in diffuser-ejector limiting exit static pressure. The exception to this was when the rocket engine was operated on air instead of steam or propellant. Operating with air did not cause an increase in the limiting exit static pressure because of the air cooling the ejector driving fluid (steam).
6. The limiting exit static pressure remained essentially constant at the limiting value obtained with only the annular-type ejector operating up to a rocket engine chamber pressure of 15 psia with or without the ejector second throat.

7. The optimum performance of the annular- or centerbody-type ejector was obtained when the ejector nozzle lip static pressure was equal to the diffuser second-throat exit static pressure for the throttled rocket engine chamber pressure.
8. If the diffuser second throat is too close to the rocket engine nozzle, such that the jet boundary impinges on the second-throat transition near the intersection with the cylindrical diffuser impingement duct, a much higher cell pressure will result.
9. A successful throttling demonstration from full power to approximately 10 percent power was made with the rocket engine and the auxiliary annular-type ejector configuration. This could not be demonstrated when the annular-type ejector was replaced by a centerbody-type ejector having equal geometric parameters.
10. The pressure distribution in the J-3 model exhaust ducting during rocket engine and ejector operation varied from approximately 1.40 psia at the diffuser-ejector exit to a peak of approximately 2.4 psia at the 55-deg miter turn and back to 2.0 psia in the exhaust header.

APPENDIX I FORCE BALANCE ANALYSIS FOR TEST CONFIGURATIONS 3a, b, and c

The general theory based on momentum analysis given in Refs. 5, 12, 13, and 14 can be used in a force balance for the annular-type ejector in test configurations 3a, b, and c to predict the diffuser-ejector limiting exit static pressure. The limiting pressure can be predicted within a few percent for the steam-driven rocket engine and steam-driven annular-type ejector with and without the ejector second throat and for the N_2O_4 and AZ-50 liquid-propellant rocket engine and steam-driven annular-type ejector with the second throat. The conditions at which the calculations were made are (1) minimum chamber pressure to which throttling was accomplished and (2) limiting diffuser-ejector exit static pressure.

The methods and equations used in the force balance analysis are as follows:

$$F'' = P''(A_{st})_r (1 + \gamma_r M''^2) \quad (I-1)$$

where

$$P'' = P_{s2}$$

as shown in Fig. I-1. A conservative value of P_{s2} for a rocket engine diffuser having a normal shock second-throat contraction area ratio is (Refs. 1 and 2 and Fig. 19a) approximately equal to the downstream normal shock static pressure. The value used was

$$P_{s2} \approx 0.90 P_y$$

Then from Ref. 9 and the chamber pressure to which throttling was made,

$$P_y = \left[f(A_d/A^*, \gamma)_r \right] P_{tr}$$

The Mach number, M'' , was calculated from the continuity equation of the form given in Ref. 13

$$M'' = \frac{m_r}{P_{s2} (A_{st})_r} \sqrt{\frac{R_r T_r}{\gamma_r g_c}}$$

where

$$m_r = \frac{(P/P_t \dot{m})_{M=1} P_{tr} A_r^*}{\sqrt{T_{tr}}}$$

By applying the ejector secondary and primary static pressure equilibrium principle from Refs. 5 and 13, then

$$P'' = P'$$

From P' and the annular-type ejector driving pressure, P_{te} , the ratio P'/P_{te} is calculated.

From Ref. 9 and the annular-type ejector nozzle throat area, A_e^* , the following are obtained:

$$A' = [f(P'/P_t, \gamma)]_e A_e^*$$

$$M' = f(P'/P_t, \gamma)_e$$

which is sufficient for calculating F' .

$$F' = P' A' [1 + \gamma_e (M')^2] \quad (I-2)$$

The force balance, neglecting wall friction, for test configuration 3a is shown in Fig. I-1, which contains the annular-type ejector without a second throat is

$$F_{ex} = F' + F'' \quad (I-3)$$

Test configurations 3b and c shown in Fig. I-2 which contain the annular-type ejector having the second throat require an additional force to balance Eq. (I-3). This force balance equation is

$$F_{ex} = F' + F'' - F_{ramp} \quad (I-4)$$

which is smaller than that in Eq. (I-3) by the amount of the ejector second-throat ramp force, F_{ramp} . The ramp force is obtained from the average ramp pressure multiplied by the projected area of the ramp, which is

$$F_{ramp} = P_{ramp} (A_d - A_{sl})_e \quad (I-5)$$

The average ramp pressure was determined from the two-dimensional oblique shock relations given in Ref. 15 as if secondary mass flow rate was zero. The oblique shock was assumed to be along a straight line from the beginning of the 5-deg ramp to the centerline of the diffuser in the plane of the entrance to the constant area ejector second throat. This gave an oblique shock angle $\phi = 28$ deg from the direction of flow near the diffuser wall at the exit of the ejector nozzle as shown in Fig. I-2. The ramp pressure was determined as the static pressure downstream of the oblique shock as follows:

$$M_{ramp} = f(M', \gamma_e, \phi)$$

giving

$$(P_t)_{ramp} = P_{te} [(P_t)_{ramp} / P_{te}]$$

and from

$$P_{ramp} / (P_t)_{ramp} = f(M_{ramp}, \gamma_e)$$

the ramp pressure was obtained as

$$P_{\text{ramp}} = (P_t)_{\text{ramp}} \left[P_{\text{ramp}} / (P_t)_{\text{ramp}} \right]$$

Actually a more correct approach would be the use of a well-defined flow field from the method of characteristics for internal flow for an open-nosed body. The oblique shock originating at the ramp lip is strengthened as it moves toward the centerline, and finally, beyond a certain point, the flow becomes subsonic behind the shock as shown on page 689 in Ref. 16. This approach for determining the second-throat ramp pressure is given in Ref. 14.

By assuming that the secondary stream does not expand or contract from the area of the rocket engine diffuser second throat, then the primary stream has freedom to expand to the annulus area $(A_d)_e = (A_{st})_r$. The measured nozzle lip static pressure for conical or contoured nozzles as shown in Figs. 15c, 19e, 20a, and 20b is higher than the isentropic value based on area ratio by a factor of 1.13 to 2.07. The smaller half-angle conical and contoured nozzles have the largest pressure multiplying factor. The pressure ratio from $A/A_e^* = 17.22$ is approximately two times the pressure ratio from $[(A_d)_e = (A_{st})_r] / A_e^* = 27.06$ given in Ref. 9. Therefore, the ramp pressure was based on the inlet conditions from A/A_e^* or M' . From the oblique shock relations given in Ref. 15, the oblique shock angle, ϕ , of the flow stream, approach Mach number, M' , and the ejector driving pressure, P_{te} , were sufficient for calculating the static pressure downstream of the oblique shock from the beginning of the ramp.

The continuity, momentum, and energy relationships when applied as given in Ref. 13 give

$$\mu(M_{ex}) = \frac{m_{ex}}{F_{ex}} \sqrt{\frac{R_{ex} (T_t)_{ex}}{g_c}} = \frac{M_{ex} \sqrt{\gamma_{ex} \left(1 + \frac{\gamma_{ex}-1}{2} M_{ex}^2\right)}}{1 + \gamma_{ex} M_{ex}^2} \quad (\text{I-6})$$

The $\mu(M)$ equation is given in Ref. 13 in a curve (Fig. II-2 of Ref. 13) as a function of γ and M . Since there are two fluids mixed in different proportions at the diffuser-ejector exit of the annular-type ejector when the rocket engine and ejector are operating, then m_{ex} , R_{ex} , γ_{ex} , and $(T_t)_{ex}$ are given as follows:

$$\begin{aligned} m_{ex} &= m_e + m_r & \gamma_{ex} &\cong \frac{(m_r/m_e) \gamma_r + \gamma_e}{1 + m_r/m_e} \\ R_{ex} &= \frac{(m_r/m_e) R_r + R_e}{1 + m_r/m_e} & (T_t)_{ex} &\cong \frac{(m_r/m_e) T_{tr} + T_{te}}{1 + m_r/m_e} \end{aligned}$$

The $\mu(M_{ex})$ was calculated from the equation

$$\mu(M_{ex}) = m_{ex}/F_{ex} \frac{\sqrt{R_{ex}(T_t)_{ex}}}{g_c}$$

and then from γ_{ex} on the subsonic side of the curve in Fig. II-2 of Ref. 13, M_{ex} is obtained. The momentum equation was then used in the form

$$(P_{ex})_{lip (theory)} = \frac{F_{ex}}{A_{ex} (1 + \gamma_{ex} M_{ex}^2)} \quad (I-7)$$

where F_{ex} is obtained from either Eq. (I-3) or (I-4), depending on the test configuration being checked (3a, b, or c). The A_{ex} is the corresponding diffuser-ejector exit area for the test configuration being checked. Since the exit pressure is affected by the length of the diffuser, a correction to Eq. (I-7) was necessary. The correction factor used to correct the theoretical value from Eq. (I-7) to the predicted value was the ratio $[(P_{ex})_{lip}/P_{te}]/(P_y/P_{tx})$ obtained for the individual ejector performance given in section 4.4.2 and Fig. 18.

Therefore,

$$(P_{ex})_{lip (pred)} = (P_{ex})_{lip (theory)} \frac{(P_{ex})_{lip}/P_{te}}{P_y/P_{tx}} \quad (I-8)$$

Actually, this correction factor may not necessarily be correct. It is known to vary with $(L/D)_e$ and may vary with secondary mass flow. The secondary mass flow could increase or decrease the correction factor depending on the value of $(L/D)_e$ as shown in Fig. 13a for a centerbody-type ejector configuration without an ejector second throat. The correction factor for the ejector second-throat configuration may decrease with secondary mass flow. The geometric parameters and conditions for which the force balance calculations were made are given in Table I-1. The results of this analysis for the three test configurations 3a, b, and c are presented in Table I-2.

Analytical results for test configurations 3b and c indicate that a correction factor less than 0.94 should be used. If wall friction or viscous forces had not been neglected and if the exact value of rocket engine exhaust gas temperature were known, closer agreement of predicted and measured exit pressure would probably have resulted.

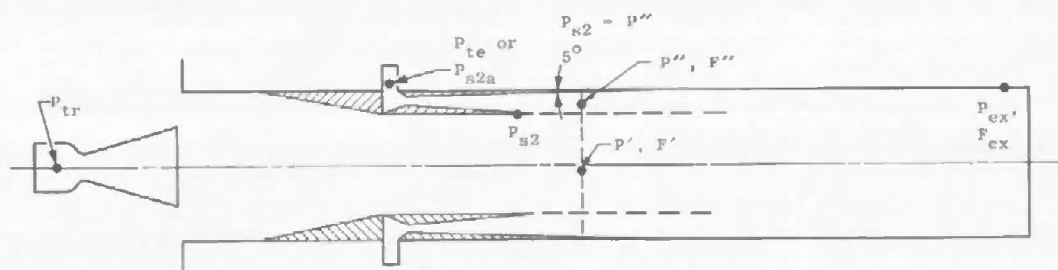


Fig. 1-1 Cold Flow without Second-Throat Test Configuration 3a

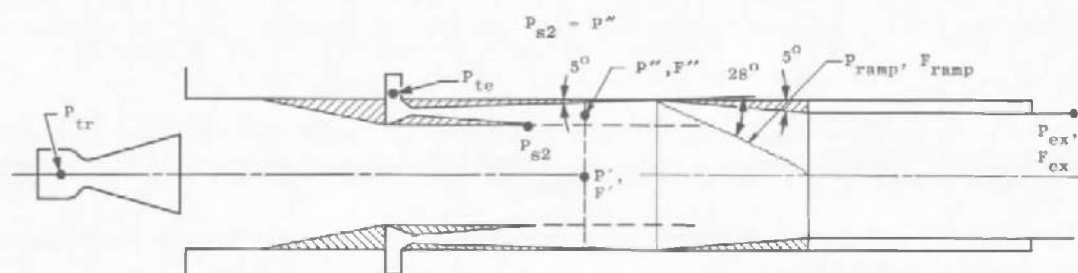


Fig. 1-2 Cold Flow with Second-Throat Test Configuration 3b
Hot Rocket with Second-Throat Test Configuration 3c

TABLE I-1
GEOMETRIC PARAMETERS AND FORCE BALANCE CONDITIONS

Parameter	Test Configuration		
	3a	3b	3c
A_r^* , in. ²	0.7512	0.7512	0.6124
$(A_{st})_r$, in. ²	27.05	27.05	27.05
$(A_d/A^*)_r$	61.89	61.89	75.57
$(A_{ne}/A^*)_r$	18.57	18.57	40.0
A_e^* , in. ²	1.8601	1.8601	1.8601
$(A_d)_e$, in. ²	77.38	77.38	77.38
$(A_{st})_e$, in. ²	--	47.99	47.99
A_{ex} , in. ²	77.38	47.99	47.99
γ_r	1.30	1.30	1.28
γ_e	1.30	1.30	1.30
R_r , $\frac{ft \cdot lb_f}{lb_m \cdot ^\circ R}$	86.0	86.0	67.0
R_e , $\frac{ft \cdot lb_f}{lb_m \cdot ^\circ R}$	86.0	86.0	86.0
T_{tr} , $^\circ R$	760	760	Assumed 4000
T_{te} , $^\circ R$	760	760	760
P_{tr} , psia	10	10	11.00
P_{te} , psia	50	50	45.66
$\frac{(P_{ex})_{11p}/P_{te}}{P_v/P_{tx}}$	0.62	0.94	0.94

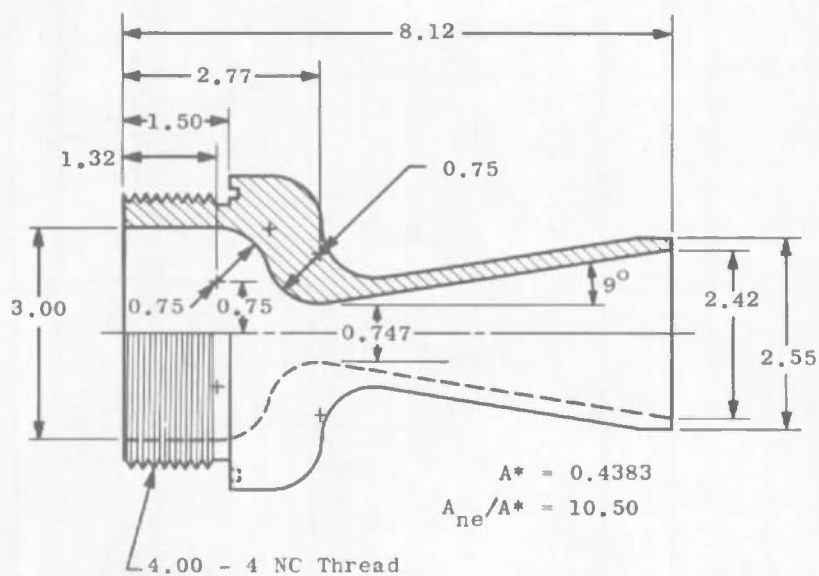
TABLE 1-2
FORCE BALANCE CHECK

Parameters	Test Configuration		
	3a	3b	3c
P_{te} , psia	50	50	45.66
P_{tr} , psia	10	10	11
F' , lbf	160.54	160.54	147.83
P' , psia	0.2224	0.2224	0.2048
F'' , lbf	10.20	10.20	8.90
P'' , psia	0.2224	0.2224	0.2048
F_{ramp} , lbf	--	25.25	23.28
P_{ramp} , psia	--	0.867	0.792
$(F_{ex})_{lip}$, lbf	170.74	145.25	133.46
$(P_{ex})_{lip}$ (theory), psia	1.7949	2.1613	2.0926
$(P_{ex})_{lip}$ (pred), psia	1.1128	2.0316	1.9671
$(P_{ex})_{lip}$ (measured), psia	1.1000	1.64	1.48

REFERENCES

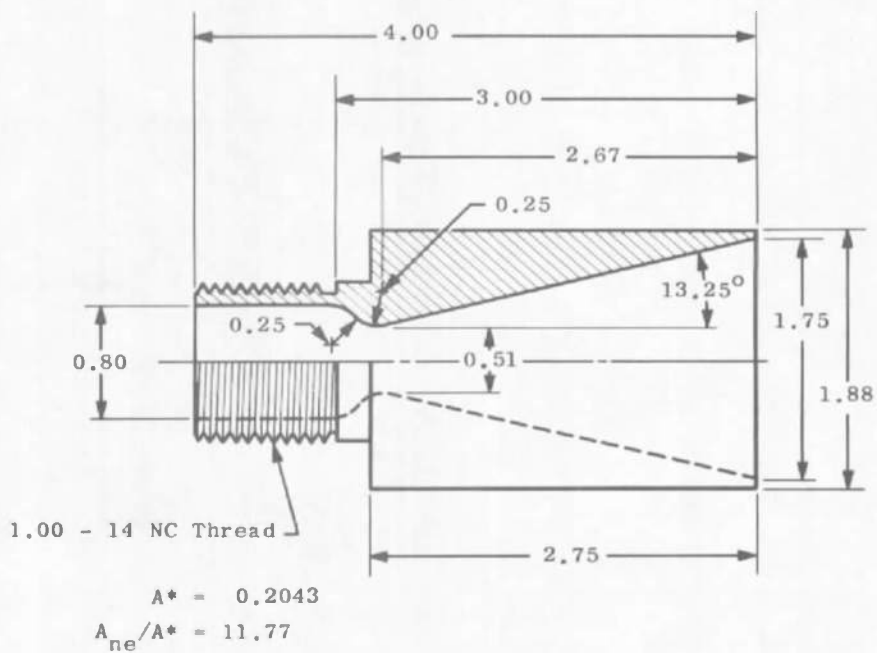
1. Bauer, R. C. and German, R. C. "The Effect of Second Throat Geometry on the Performance of Ejectors without Induced Flow." AEDC-TN-61-133 (AD267263), November 1961.
2. Hale, J. W. and Gobbell, W. C. "Diffuser Development for Throttleable Engines." AEDC-TR-65-7 (AD458437), March 1965.
3. Hale, James W. "Investigation of Two-Nozzle Cluster Diffuser-Ejector with and without Ejected Mass." AEDC-TDR-63-130 (AD422419), November 1963.
4. Hale, James W. "Influence of Pertinent Parameters on Ejector-Diffuser Performance with and without Ejected Mass." AEDC-TDR-64-134 (AD602770), July 1964.
5. Lewis, W. G. E. and Drabble, J. S. "Ejector Experiments." NGTE R 151 (N34389), February 1954.
6. Hale, James W. "Auxiliary Ejector Effects on Rocket-Driven Diffuser Performance during Thrust Variation." AEDC-TDR-63-188, September 1963.
7. Bauer, R. C. and German, R. C. "Some Reynolds Number Effects on the Performance of Ejectors without Induced Flow." AEDC-TN-61-87 (AD262734), August 1961.
8. Hale, James W. "Comparison of Diffuser-Ejector Performance with Five Different Driving Fluids." AEDC-TDR-63-207 (AD420813), October 1963.
9. Wang, C. J., Peterson, J. B., and Anderson, R. "Gas Flow Tables." GM-TR-154, March 1958.
10. Barton, D. L. and Taylor, D. "An Investigation of Ejectors without Induced Flow." AEDC-TN-59-145 (AD229860), December 1959.
11. Latvala, E. K. "Spreading of Rocket Exhaust Jets at High Altitudes." AEDC-TR-59-11 (AD215866), June 1959.
12. Panesci, J. H. and German, R. C. "An Analysis of Second-Throat Diffuser Performance for Zero-Secondary-Flow Ejector Systems." AEDC-TDR-63-249 (AD426336), December 1963.

13. Lynch, G. R. and Carman, C. T. "An Investigation of the Performance of a Hot-Gas Jet Pump with and without Induced Flow." AEDC-TDR-64-234 (AD452985), December 1964.
14. German, R. C. and Panesci, J. H. "Improved Methods for Determining Second-Throat Diffuser Performance of Zero-Secondary-Flow Ejector Systems." AEDC-TR-65-124 (AD466580), July 1965.
15. Edelfelt, Ivan H. "Graphical Presentation of Compressible Flow Functions." GE R52GL-300, December 1952.
16. Shapiro, Ascher H. The Dynamics and Thermodynamics of Compressible Fluid Flow. Vol. II, pp 688 and 689. Ronald Press Company, New York, 1953-54.



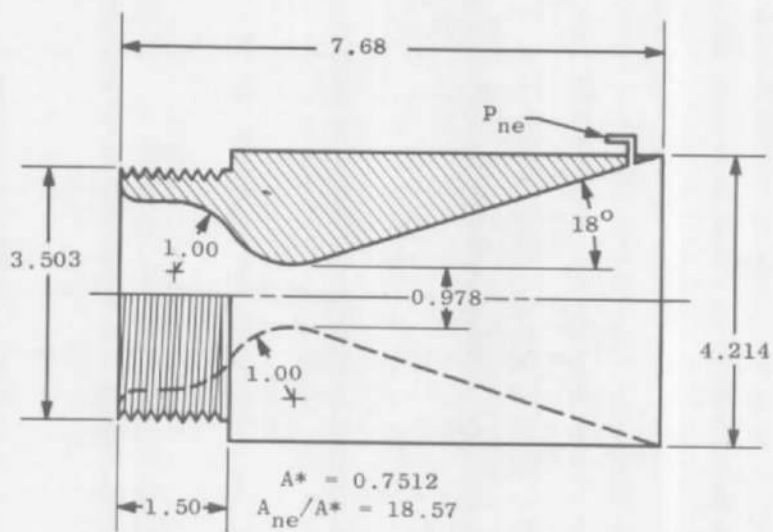
All Dimensions in Inches

o. Configuration A



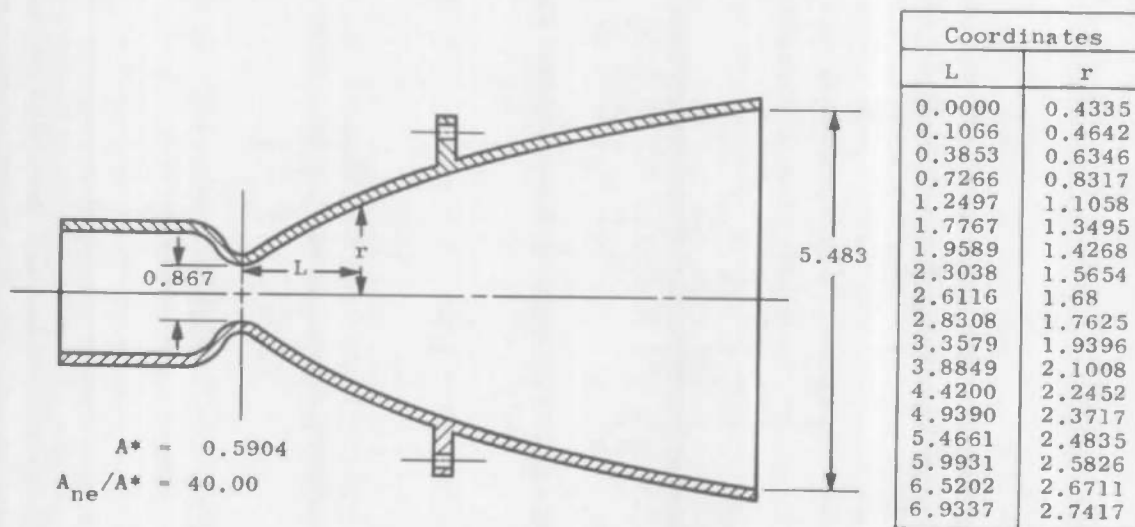
b. Configuration B

Fig. 1 Details of Simulated Rocket Engine Nozzles and Model Rocket Engine



All Dimensions in Inches

c. Configuration C



d. Configuration D

Fig. 1 Concluded

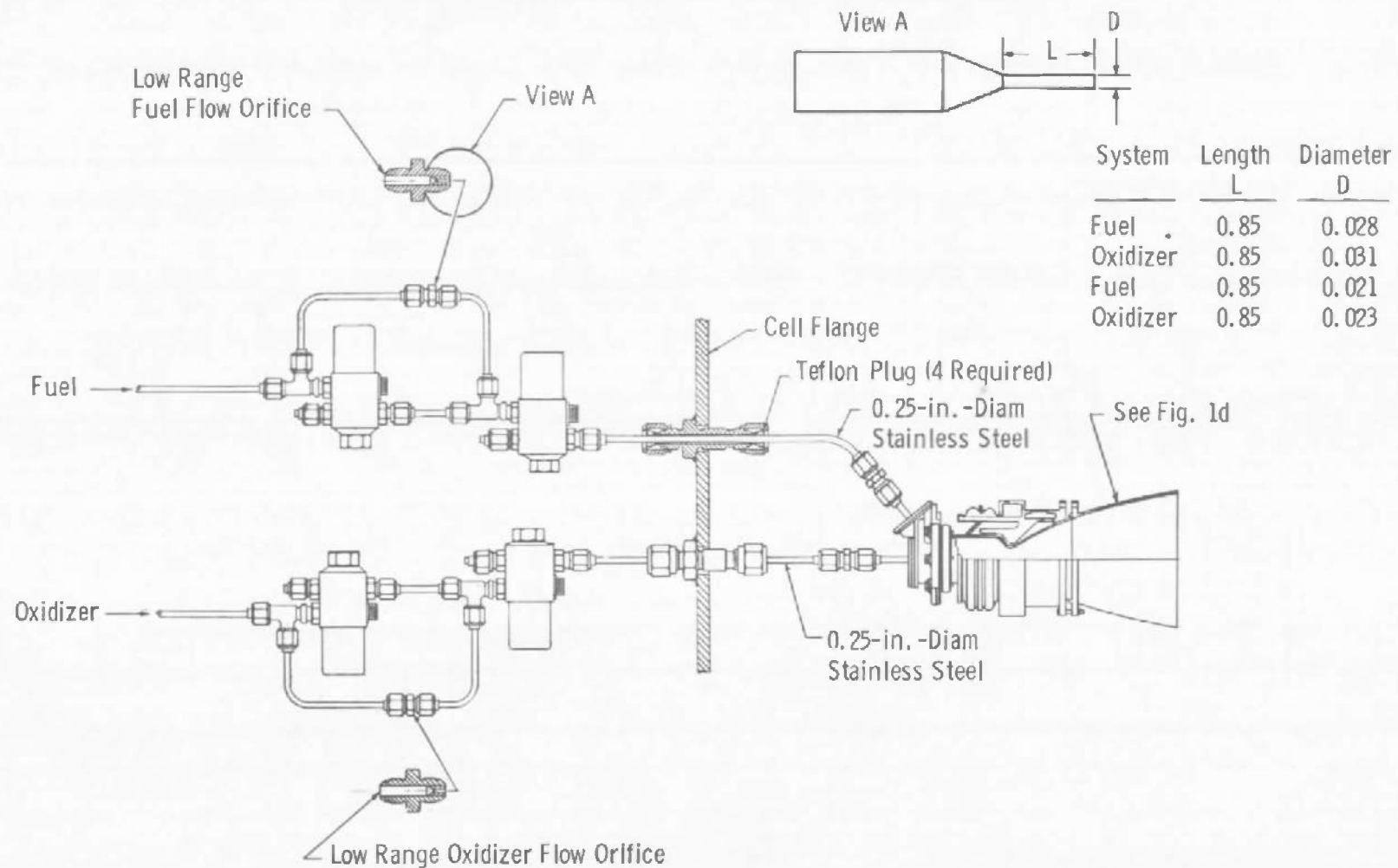


Fig. 2 Model Rocket Engine Propellant System for Configuration D Engine Throttling

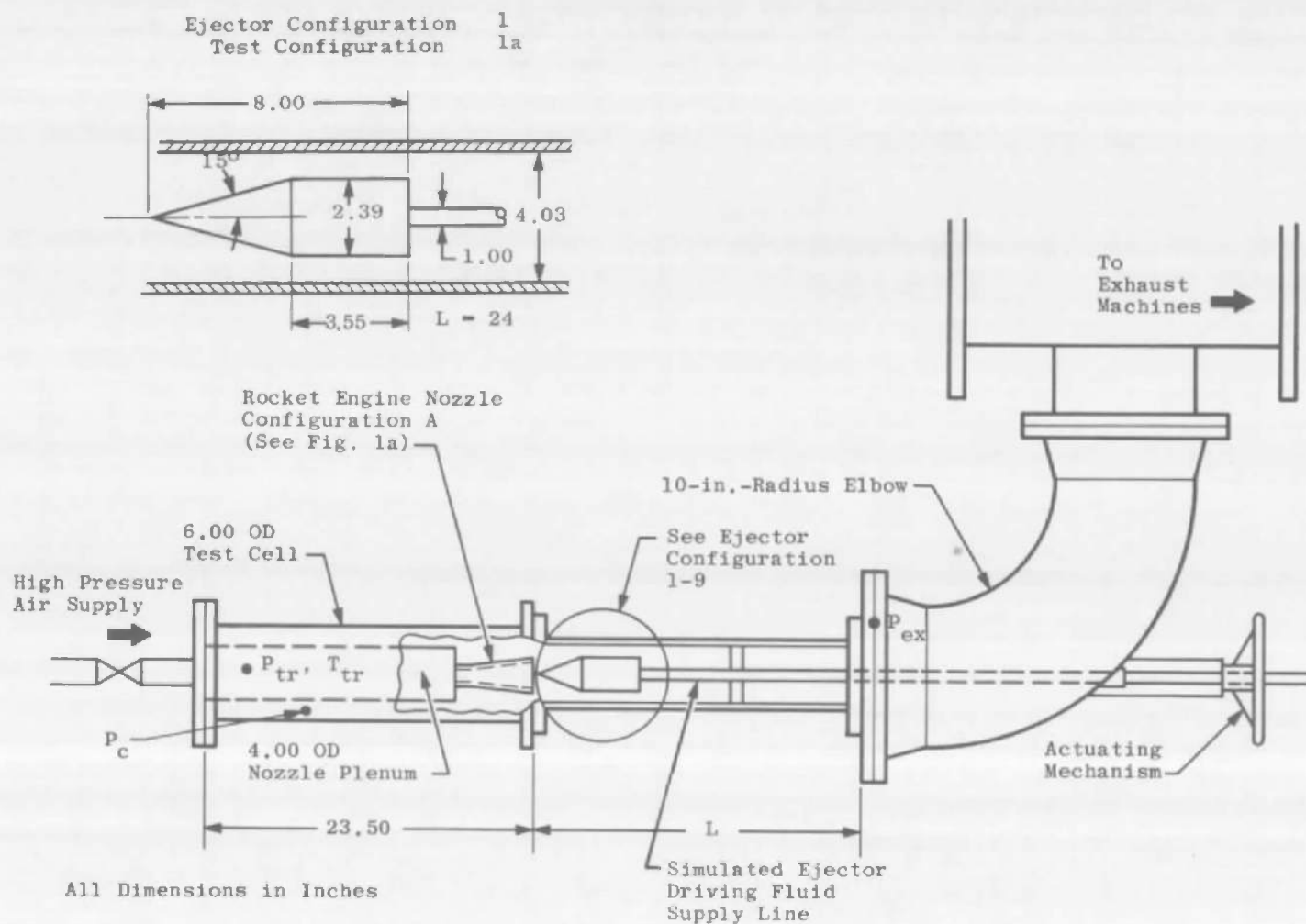
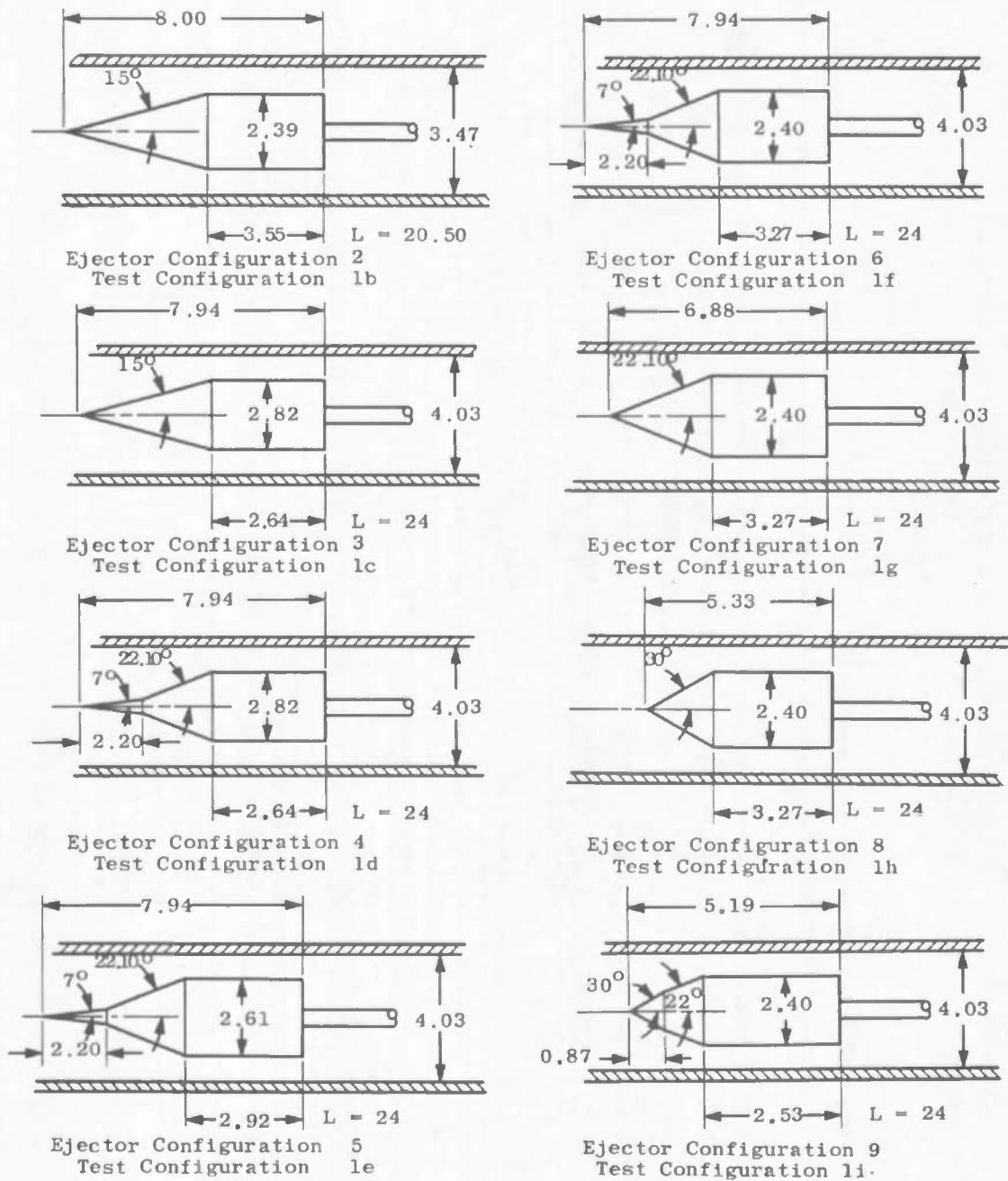
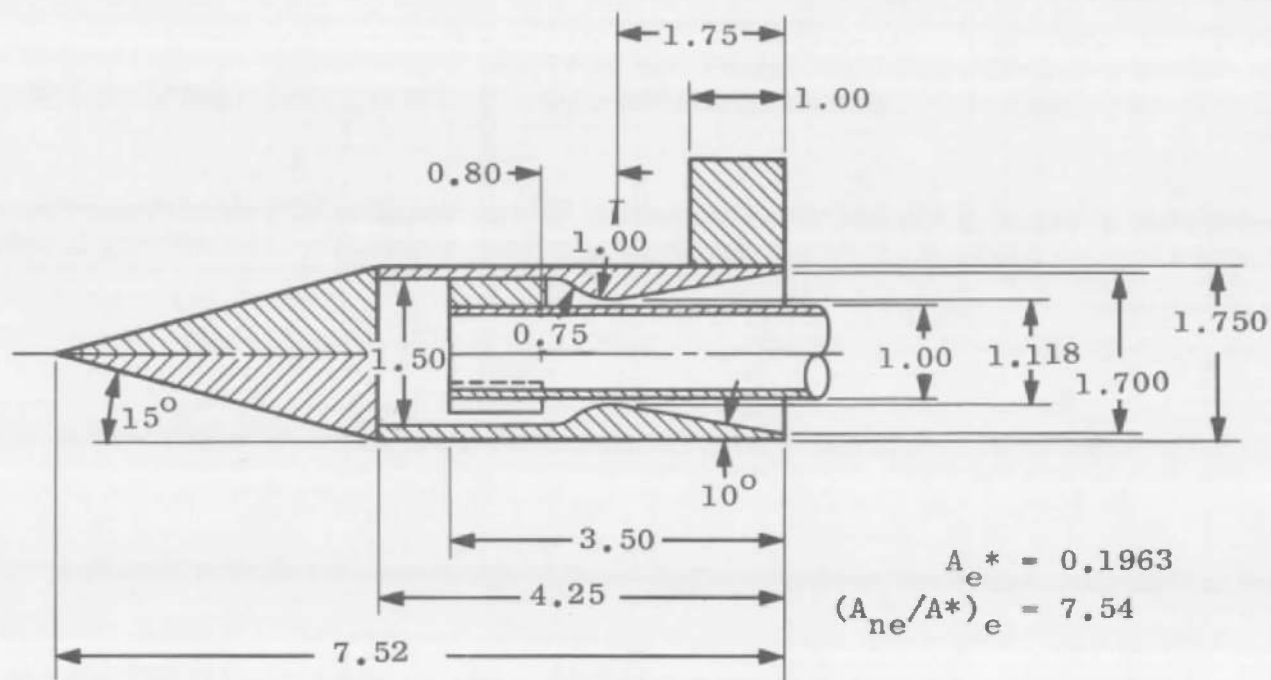


Fig. 3 Details for Centerbody-Type Ejector Configurations 1 through 9



All Dimensions in Inches

Fig. 3 Concluded



All Dimensions in Inches

Fig. 4 Details of Centerbody-Type Auxiliary Ejector Configuration 10

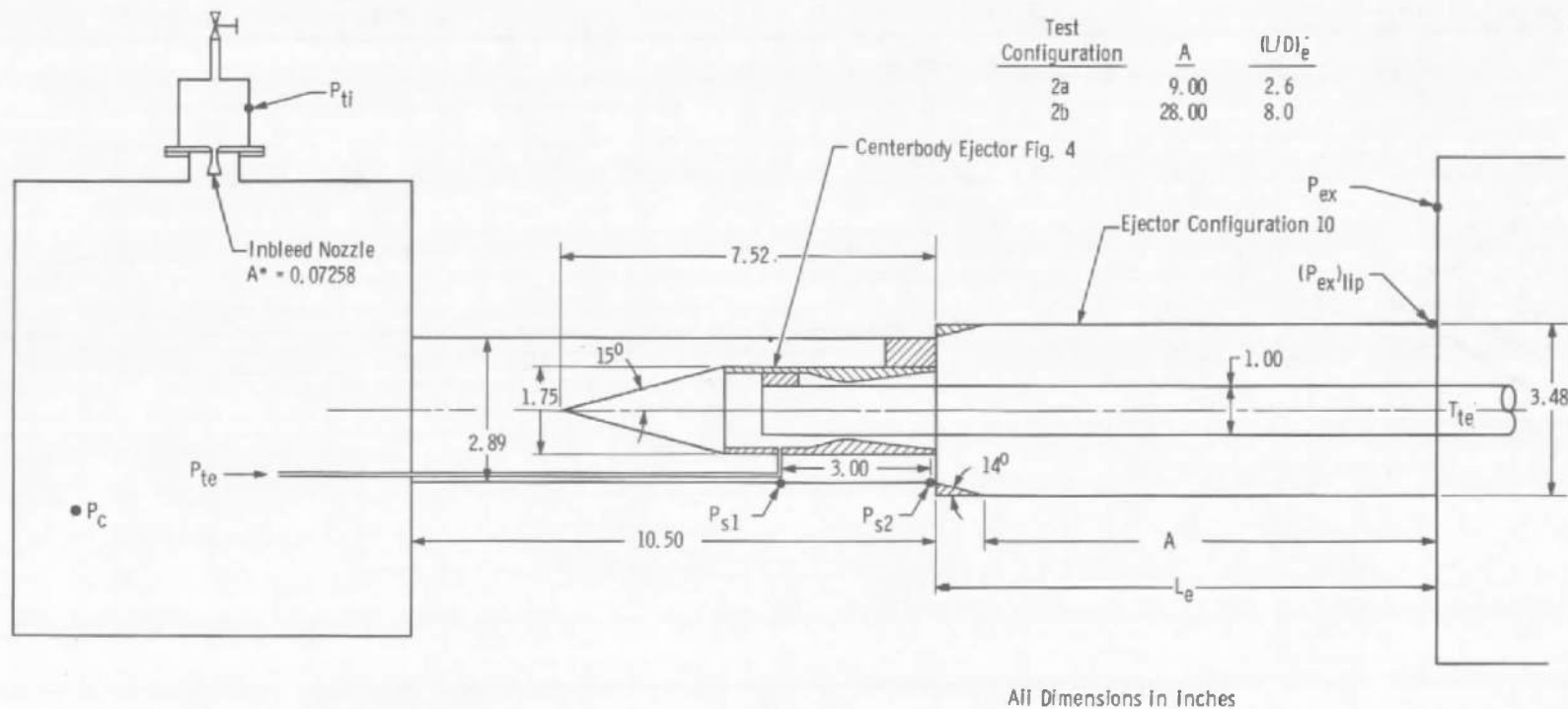


Fig. 5 Test Configurations 2a and b for Centerbody-Type Ejector Configuration 10

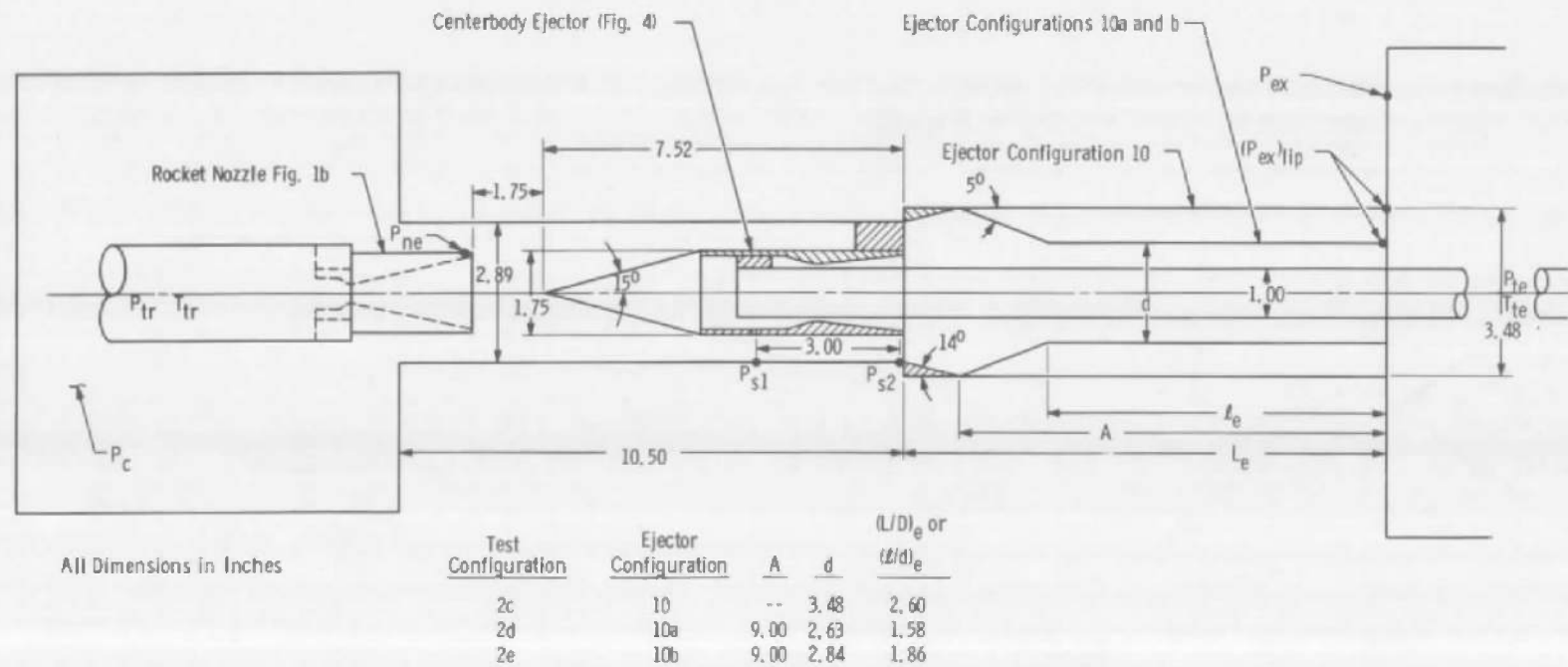


Fig. 6 Test Configurations 2c, d, and e for Centerbody-Type Ejector Configurations 10, 10a, and 10b

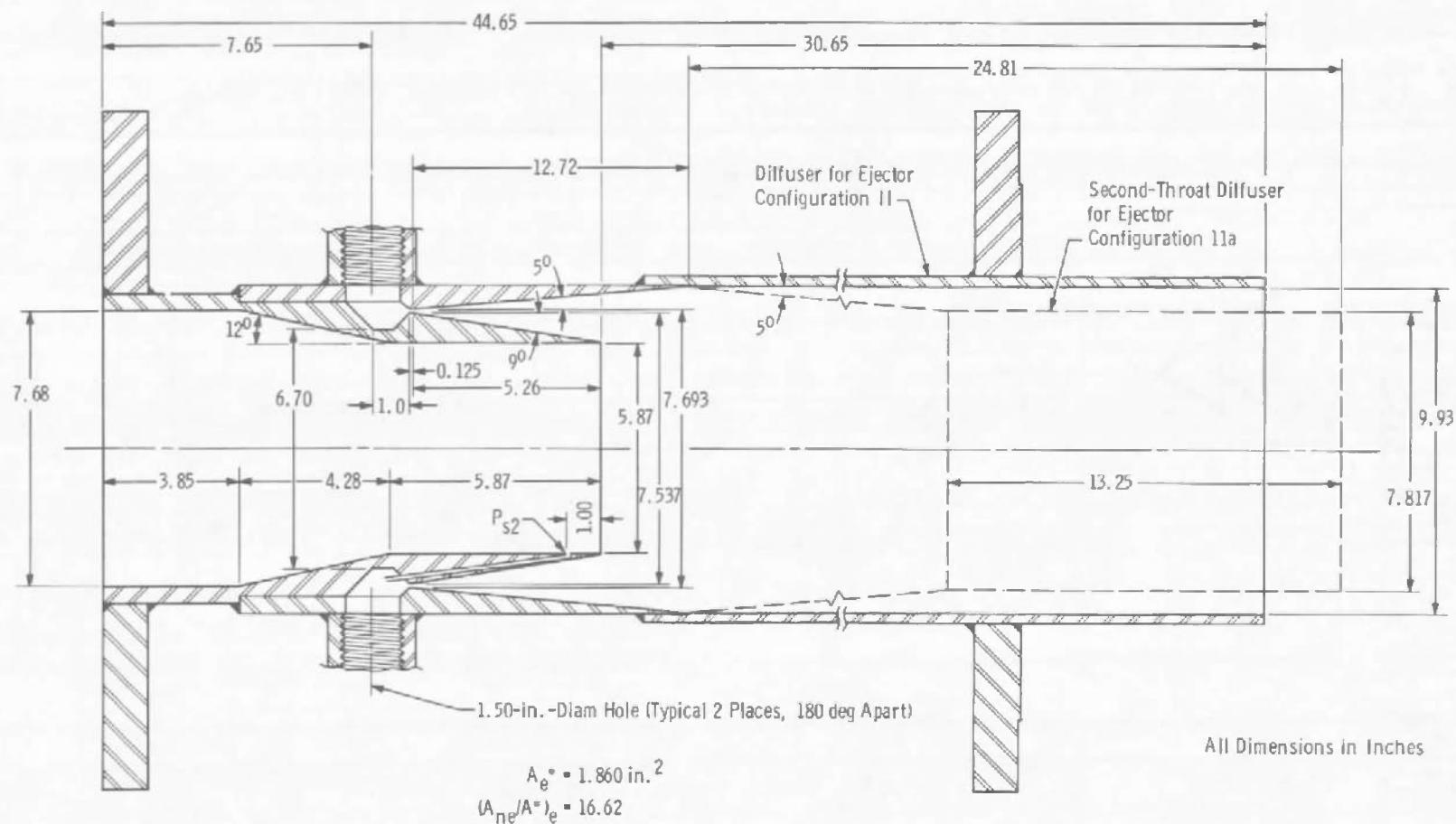


Fig. 7 Details of Annular-Type Auxiliary Ejector Configurations 11 and 11a

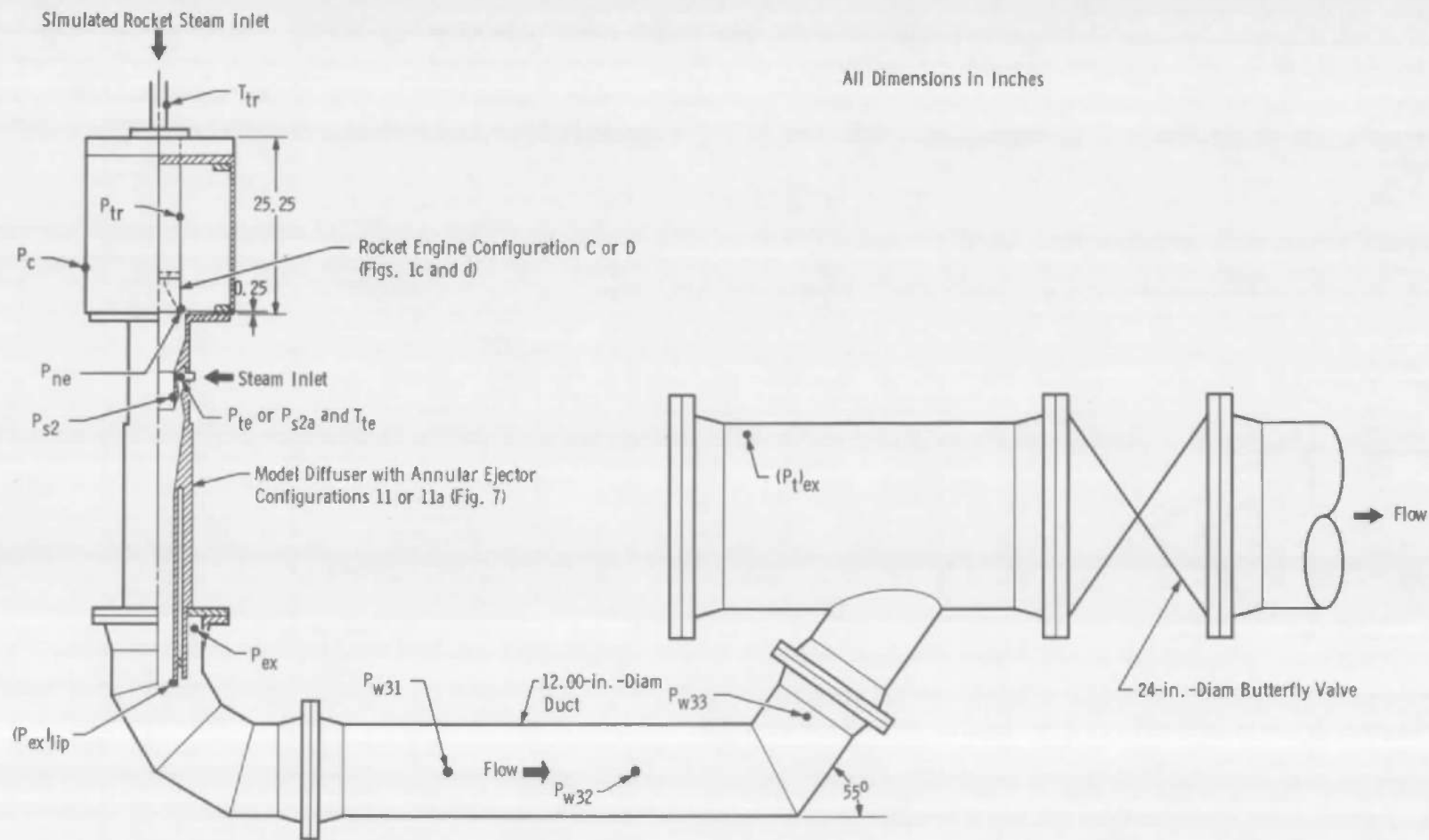


Fig. 8 J-3 Model Installation in Propulsion Research Area (R-2C-2) for Test Configurations 3a, b, and c

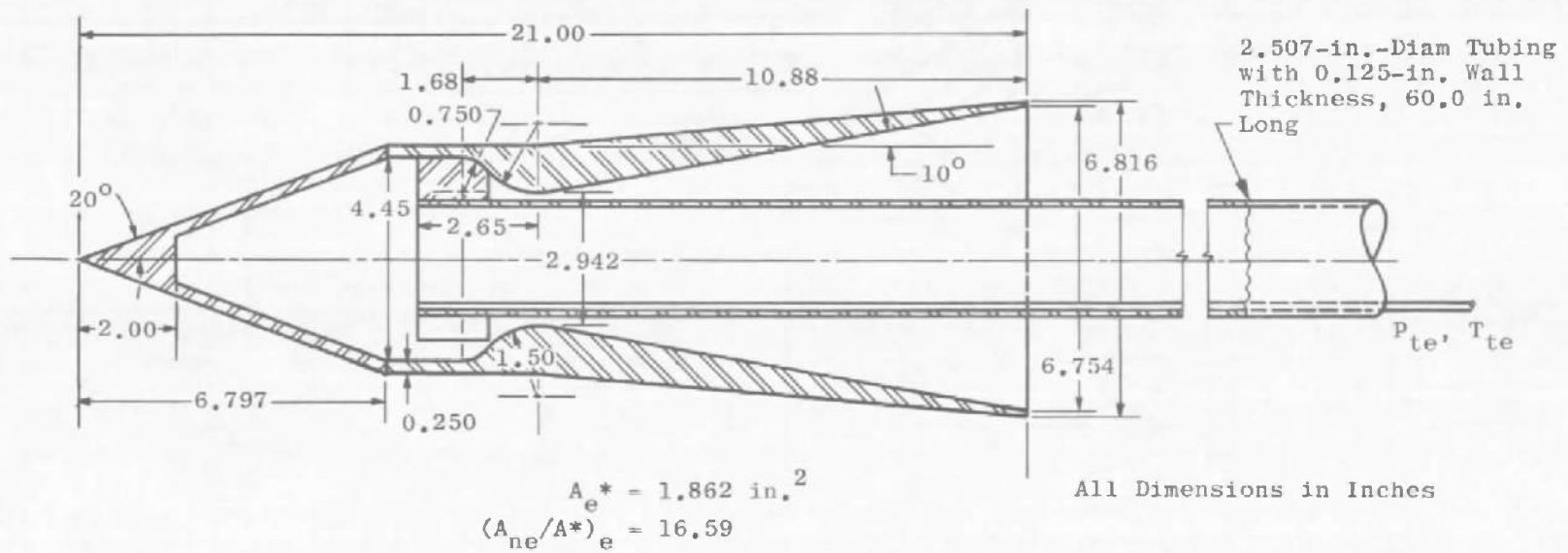


Fig. 9 Details of Centerbody-Type Ejector Configuration 12

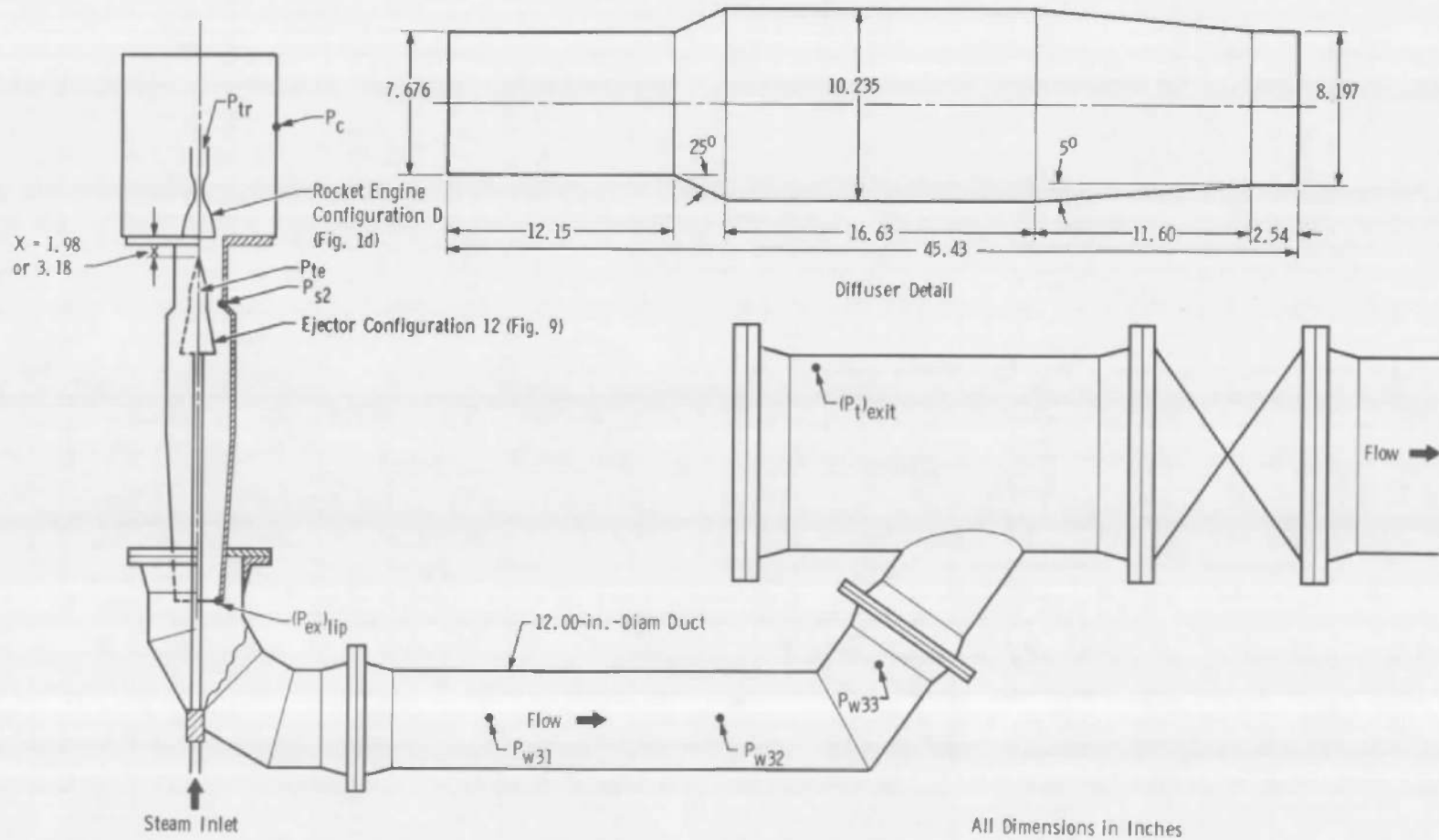
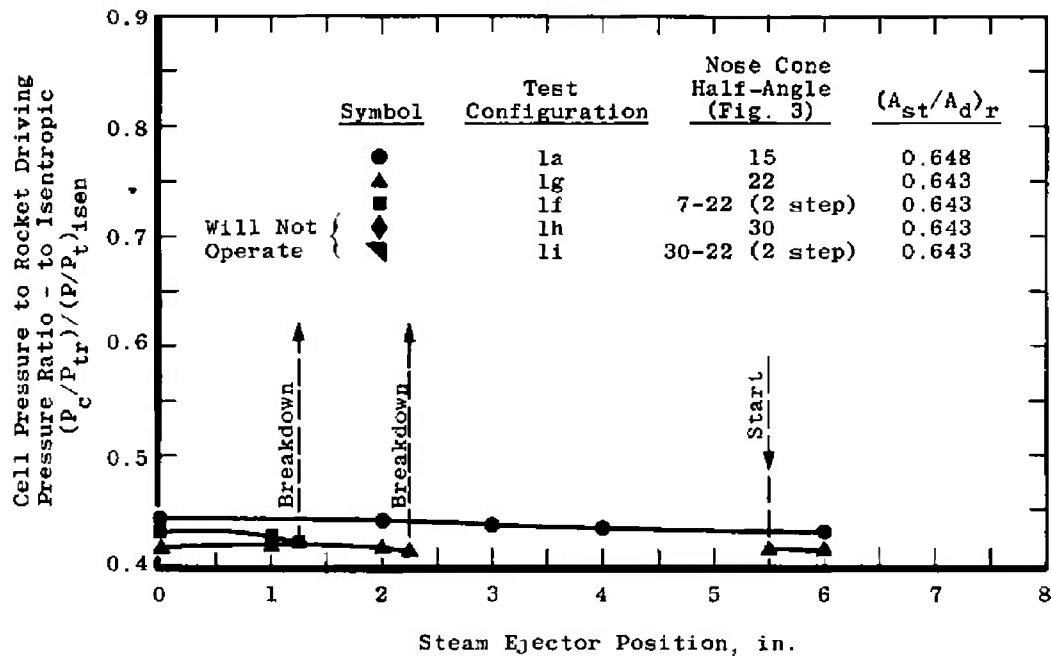
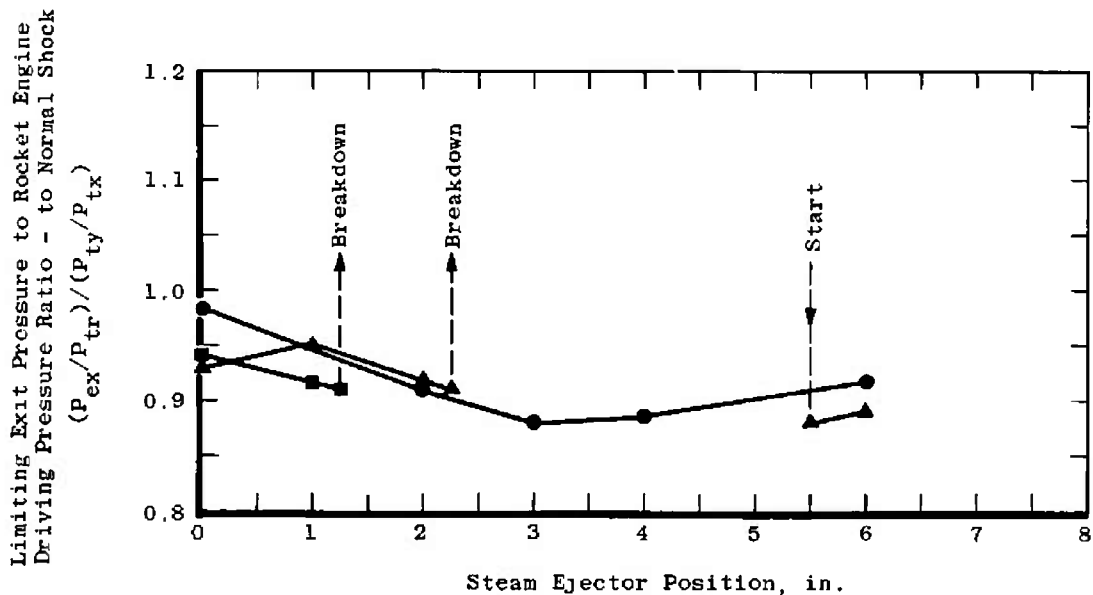


Fig. 10 J-3 Model Installation in Propulsion Research Area (R-2C-2) for Test Configuration 4



a. Centerbody-Type Ejector Position Limitation for Various Nose Cone Angles



b. Centerbody-Type Ejector Position Effect on Driving Pressure Ratio for Various Centerbody Nose Cone Angles

Fig. 11 Performance Evaluation of Phase I, Test Configurations with Diffusers having Normal Shock Contraction

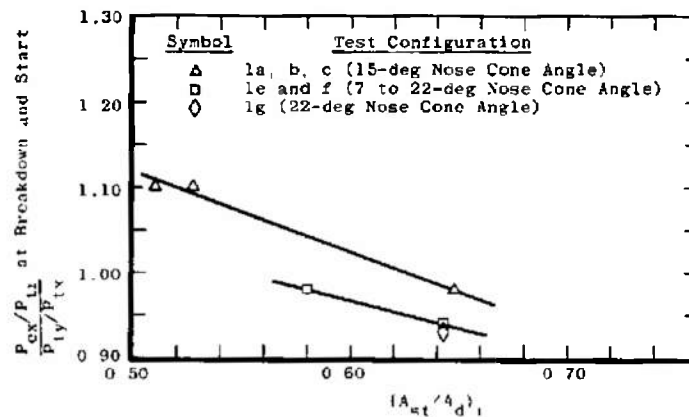
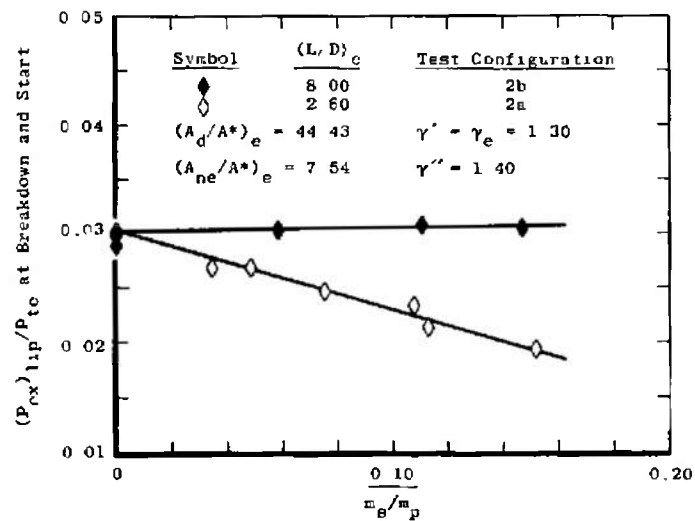
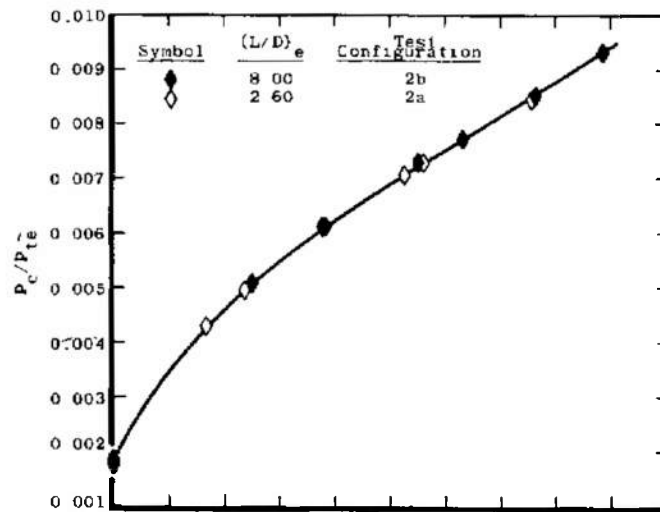


Fig. 12 Diffuser Contraction Area Ratio Effect on Driving Pressure Ratio for Various Centerbody Nose Cone Angles

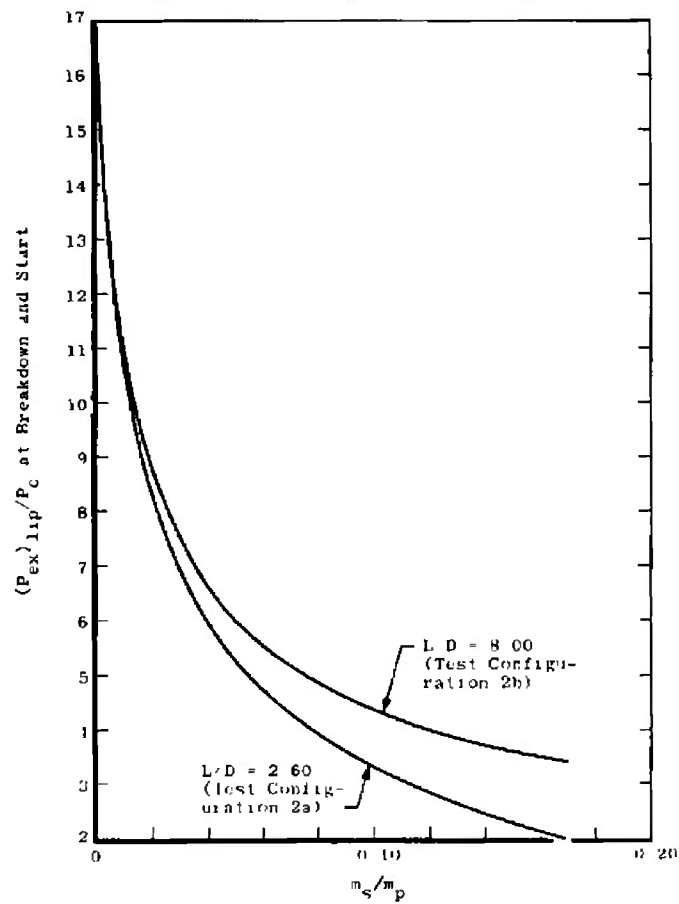


a. Secondary-to-Primary Mass Ratio Influence on the Limiting Driving Pressure Ratio

Fig. 13 Centerbody-Type Ejector Performance for Test Configurations 2a and b having $(L/D)_e = 2.6$ and 8.0



b. Secondary-to-Primary Mass Ratio Influence on Cell-to-Driving Pressure Ratio



c. Secondary-to-Primary Mass Ratio Influence on Rise Ratio

Fig. 13 Concluded

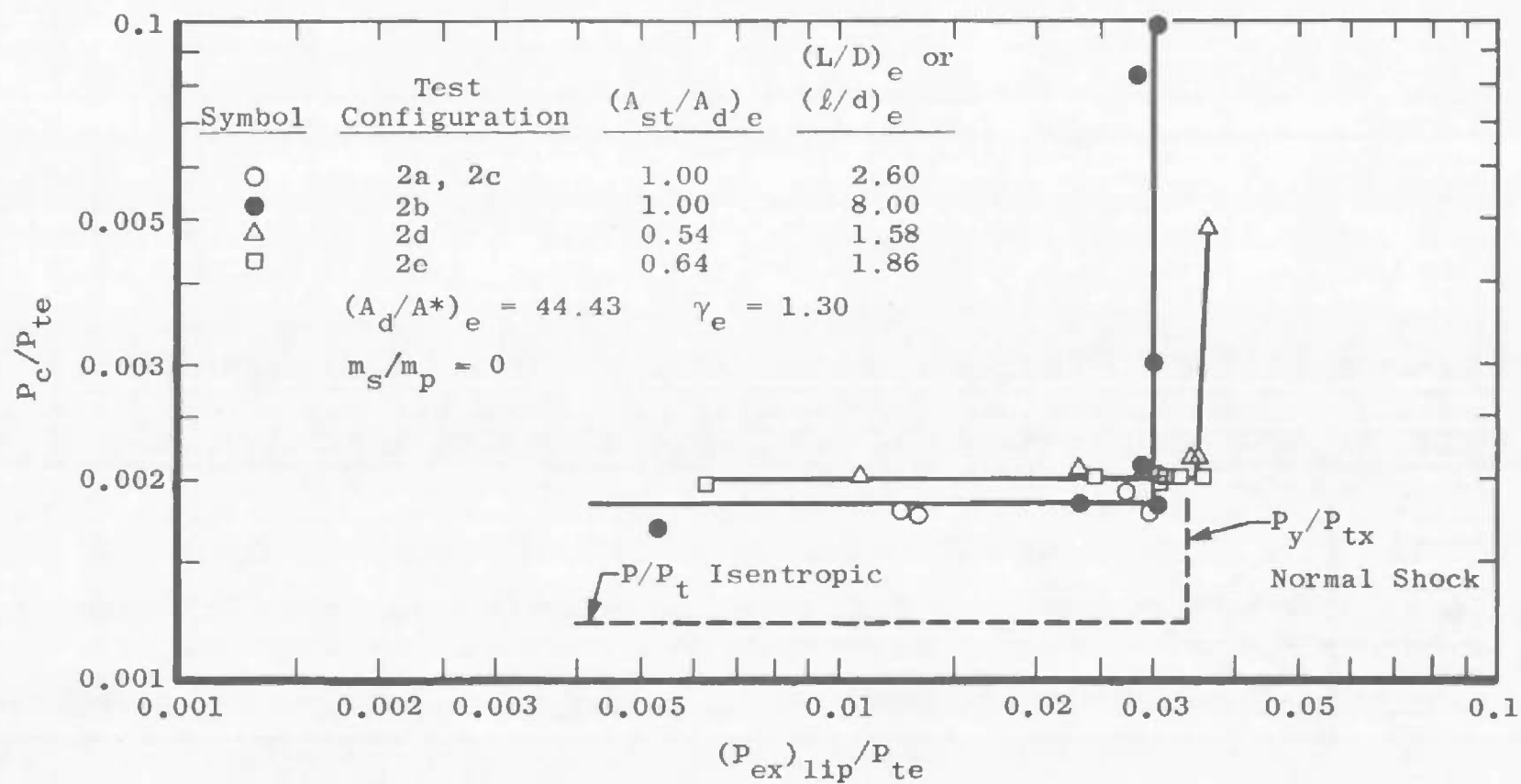
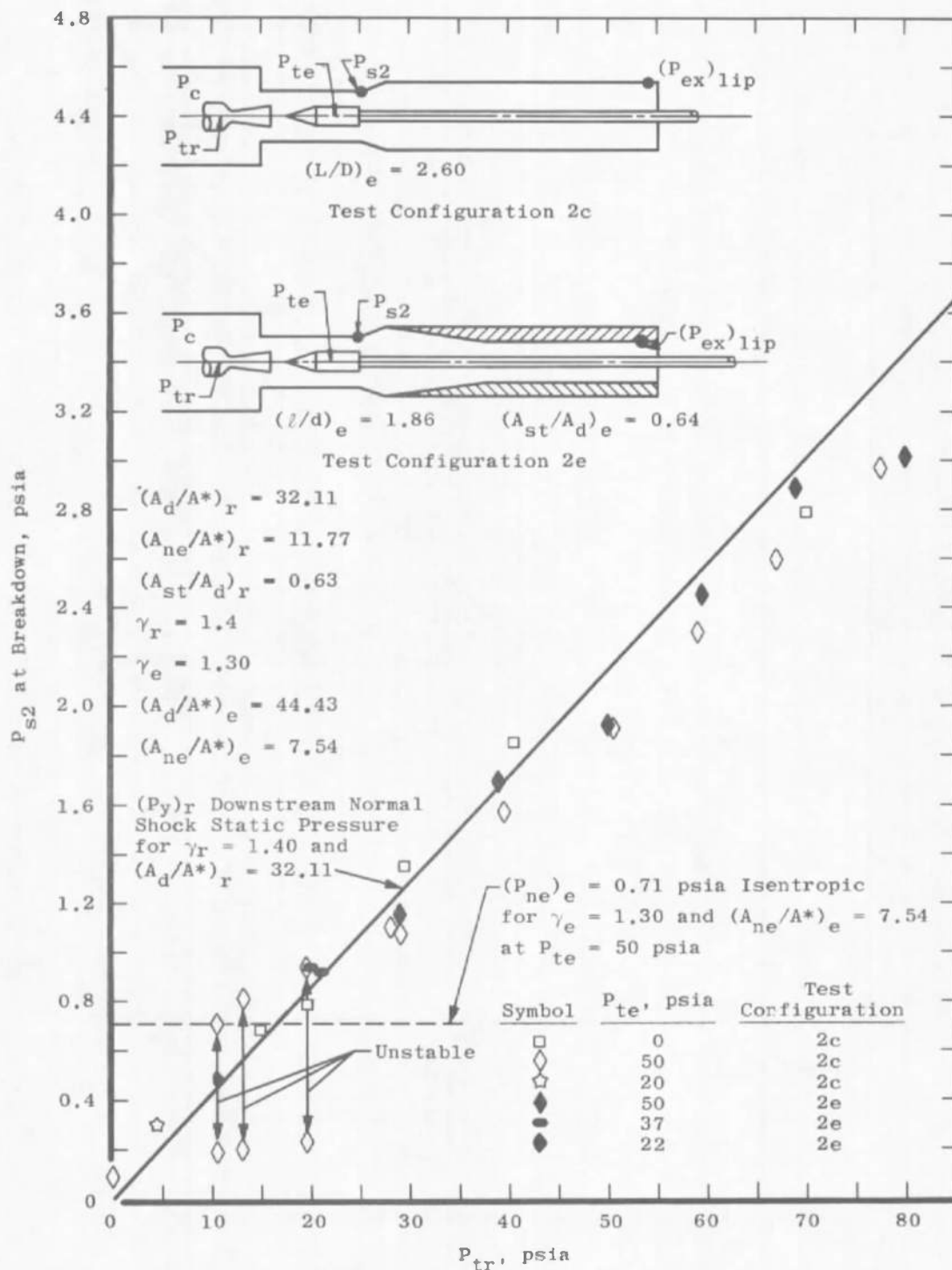
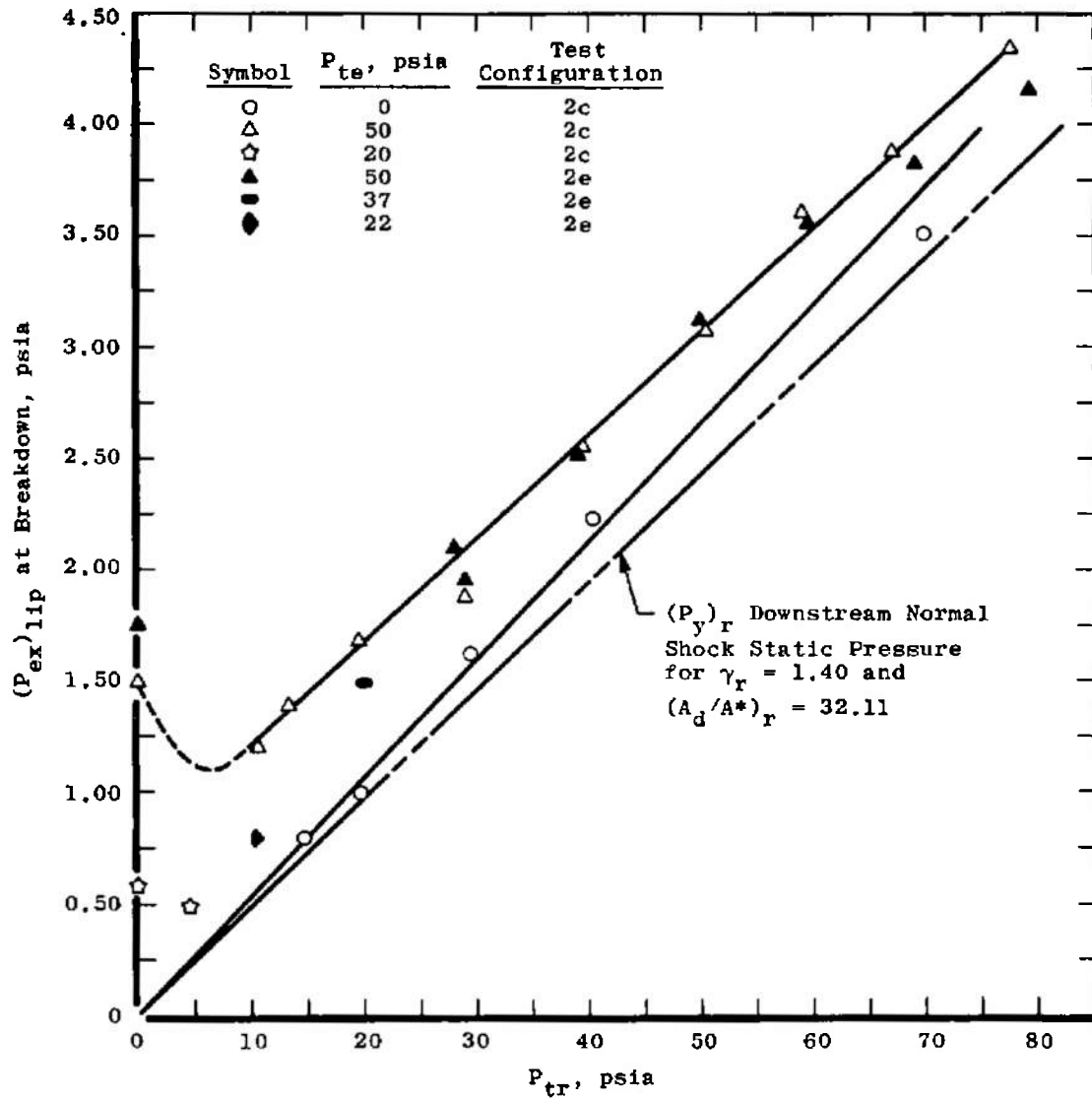


Fig. 14 Centerbody-Type Ejector Performance for Test Configurations 2c, d, and e



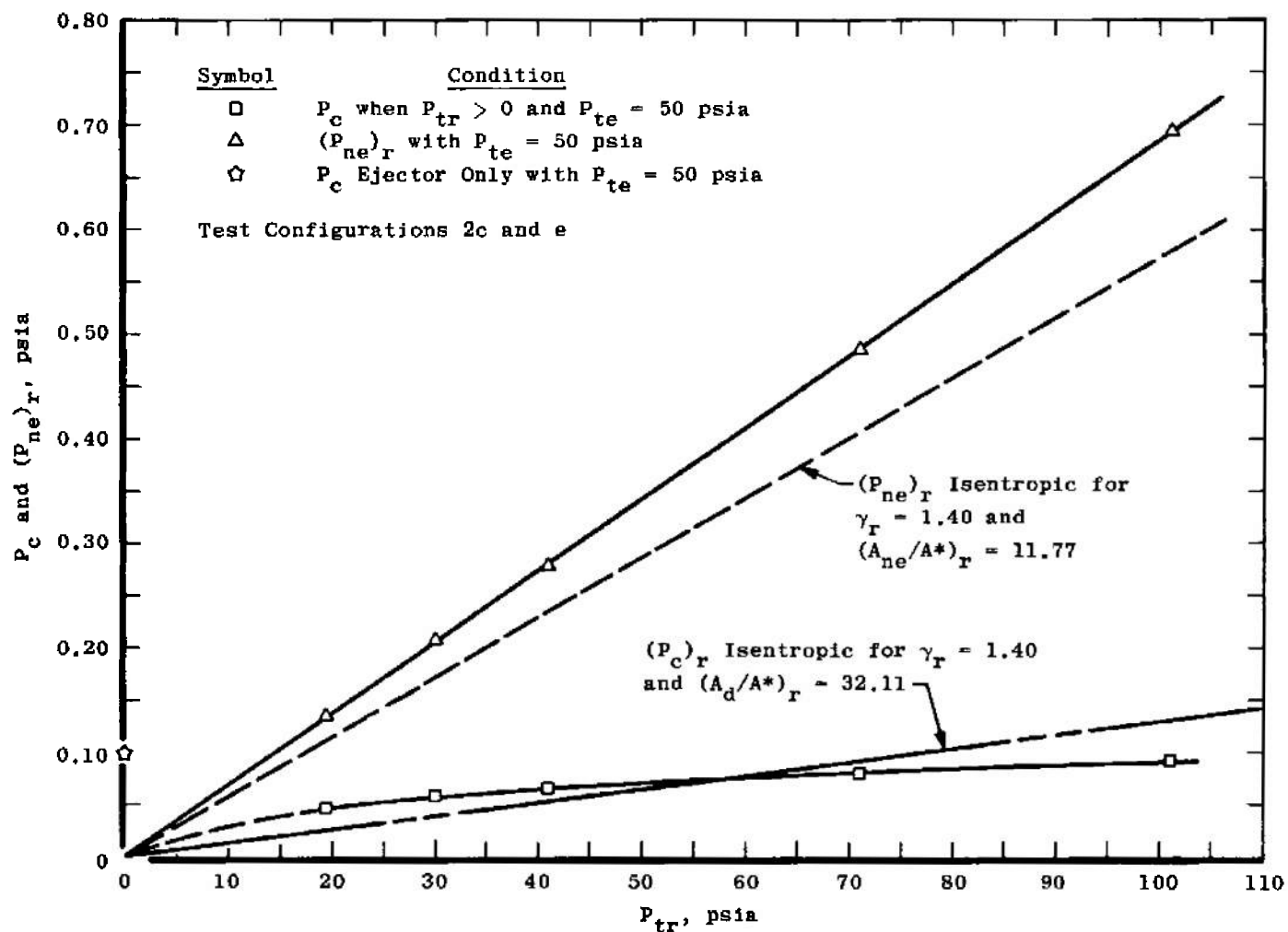
a. Diffuser Limiting Second-Throat Exit Static Pressure Performance

Fig. 15 Air-Driven Rocket Engine and Steam-Driven Centerbody-Type Ejector Performance for Test Configurations 2c through e



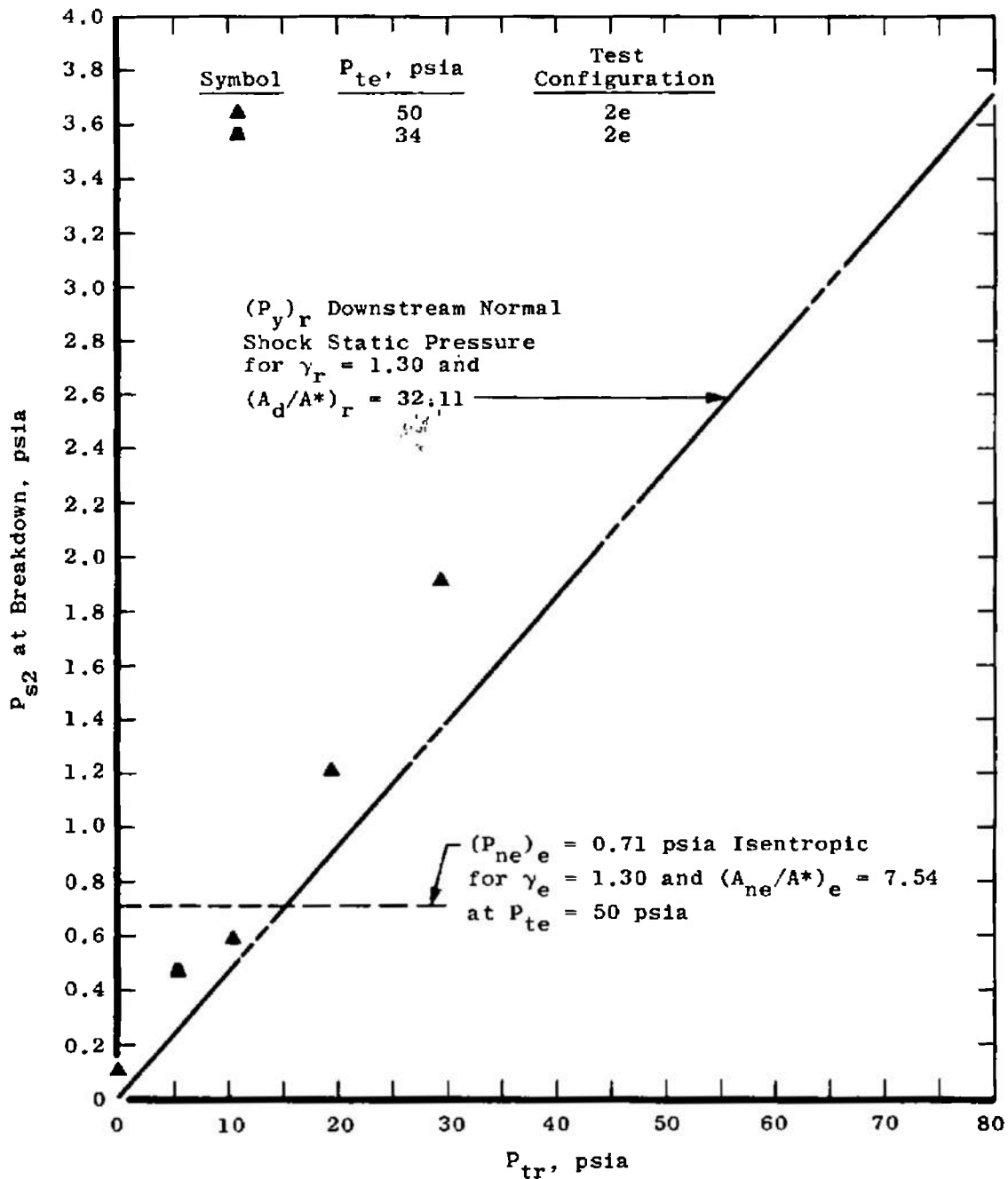
b. Ejector Limiting Exit Static Pressure Performance

Fig. 15 Continued



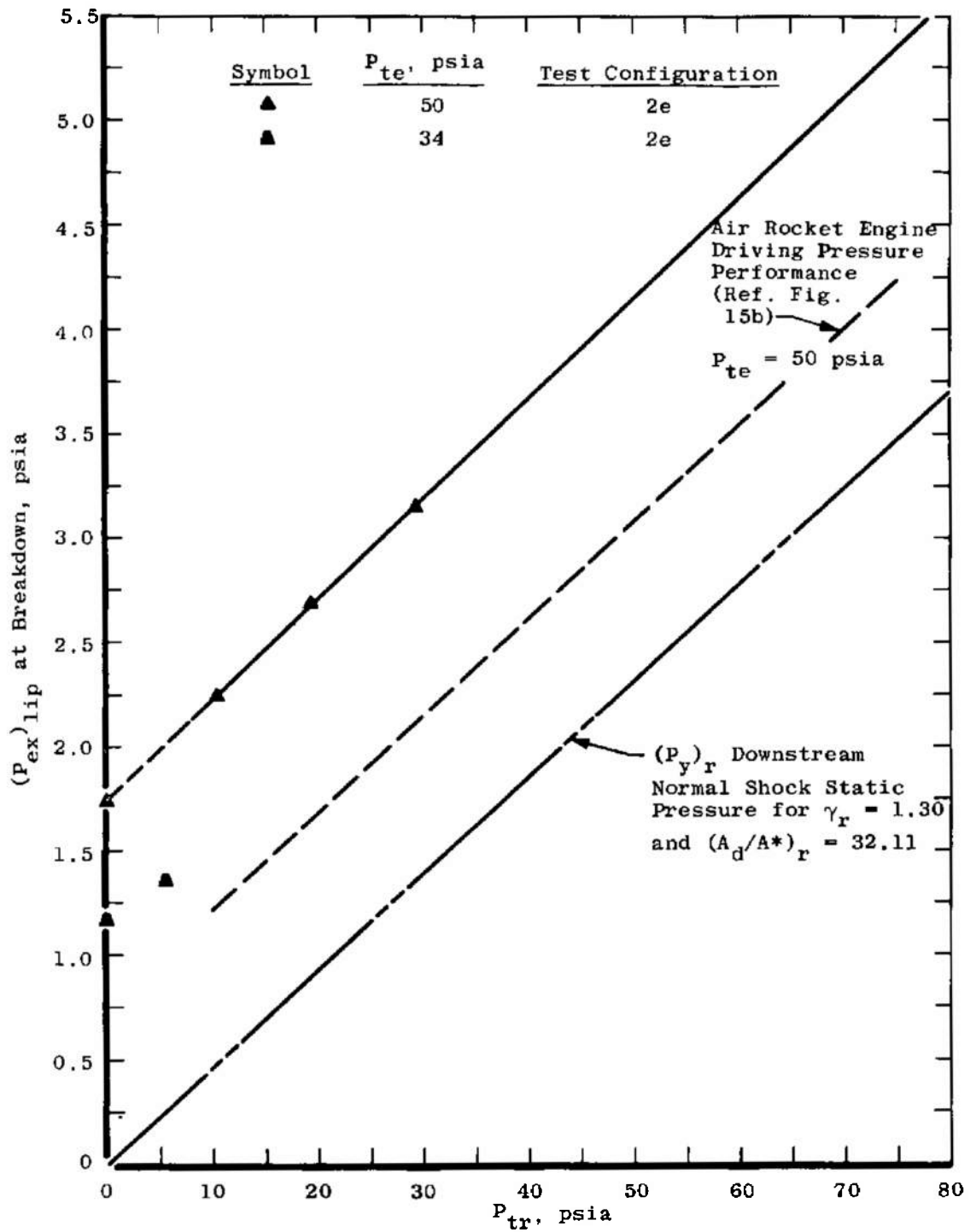
c. Minimum Cell Pressure and Rocket Engine Nozzle Lip Static Pressure Performance

Fig. 15 Concluded



a. Diffuser Limiting Second-Throat Exit Static Pressure Performance

Fig. 16 Steam-Driven Rocket Engine and Steam-Driven Centerbody-Type Ejector Performance for Test Configuration 2e



b. Ejector Limiting Exit Static Pressure Performance

Fig. 16 Concluded

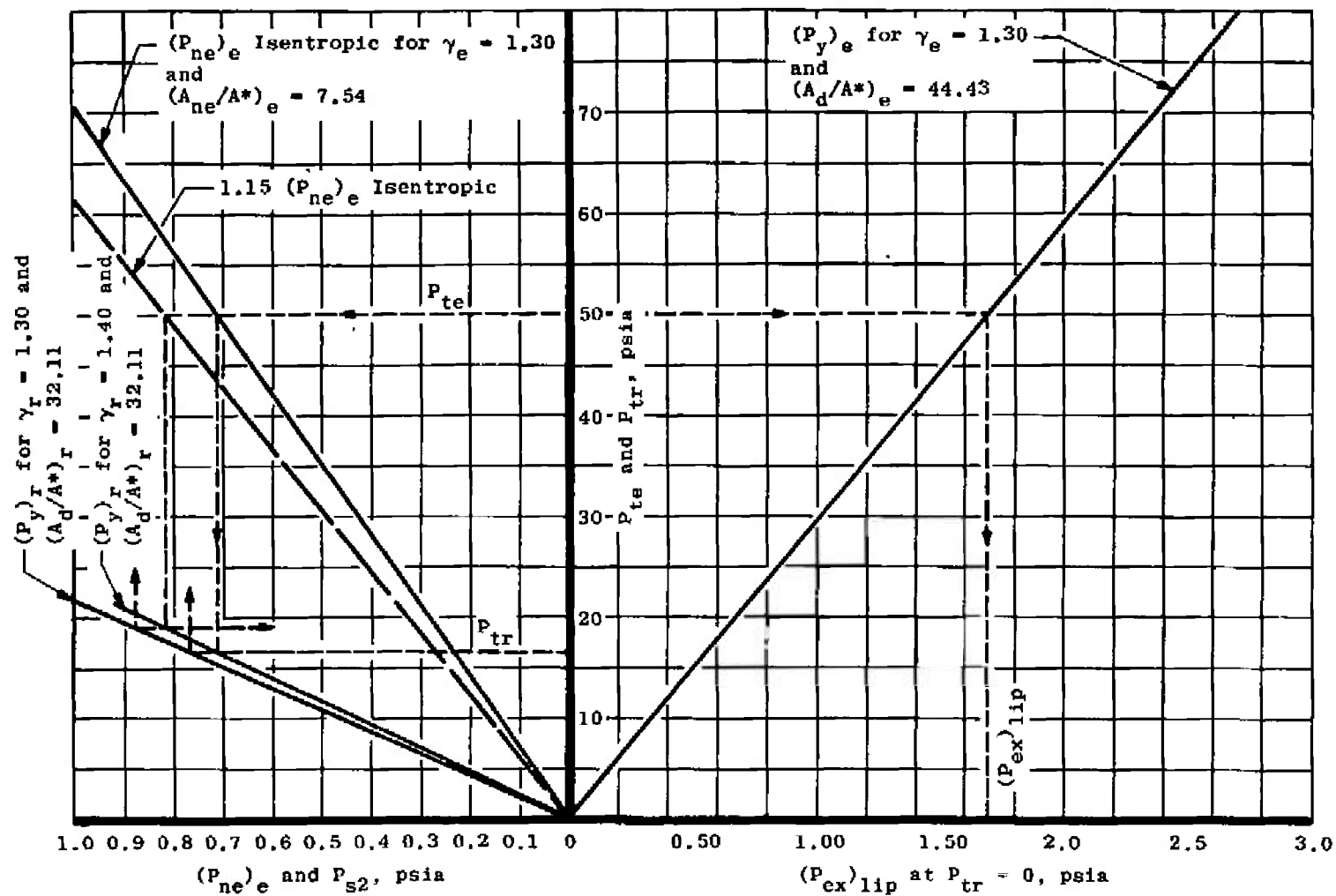


Fig. 17 Nomogram of Rocket Engine Chamber Pressure Throttling Limitations for Test Configurations 2c and e

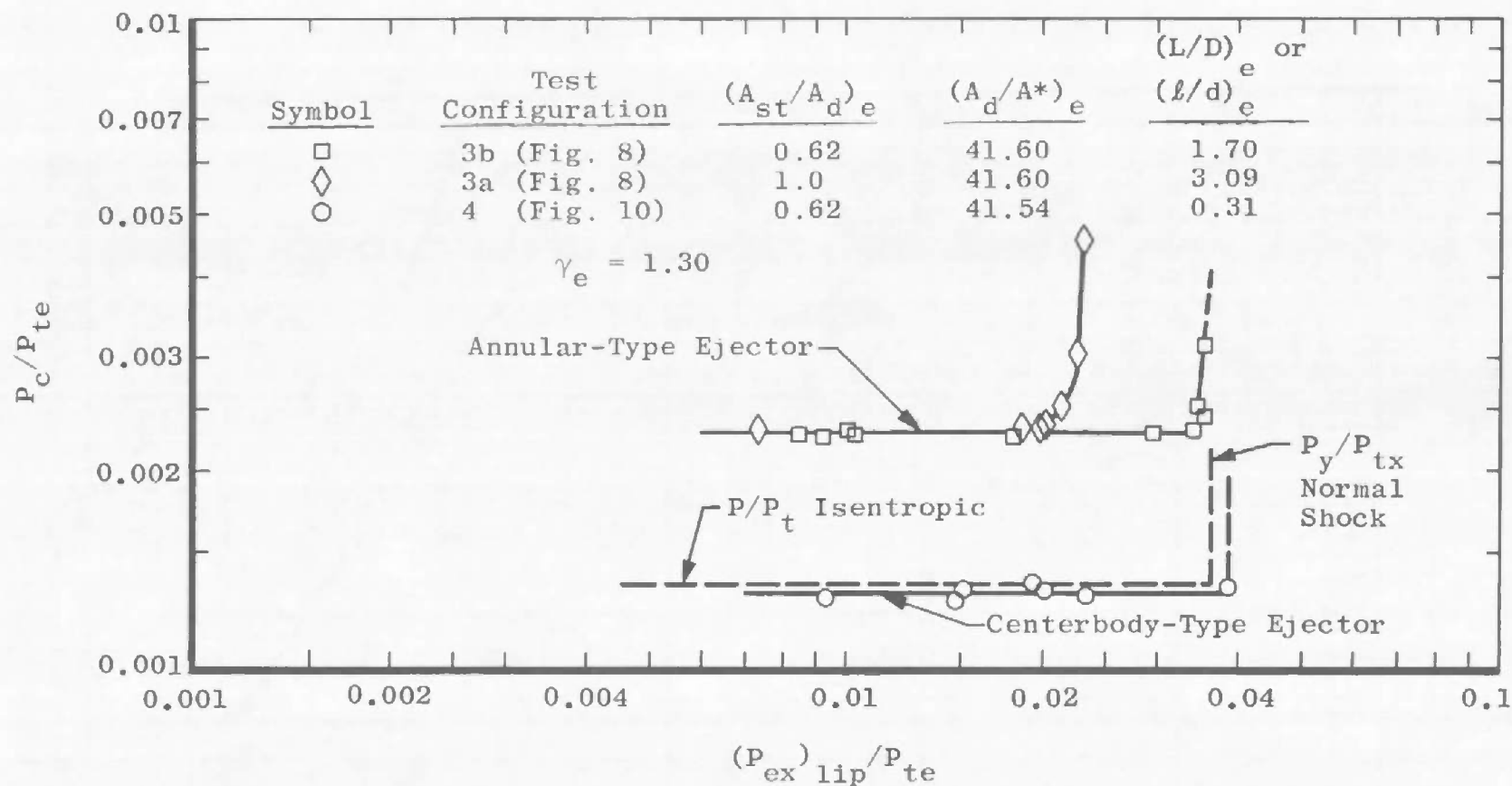
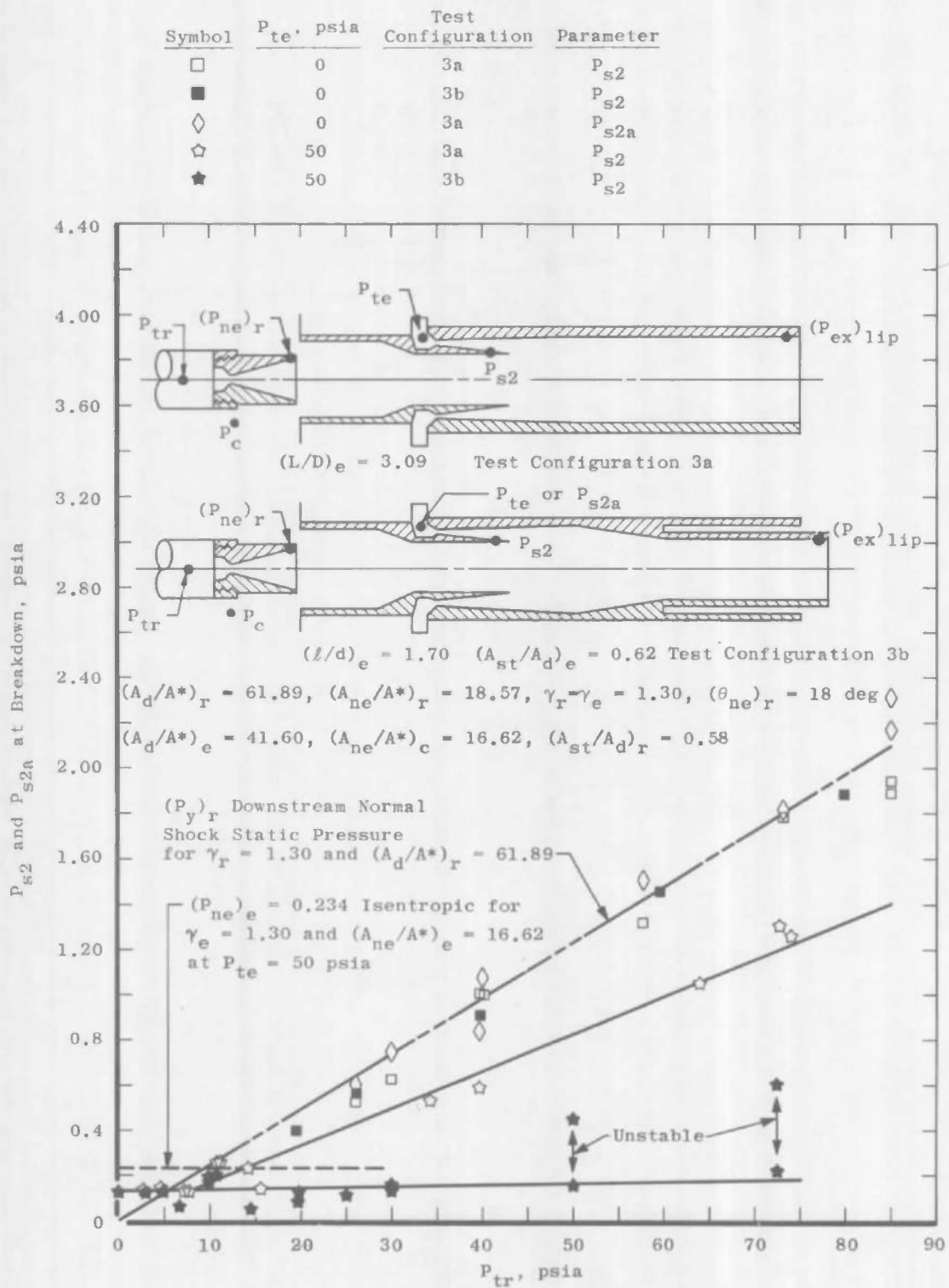
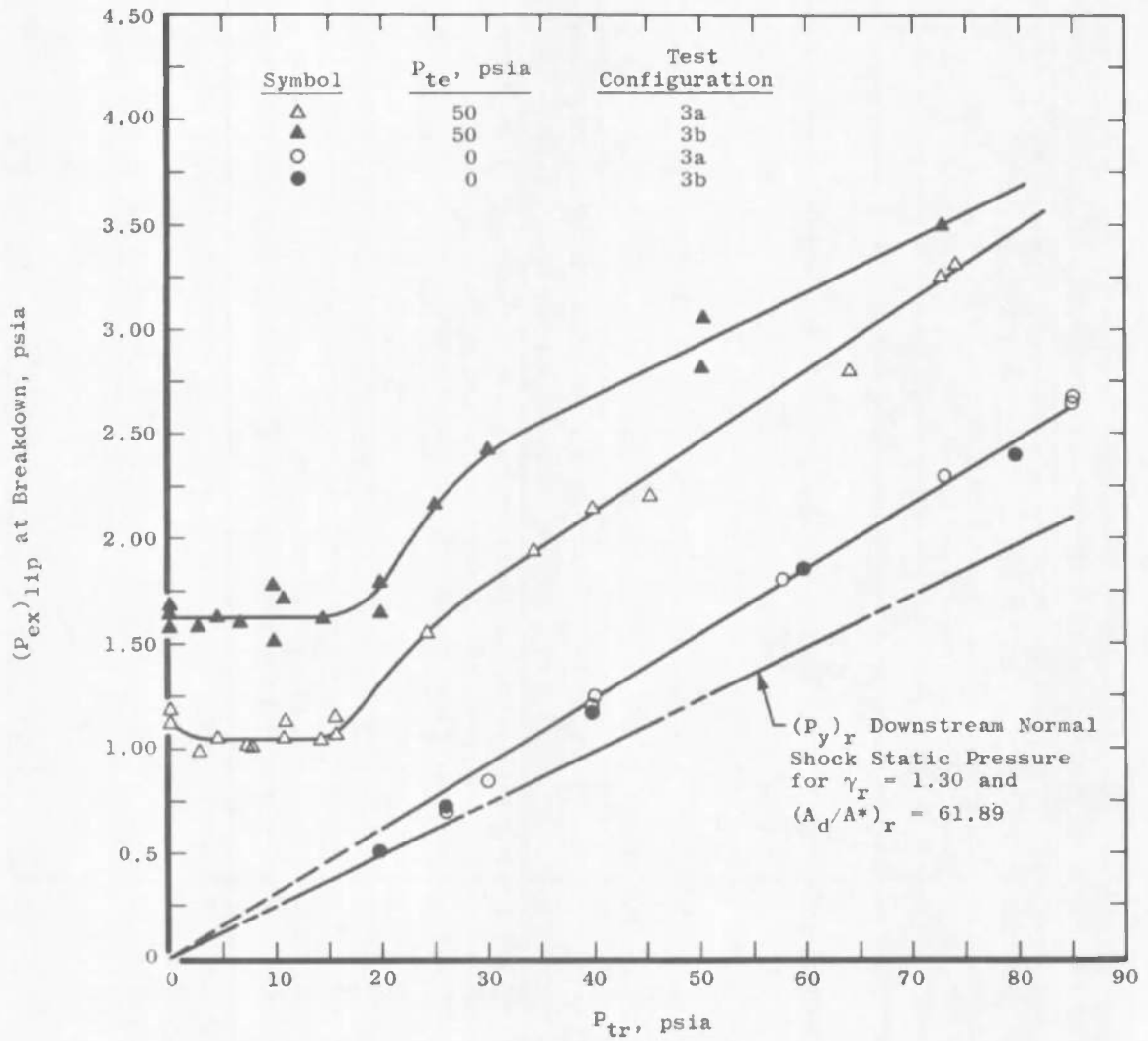


Fig. 18 Annular-Type and Centerbody-Type Ejector Performance for Test Configurations 3a, 3b, and 4



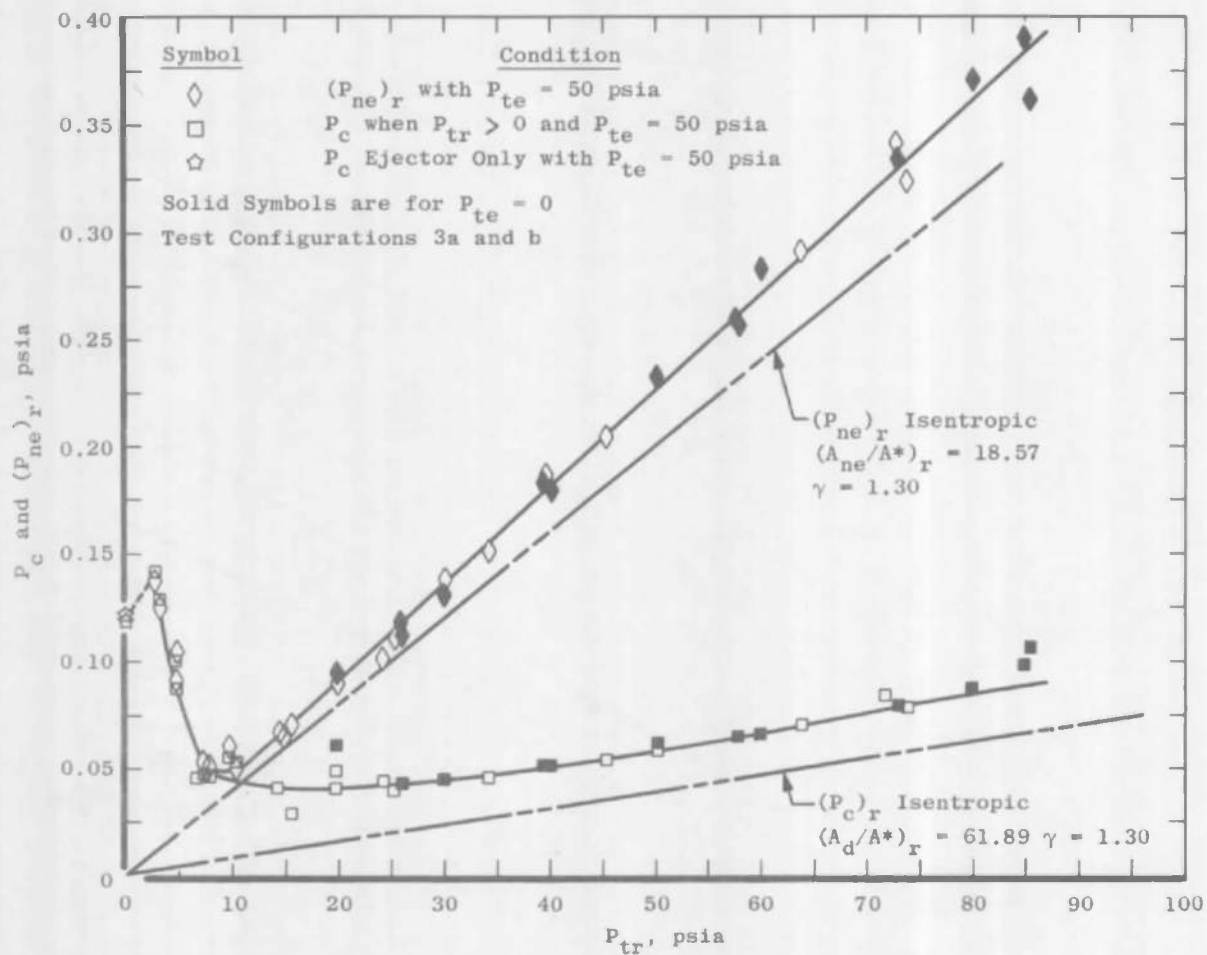
a. Diffuser Limiting Second-Throat Exit Static Pressure Performance

Fig. 19 Steam-Driven Rocket Engine and Steam-Driven Annular-Type Ejector Performance for Test Configurations 3a and b



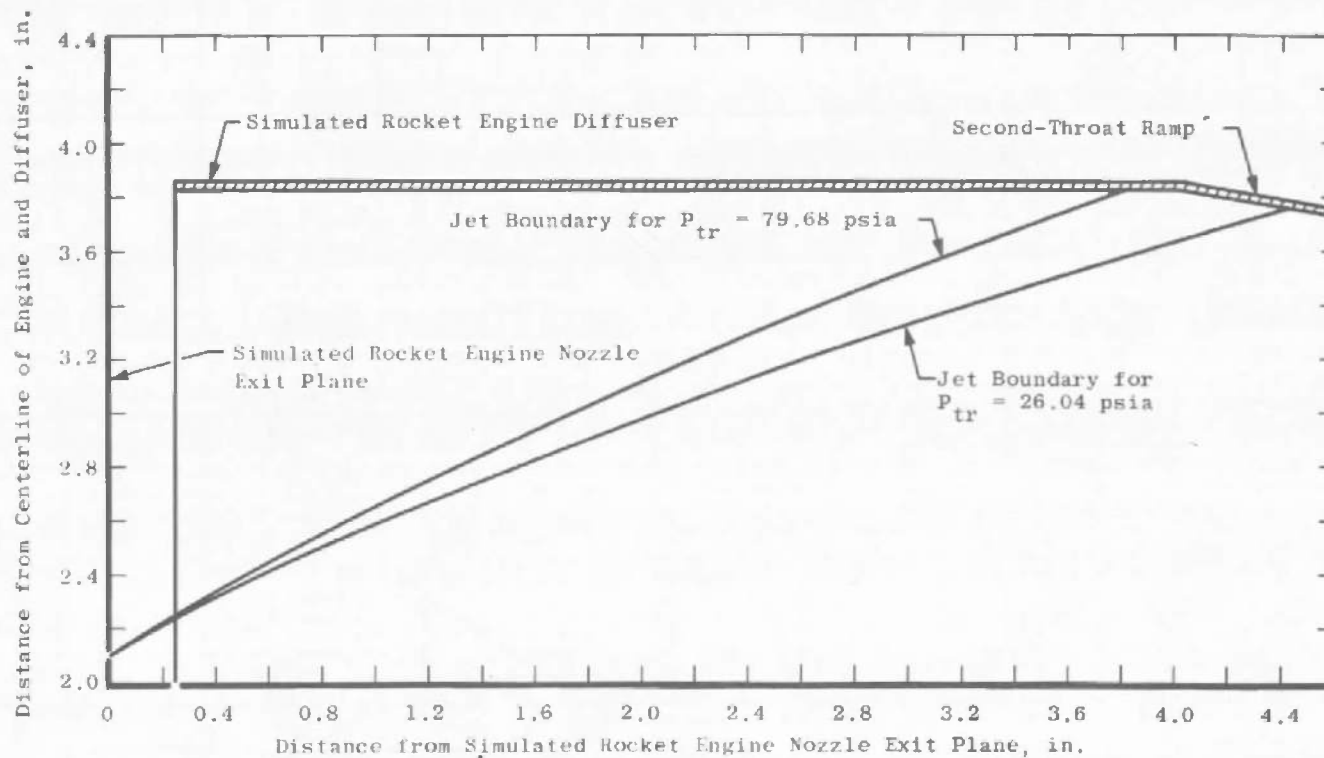
b. Ejector Limiting Exit Static Pressure Performance

Fig. 19 Continued



c. Minimum Cell Pressure and Rocket Engine Nozzle Lip Static Pressure Performance

Fig. 19 Continued



d. Rocket Engine Jet Boundary Impingement Variation with Change in Chamber Pressure

Fig. 19 Concluded

Symbol	P_{tr} , psia	P_{te} , psia	$(P_{ex})_{lip}$, psia	$(P_t)_{ex}$, psia	P_{s2} , psia
See Note					
\square	92.68—20.12	58.44	1.48—1.37	2.00	0.16—0.24
\triangle	48.93—13.04	46.58	1.46—1.43	2.01	0.13—0.14
\circ	47.11—12.00	45.89	1.43—1.41	1.96	0.11—0.13
Δ	97—20	57.54	0.51—0.50	0.52	0.16—0.17

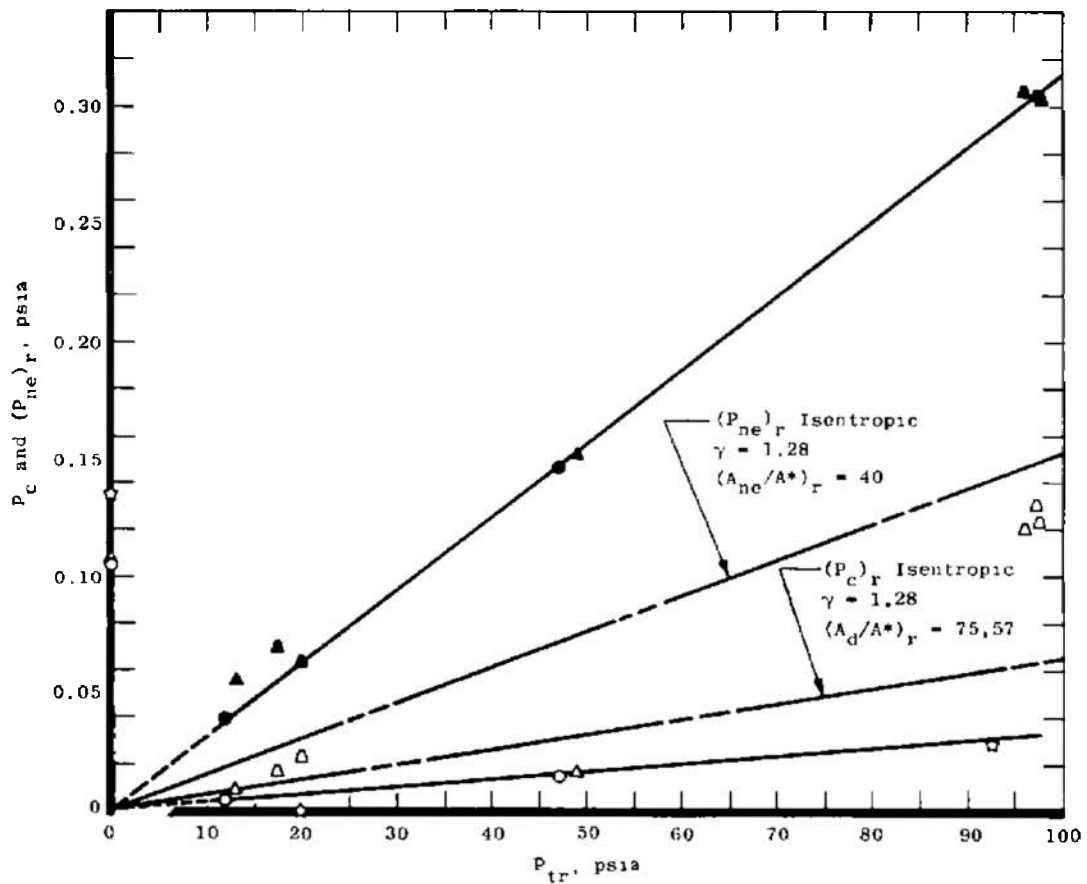
Open Symbol - P_c $(A_{st}/A_d)_r = 0.58$

Closed Symbol - $(P_{ne})_r$ $(A_{st}/A_d)_e = 0.62$

$(A_d/A^*)_e = 41.60$ $\gamma_e = 1.30$ $(\ell/d)_e = 1.70$

$(A_{ne}/A^*)_e = 16.62$

Note: Rocket Engine Nozzle Exit Moved Upstream 1.194 in.



a. Annular-Type Ejector Test Configuration 3c

Fig. 20 Throttling Performance of N_2O_4 and AZ-50 Liquid-Propellant Rocket Engine for Test Configurations 3c and 4

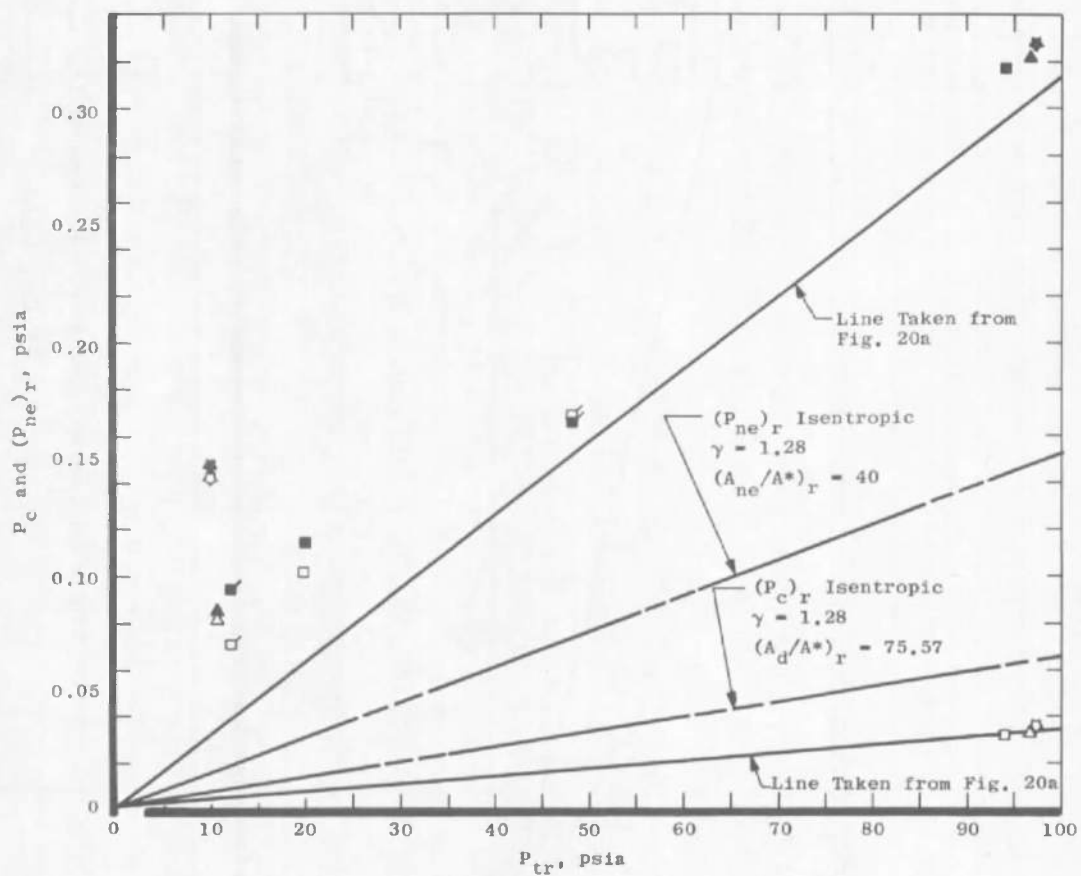
Symbol	P_{tr} , psia	P_{te} , psia	$(P_{ex})_{lip}$, psia	$(P_t)_{ex}$, psia	P_{s2} , psia
See Note	97.35-9.90	40.46	1.24-0.88	1.08	0.54-0.30
	96.83-10.69	40.23	1.22-0.57	0.60	0.52-0.22
	94.10-19.99	50.25	0.91-0.59	0.64	0.56-0.27
	48.11-12.11	44.27	0.78-0.53	0.64	0.43-0.22

Open Symbol - P_c $(A_{st}/A_d)_r = 0.58$

Closed Symbol - $(P_{ne})_r$ $(A_{st}/A_d)_e = 0.62$

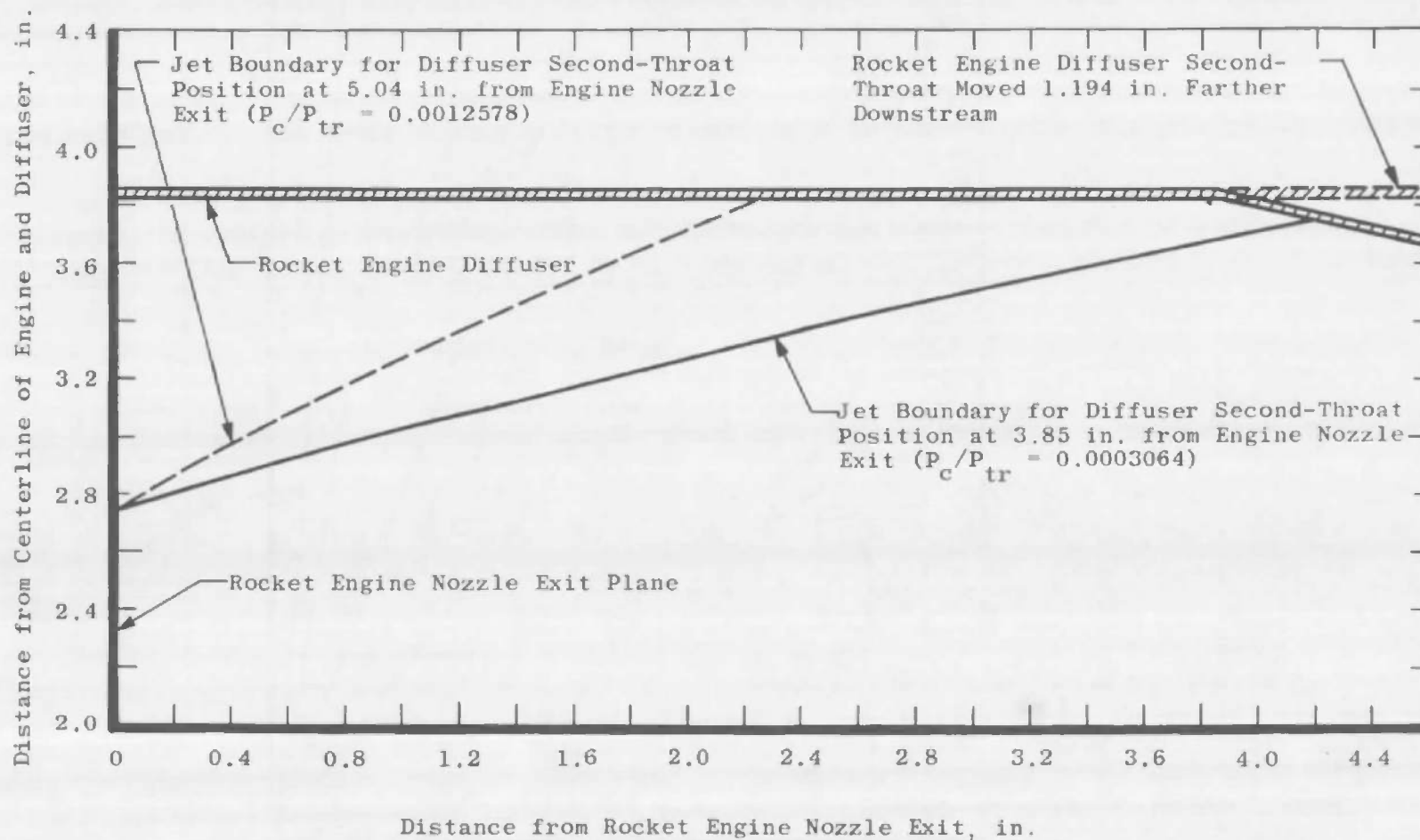
$(A_d/A^*)_e = 41.54$ } $\gamma_e = 1.30$ $(f/d)_e = 0.31$
 $(A_{ne}/A^*)_e = 16.59$

Note: Rocket Engine Nozzle Exit Moved Upstream 1.194 in.



b. Centerbody-Type Ejector Test Configuration 4

Fig. 20 Continued



c. Rocket Engine Jet Boundary Change with Position for Test Configuration 3c

Fig. 20 Concluded

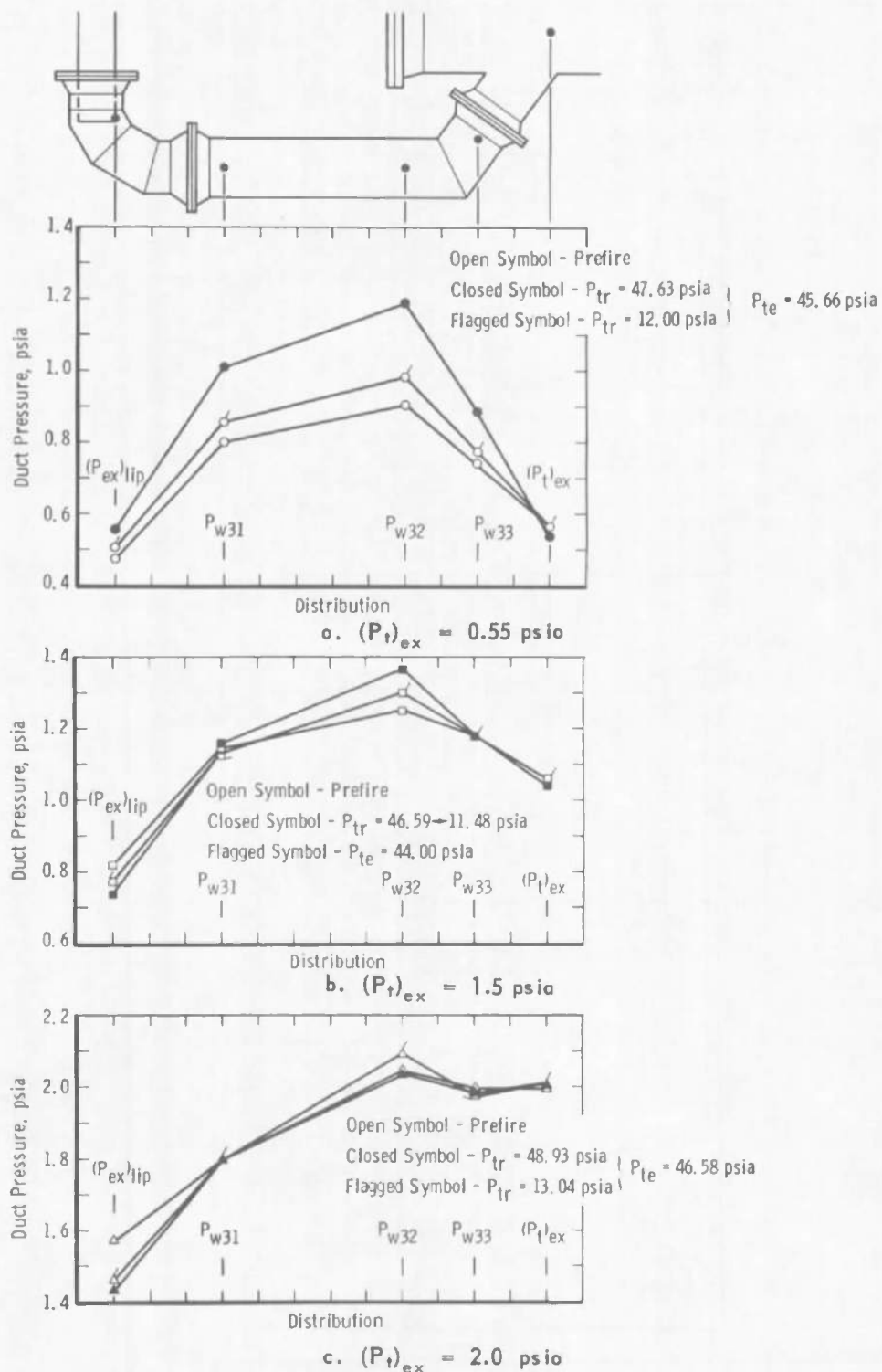


Fig. 21 J-3 Model Duct Pressure Distribution for Test Configuration 3c with $P_{te} = 43$ psia and Throttling from $P_{tr} = 50$ to 10 psia

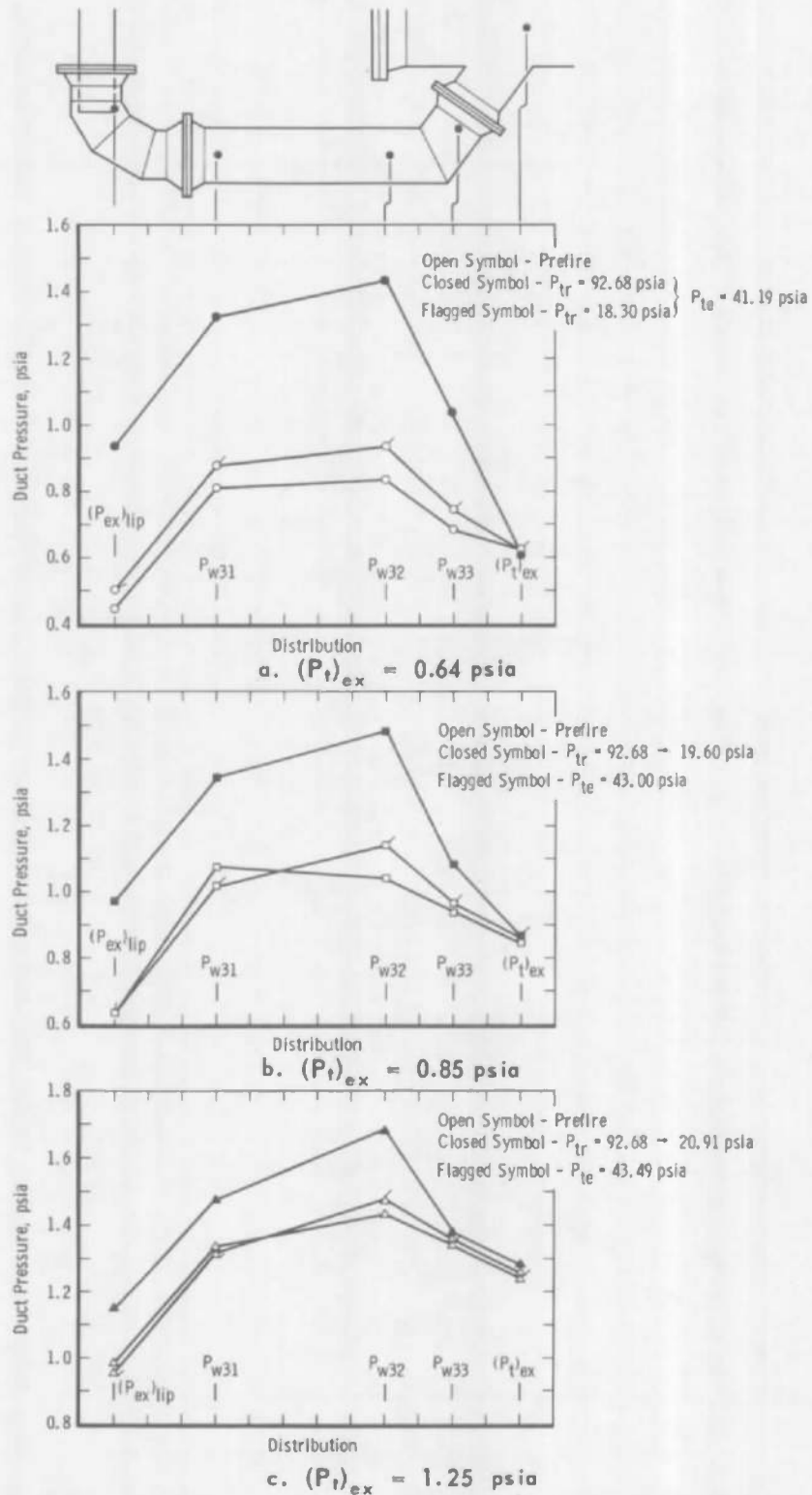


Fig. 22 J-3 Model Duct Pressure Distribution for Test Configuration 3c with $P_{te} = 40$ psia and Throttling from $P_{tr} = 20$ psia

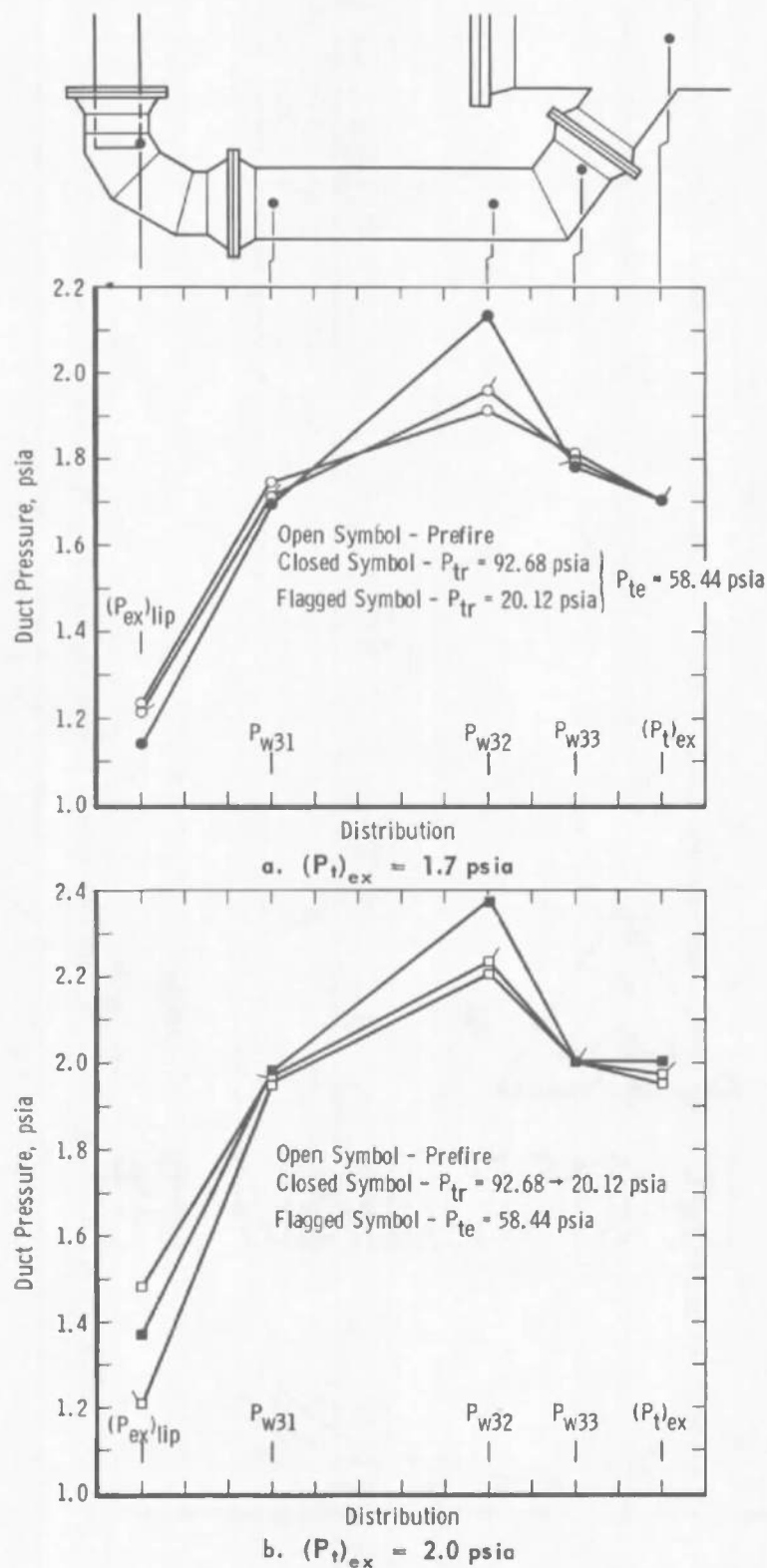


Fig. 23 J-3 Model Duct Pressure Distribution for Test Configuration 3c with $P_{te} = 56$ psia and Throttling from $P_{tr} = 100$ to 10 psia

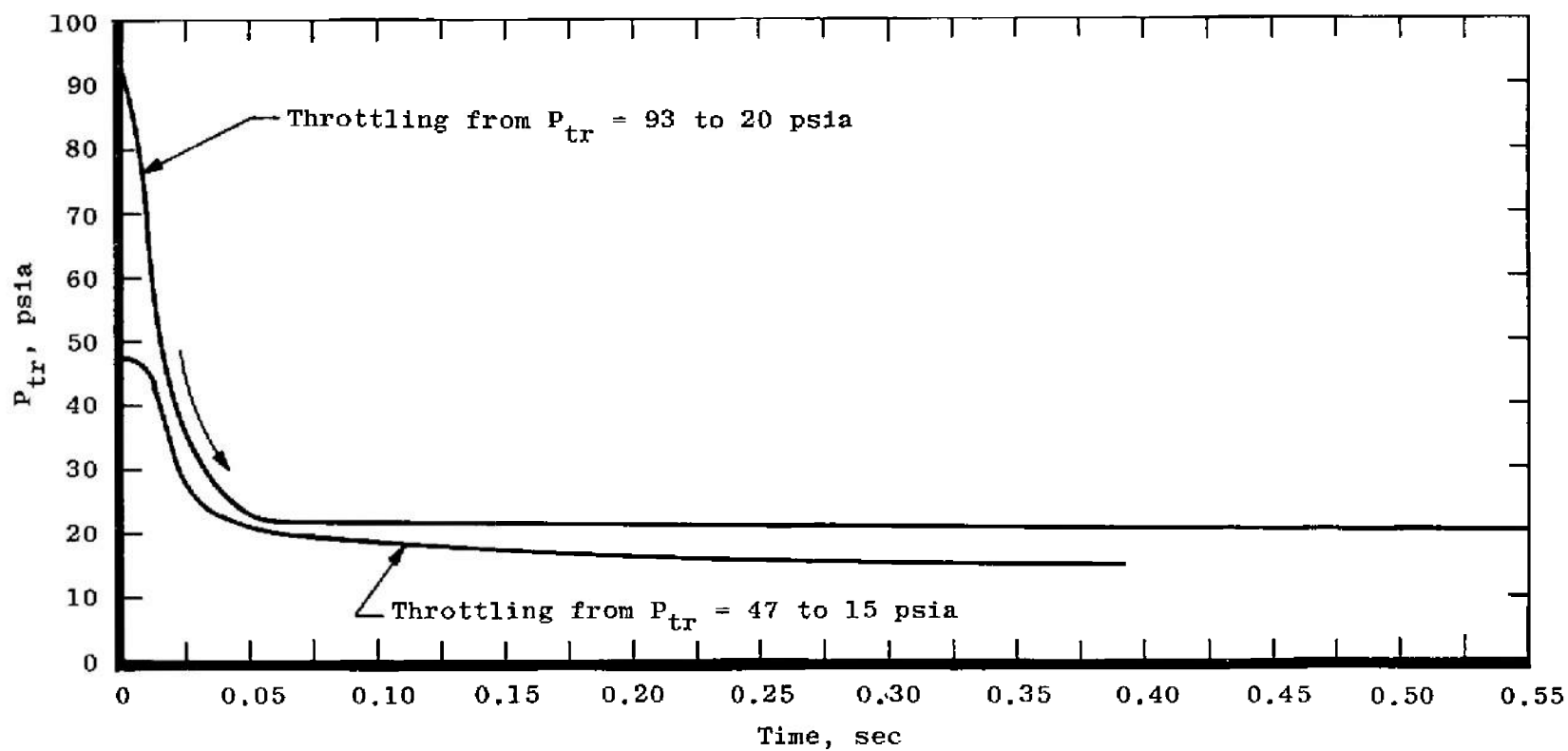


Fig. 24 Typical Transient of Rocket Engine Chamber Pressure

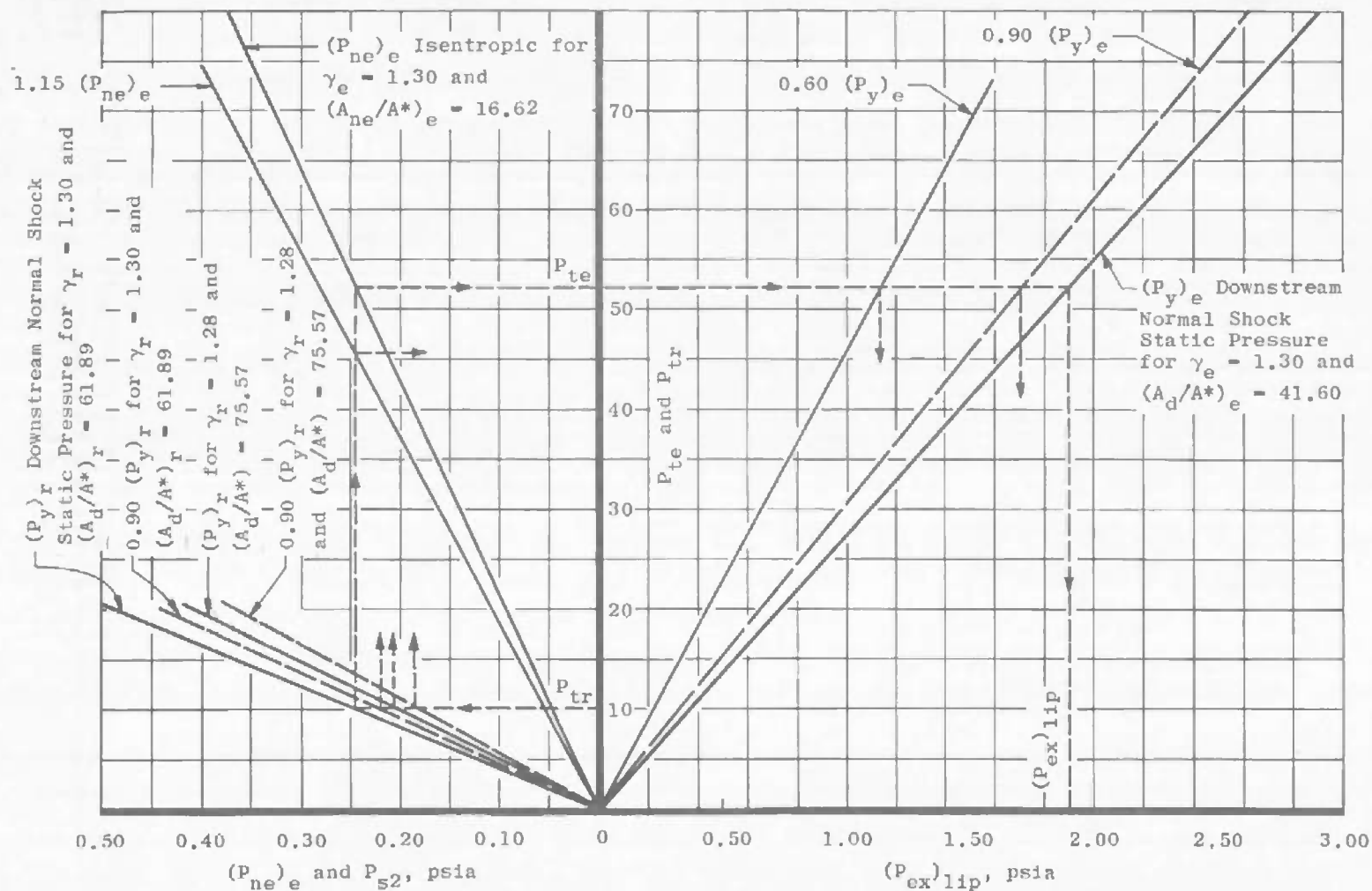


Fig. 25 Nomogram of Rocket Engine Chamber Pressure Throttling Limitations for Test Configurations 3a, b, and c

TABLE I
DESCRIPTION OF ROCKET ENGINE NOZZLE CONFIGURATIONS

Nozzle Configuration (Fig. 1)	Nozzle Geometry			
	d^* , in.	d_{ne} , in.	θ , deg	A_{ne}/A^*
A (Conical)	0.747	2.42	9.00	10.50
B (Conical)	0.51	1.75	13.25	11.77
C (Conical)	0.978	4.214	18.00	18.57
D (Contoured Nozzle Rocket Engine)	0.867	5.48	9.75	40.00

TABLE II
DESCRIPTION OF TEST CONFIGURATIONS

Test Phase	Test Configuration No.	Hot Jet Engine Nozzle Configuration (Fig. 1)	Ejector Configuration (Figs. 3, 5, 6, 8, and 10)	$(A_{01}/A_d)_e$	$(A_{02}/A_d)_e$	$(A_d/A^*)_e$	$(A_d/A^*)_e$	$(A_{02}/A^*)_e$	$(A_{01}/A^*)_e$	$(\theta_{02})_e$	$(\theta_{01})_e$	$(1/\eta)_e$ or $(L/D)_e$ or
I	1a	A	1*	1.00	0.648	29.05	--	--	10.50	--	9.00	--
	b	A	2*	1.00	0.527	31.58	--	--	10.50	--	9.00	--
	c	A	3*	1.00	0.510	29.05	--	--	10.50	--	9.00	--
	d	A	4*	1.00	0.510	29.05	--	--	10.50	--	9.00	--
	e	A	5*	1.00	0.580	29.05	--	--	10.50	--	9.00	--
	f	A	6*	1.00	0.643	29.05	--	--	10.50	--	9.00	--
	g	A	7*	1.00	0.643	29.05	--	--	10.50	--	9.00	--
	h	A	8*	1.00	0.643	29.05	--	--	10.50	--	9.00	--
	i	A	9*	1.00	0.643	29.05	--	--	10.50	--	9.00	--
II	2a	--	10 [†]	1.00	0.633	--	44.43	7.54	--	10.00	--	2.60
	b	--	10 [†]	1.00	0.633	--	44.43	7.54	--	10.00	--	8.00
III	2c	B	10 [†]	1.00	0.633	32.11	44.43	7.54	11.77	10.00	13.25	2.60
	d	B	10a [†]	0.54	0.633	32.11	44.43	7.54	11.77	10.00	13.25	1.58
	e	B	10b [†]	0.64	0.633	32.11	44.43	7.54	11.77	10.00	13.25	1.86
	3a	C	11 [†]	1.00	0.585	61.89	41.60	16.62	18.57	Ref. Fig. 7	18.00	3.09
	b	C	11a [†]	0.62	0.585	61.89	41.60	16.62	18.57	Ref. Fig. 7	18.00	1.70
IV	3c	D	11a [†]	0.62	0.585	75.57	41.60	16.62	40.00	Ref. Fig. 7	9.75	1.70
	4	D	12*	0.62	0.585	75.57	41.54	16.59	40.00	10.00	9.75	0.31

Ejector Configuration Note: * = Centerbody-Type Ejector

† = Annular-Type Ejector

TABLE III
SUMMARY OF COLD-FLOW CENTERBODY-TYPE EJECTOR BLOCKAGE STUDY (Phase I)

Test Config (Fig. 3)	Ejector Config (Fig. 3)	$(A_{01}/A_d)_t$	$(A_{01}/A_d)_{opt}$	$(A_d/A^*)_t$	Nozzle Cont. Half-Angle, δ , deg	Average Values at Zero Position		Position of Centerbody, in					
						$(P_t/P_t)_{start}$ $(P_t/P_t)_{max}$	P_{01}/P_t P_{01}/P_{01}	$P_{01} = 0 \rightarrow 100$ psia		F_{01} Decrease After Breakdown		Varied Position When P_{01} & P_{01} = Constant	
								Start	No-Start	Start	No-Start	Start	No-Start
1a	1	0.648	1.00	29.1	15	0.44	0.98	0, 2, 3, 4, 6	--	0, 2, 3, 4, 6	--	--	--
1b	2	0.527	0.81	21.6	15	0.40	1.10	0, 1	2, 3, 4, 5	0	1	--	--
1c	3	0.510	0.79	28.1	15	0.40	1.10	0, 1	2, 2.5, 4, 5, 6	0	1, 2, 2.5, 4, 5, 6	0 \rightarrow 2.50	2.50 \rightarrow 6
1d	4	0.510	0.79	29.1	7-22 (2-Step)	--	--	--	0, 1, 2, 3, 4, 5, 6	--	--	--	--
1e	5	0.580	0.90	29.1	7-22 (2-Step)	0.42	0.93	0, 0.5	1, 2, 5, 4, 6	--	0, 0.5, 1, 2, 5, 4, 6	0 \rightarrow 2.63	2.63 \rightarrow 6
1f	6	0.643	1.00	29.1	7-22 (2-Step)	0.43	0.94	0, 1, 1.25	1.5, 1.38	0, 1, 1.25	1.50, 4.38	0 \rightarrow 4.38	--
1g	7	0.643	1.00	29.1	22	0.42	0.93	0, 1, 2, 2.25, 5, 50, 6	3.5	1, 6	0, 2, 2.5, 2.50, 3, 5, 5.50	0 \rightarrow 6	--
1h	8	0.643	1.00	29.1	30	--	--	--	0, 1, 2, 3, 4, 5, 6, 6.25, 6.78, 6	--	--	--	--
1i	9	0.643	1.00	29.1	30-22 (2-Step)	--	--	--	0, 1, 2, 3, 4, 5, 6	--	--	--	--

UNCLASSIFIED

Security Classification

DOCUMENT CONTROL DATA - R&D

(Security classification of title, body of abstract and indexing annotation must be entered when the overall report is classified)

1 ORIGINATING ACTIVITY (Corporate author) Arnold Engineering Development Center ARO, Inc., Operating Contractor Arnold AF Station, Tennessee		2a REPORT SECURITY CLASSIFICATION UNCLASSIFIED	
		2b GROUP N/A	
3 REPORT TITLE DIFFUSER AUXILIARY EJECTOR DEVELOPMENT FOR THE DESIGN OF THE J-3 LEM DESCENT EXHAUST SYSTEM			
4 DESCRIPTIVE NOTES (Type of report and inclusive dates) N/A			
5 AUTHOR(S) (Last name, first name, initial) Hale, J. W. and Gobbell, W. C., ARO, Inc.			
6 REPORT DATE February 1966	7a TOTAL NO OF PAGES 83	7b NO OF REFS 16	
8a CONTRACT OR GRANT NO AF 40(600)-1200 b XXXXXXXX Program Element 65402234 c d	9a ORIGINATOR'S REPORT NUMBER(S) AEDC-TR-65-255 9b OTHER REPORT NO(S) (Any other numbers that may be assigned this report) N/A		
10 AVAILABILITY/LIMITATION NOTICES Qualified users may obtain copies of this report from DDC. Release to foreign governments or foreign nationals must have prior approval of AEDC.			
11 SUPPLEMENTARY NOTES N/A		12 SPONSORING MILITARY ACTIVITY Arnold Engineering Development Center Air Force Systems Command Arnold AF Station, Tennessee	
13 ABSTRACT A four-phase investigation was conducted to select a rocket engine diffuser auxiliary ejector configuration. The configuration was required to maintain test cell pressure sufficiently low to keep the rocket engine nozzle flowing full at 10 percent of full power while operating against an exit pressure of approximately 1.50 psia. The investigation was in sup- port of the LEM Descent test program scheduled for the J-3 test cell. The annular-type auxiliary ejector was selected because of its superior performance over the centerbody-type ejector. A successful model rocket engine throttling demonstration to 10 percent of full power was made with the annular-type auxiliary ejector. An ejector second throat (having a contraction area ratio of 0.62) was used to increase the limit- ing diffuser exit pressure. Pressure distribution through the J-3 model ducting was obtained at various exhaust header pressures.			

UNCLASSIFIED
Security Classification

KEY WORDS

rocket engine testing
altitude test facilities
ejectors
diffusers
APOLLO LEM engine

INSTRUCTIONS

- 1. ORIGINATING ACTIVITY:** Enter the name and address of the contractor, subcontractor, grantee, Department of Defense activity or other organization (*corporate author*) issuing the report.

- 2a. REPORT SECURITY CLASSIFICATION:** Enter the overall security classification of the report. Indicate whether "Restricted Data" is included. Marking is to be in accordance with appropriate security regulations.

- 2b. GROUP:** Automatic downgrading is specified in DoD Directive 5200.10 and Armed Forces Industrial Manual. Enter the group number. Also, when applicable, show that optional markings have been used for Group 3 and Group 4 as authorized.

3. REPORT TITLE: Enter the complete report title in all capital letters. Titles in all cases should be unclassified. If a meaningful title cannot be selected without classification, show title classification in all capitals in parenthesis immediately following the title.

4. **DESCRIPTIVE NOTES:** If appropriate, enter the type of report, e.g., interim, progress, summary, annual, or final. Give the inclusive dates when a specific reporting period is covered.

5. **AUTHOR(S):** Enter the name(s) of author(s) as shown on or in the report. Enter last name, first name, middle initial. If military, show rank and branch of service. The name of the principal author is an absolute minimum requirement.

- 6. REPORT DATE.** Enter the date of the report as day, month, year, or month, year. If more than one date appears on the report, use date of publication.

- 7a. TOTAL NUMBER OF PAGES:** The total page count should follow normal pagination procedures, i.e., enter the number of pages containing information.

- 7b. NUMBER OF REFERENCES: Enter the total number of references cited in the report.

- 8a. CONTRACT OR GRANT NUMBER: If appropriate, enter the applicable number of the contract or grant under which the report was written.

- 8b, 8c, & 8d. PROJECT NUMBER:** Enter the appropriate military department identification, such as project number, subproject number, system numbers, task number, etc.

- 9a. ORIGINATOR'S REPORT NUMBER(S).** Enter the official report number by which the document will be identified and controlled by the originating activity. This number must be unique to this report.

- 9b. OTHER REPORT NUMBER(S): If the report has been assigned any other report numbers (either by the originator or by the sponsor), also enter this number(s).

10. AVAILABILITY/LIMITATION NOTICES: Enter any limitations on further dissemination of the report, other than those

imposed by security classification, using standard statements such as:

- (1) "Qualified requesters may obtain copies of this report from DDC."
- (2) "Foreign announcement and dissemination of this report by DDC is not authorized."
- (3) "U. S. Government agencies may obtain copies of this report directly from DDC. Other qualified DDC users shall request through _____."
- (4) "U. S. military agencies may obtain copies of this report directly from DDC. Other qualified users shall request through _____."
- (5) "All distribution of this report is controlled. Qualified DDC users shall request through _____."

If the report has been furnished to the Office of Technical Services, Department of Commerce, for sale to the public, indicate this fact and enter the price, if known.

11. SUPPLEMENTARY NOTES: Use for additional explanatory notes.

- 12. SPONSORING MILITARY ACTIVITY:** Enter the name of the departmental project office or laboratory sponsoring (paying for) the research and development. Include address.

- 13 **ABSTRACT:** Enter an abstract giving a brief and factual summary of the document indicative of the report, even though it may also appear elsewhere in the body of the technical report. If additional space is required, a continuation sheet shall be attached

It is highly desirable that the abstract of classified reports be unclassified. Each paragraph of the abstract shall end with an indication of the military security classification of the information in the paragraph, represented as (TS), (S), (C), or (U)

There is no limitation on the length of the abstract. However, the suggested length is from 150 to 225 words.

- 14. KEY WORDS.** Key words are technically meaningful terms or short phrases that characterize a report and may be used as index entries for cataloging the report. Key words must be selected so that no security classification is required. Identifiers, such as equipment model designation, trade name, military project code name, geographic location, may be used as key words but will be followed by an indication of technical context. The assignment of links, rules, and weights is optional.

UNCLASSIFIED

Security Classification